Investigating the role of sodium-glucose cotransporter 2 modulation in metabolic syndrome induced-chronic kidney disease mouse model

Véronique Cheff

A thesis submitted in partial fulfillment of the requirements for the

Master's degree in Cellular and Molecular Medicine

Department of Cellular and Molecular Medicine

Faculty of Medicine

University of Ottawa

uOttawa

L'Université canadienne
Canada's university

ABSTRACT

Chronic kidney disease (CKD) is a worldwide health burden with increases risk of end-stage renal function if left untreated. CKD induced in the context of metabolic syndrome (MS) increases risks of hypertension, hyperglycemia, excess body fat and dyslipidemia. Our Centre previously generated a renin-dependent hypertensive/ type-1 diabetic mouse model and lead to the development of several signs associated with human diabetic kidney disease (DKD), however the extent and impact of dyslipidemia in this model remains unknown. We hypothesized that combining a high-fat diet (HFD) regimen onto the hypertensive/ diabetic phenotype would mimic features of MS induced-CKD in mice. An 8-week-old male genetically hypertensive mice (Lin+) were subjected to streptozotocin (STZ) intraperitoneal (i.p.) injections (50 mg/kg, 5 days consecutive) to induce hyperglycemia. Four-weeks later hypertensive/ diabetic mice (Lin+ mouse with induced beta cells death, also known as LinSTZ) were fed a 60% kCal HFD for 8 weeks. This study shows that HFD-fed LinSTZ mice developed less glomerular hypertrophy, scarring and albuminuria and hepatocytes fat accumulation at endpoint than regular-diet fed littermates. Moreover, antidiabetic drug Canagliflozin, dosed at 30 mg/kg body weight, showed reno-protection in the LinSTZ mice model. Taken together, our results show that LinSTZ mice fed a HFD did not lead to a more robust model of MS-induced CKD. In fact, several indices of renal injury were reduced by feeding LinSTZ mice a HFD or treating them with Canagliflozin.

ABSTRACT (French Version)

La maladie rénale chronique (MRC) induite par le syndrome métabolique (SM) implique l'hypertension, l'hyperglycémie, l'excès de graisse corporelle et la dyslipidémie. Précédemment étudié par notre Centre, le modèle de souris avec les phénotypes de l'hypertension dépendant de la rénine et du diabète de type-1 souligne plusieurs signes associés à la néphropathie diabétique humaine, mais l'impact de la dyslipidémie dans ce modèle restent inconnus. L'hypothèse de cette étude est de combiner un régime alimentaire riche en graisses sur le modèle hypertensif et d'hyperglycémie pour obtenir un nouveau modèle d'insuffisance rénale chronique induit par SM. À cette fin, des souris mâles génétiquement hypertensifs (Lin +) âgées de 8 semaines ont été soumises à des injections intra-péritonéale (i.p.) de streptozotocine (STZ) (50 mg / kg, 5 jours consécutif) pour induire une hyperglycémie. Quatre semaines plus tard, les souris hypertensives et diabétiques (LinSTZ) ont été nourries avec un régime haut en lipides (HFD) à 60% kCal pendant 8 semaines. Cette étude montre que les souris LinSTZ nourries avec HFD ont développé moins d'hypertrophie glomérulaire, de cicatrices rénales, d'albuminurie et d'accumulation de graisse hépatocytaire que les souris nourris avec un régime régulier. Cependant, le traitement antidiabétique Canagliflozine, dosé à 30 mg/ kg de poids corporel, a montré une protection rénale chez le modèle de souris LinSTZ. Ensemble, nos résultats suggèrent que l'alimentation HFD dans LinSTZ n'a pas conduit à un modèle plus robuste de MRC induit par la SM. En fait, plusieurs indices de lésion rénale ont été réduits en nourrissant des souris LinSTZ avec un HFD ou en les traîtant avec de la Canagliflozine.

LIST OF JOURNAL ARTICLES (2020-2021)

1. Nasrallah R, Zimpelmann J, **Cheff V**, Thibodeau JF, Burns KD, Hébert RL. Collecting duct PGE2 responses reduce water loss with empagliflozin in mice with type 2 diabetes mellitus. Journal of Clinical Nephrology. DOI: 10.29328/journal.jcn.1001069. J Clin. Nephrol. 2021; 5: 023-030.

2. Simard JC*, Thibodeau JF*, Leduc M, Tremblay M, Laverdure A, Sarra-Bournet F, Gagnon W, Ouboudinar J, Richard J, Gervais L, Felton A, Letourneau S, Geerts L, Cloutier MP, Hince K, Corpuz R, Blais A, Marques-Quintela V, Duceppe JF, Abbott SD, Zacharie B, Blais A, **Cheff V**, Laurin P, Laplante SR, Kennedy CRJ, Hébert RL, Leblond FA, Grouix B, Gagnon L. Fatty Acid Mimetic PBI-4547 Restores Metabolic Homeostasis via GPR84 in Mice with Non-Alcoholic Fatty Liver Disease. Sci., Rep., **10**, Article number: 12778 pp. 1 – 16. 2020.

1. **Cheff V**, Blais A, Holterman CE, Thibodeau JF, Hébert RL. *Characterization of a Novel Mouse Model of Metabolic Syndrome Induced-Chronic Kidney Disease*. WCN-ISN 2021. (Poster presentation by V Cheff, WCN April 2021).

2. **Cheff V**, Blais A, Holterman CE, Hébert RL, Kennedy CRJ, Thibodeau JF. *Dual GPR40/GPR84 fatty acid receptor deletion improves adenine-induced renal injury in mice*. ERA-EDTA 2020. (Submitted for Poster presentation by JF Thibodeau)

3. **Cheff V**, Blais A, Holterman CE, Thibodeau JF, Hébert RL. *Characterization of a novel mouse model of metabolic syndrome-induced chronic kidney disease*. CMM seminars I course (CMM83242) May 2020. (Poster presentation by V Cheff)

TABLE OF CONTENTS

LIST OF TABLES

LIST OF FIGURES

LEGEND (ALPHABETICAL)

ATP	Adenosine triphosphate
ALT	Alanine aminotransferase
ACR	Albumin to creatinine ratio
AHA	American Heart Association
Ang II	Angiotensin II
ARB	Angiotensin type 1 receptor blocker
ACEi	Angiotensin-converting enzyme inhibitors
AMDCC	Animal Models of Diabetic Complications Consortium
AUC	Area under the curve
AST	Aspartate aminotransferase
BP	Blood pressure
BSA	Bovine serum albumin
Cana	Canagliflozin
CV	Cardiovascular
CVD	Cardiovascular disease
CKD	Chronic kidney disease
CD	Collecting duct
cDNA	Complementary deoxyribonucleic acid
DKD	Diabetes kidney disease
DN	Diabetic nephropathy
DBP	Diastolic blood pressure
DT	Distal tubule
ESRD	End-stage renal disease
EC	Endothelial cell
eGFR	Estimated glomerular filtration rate
FITC	Fluorescein isothiocyanate
GBM	Glomerular basement membrane
GFB	Glomerular filtration barrier
GFR	Glomerular filtration rate
HDL	High density lipoprotein
HFD	High fat diet

HPLC	High pressure liquid chromatography
i.p.	Intraperitoneal
LDL	Low density lipoprotein
MD	Macula densa
mRNA	Messenger ribonucleic acid
MS	Metabolic syndrome
NO	Nitric oxide
NAFLD	Nonalcoholic fatty liver disease
OCT	Optimal cutting temperature
PFA	Paraformaldehyde
PAS	Periodic Acid Schiff
PBS	Phosphate buffer saline
PT	Proximal tubule
qPCR	Quantitative polymerase chain reaction
RPF	Renal plasma flow
RAAS	Renin-angiotensin-aldosterone system
RT	Reverse transcription
RNA	Ribonucleic acid
Na^+	Sodium
SGLT-2	Sodium-glucose cotransporter 2
STZ	Streptozotocin
SBP	Systolic blood pressure
TAL	Thick ascending limb
TGF	Tubulo-glomerular feedback
TIF	Tubulointerstitial fibrosis
T1DM	Type-1 diabetes mellitus
T2DM	Type-2 diabetes mellitus
WAT	White adipose tissue
WT	Wildtype
α-SMA	α-smooth muscle actin

ACKNOWLEDGMENTS

First, I would like to thank my supervisor Dr. Richard L. Hébert for giving me, a small-town French girl, the opportunity to join his research laboratory and complete my master's degree in his laboratory. I greatly improved my studies management and developed a stronger self-confidence under his guidance in his laboratory. I would also like to thank my former co-supervisor Dr. Jean-François Thibodeau, for all his guidance, assistance and encouragement. With your incredible patience, I have developed laboratory skills that will forever be forged in me. Thank you for believing in me since day one in the lab!

Many thanks to all the members at the Kidney Research Centre over the past two years. In particular, Chet Holterman, Amelie Blais, Mayra Trentin-Sonoda, Hannah Battaion, Alex Gutsol and Lihua (Julie) Zhu, thank you for your help. I appreciate it a lot.

I appreciate very much the guidance and support of my advisor committee members, Drs Chris Kennedy and Mario Tiberi. I would like to thank them for their time and patience in reading my reports and for pushing me to continuously improve my work with helpful suggestions.

A big thanks to the University of Ottawa`s animal care facility for their non-stop support with animal studies and metabolic cages clean-up, especially Carine and Stephanie. Thank you for making my job easier and keeping the animals safe. Also, to the Department of pathology who never turned me down, keep up the good work!

Finally, another big thank you to my family for their continued support throughout my study. Without them, I wouldn't have had the motivation and determination to further my education in a domain that I'm passionate about. Je vous remercie d'avoir cru en moi, je suis fière de ma personne.

Statement of contributions:

Veronique Cheff performed mouse breeding, project management and all *in vivo* and *in vitro* experiments and associated data analysis.

Chet Holterman and **Mayra Trentin-Sonoda** performed mice cardiac perfusion at sacrifice and collected respected tissue for analysis.

Amelie Blais and **Hannah Battaion** supervised and reviewed data analysis for unbiased results.

Alex Gutsol performed kidney sections immunofluorescence staining and morphology scoring.

Richard L. Hébert, Principal Investigator and intellectual support, conceived to lead the project and supervised the analysis of the data.

COPYRIGHTED CONTENTS

No copyrighted contents were used and are to be declared in the document.

1.1 The kidney

The kidney is a vital organ in the body responsible for plasma filtration and elimination of metabolic waste by the formation of urine [1]. All mammals have two kidneys, located in the retroperitoneal space of the abdominal cavity and each kidney have approximately 1 million nephrons playing an essential role as the filtering unit of the kidney. A nephron physiological anatomy is composed of a glomerulus segment followed by a tubular network. The glomerular is well organized and is composed of a high density of endothelial cells (EC), glomerular basement membrane (GBM) and specialized terminally differentiated epithelial cells known as podocytes [2]. When blood is sent to the kidney via the renal artery for filtration, it reaches the glomerular filtration barrier (GFB) by the capillary beds of the afferent arteriole of each glomerulus. An average of 20% of the cardiac plasma flow is filtered by the kidney. The non-filtered plasma (80%) automatically leaves the glomerulus by the efferent arteriole for proper blood flow circulation.

The tubular compartment is also well organized for reabsorption and secretion of various electrolytes and metabolites, such as sodium, potassium, or glucose to maintain proper osmolality. It is composed of the proximal tubule (PT), the loop of Henle composed of the thin descending limb and the thick ascending limb, the distal tubule (DT), and the collecting duct (CD) all well-organized along the nephron [2]. Of particular interest, the loops of Henle are responsible for the counter-current multiplier and exchanger mechanisms. The excretion of urine allows to the elimination of toxins and metabolic wastes from the body. Together, the glomerulus and the tubules of the nephrons are essentials for proper renal function and body homeostasis.

1.2 Normal kidney function

Every day, approximately 180 liters of plasma is filtered by the kidneys and produce an average of 1.5 Liter of urine output eliminated from the body [3]. To better assess kidney function, clinicians are required this property by measuring the glomerular filtration rate (GFR). The assessment of kidney function is also performed by measuring the urinary albumin excretion and albumin/ creatinine ratio (ACR). The GFR and ACR are both efficient measurements to validate the renal function.

The glomerular filtration rate (GFR) is the renal clearance ratio and is calculated by the volume filtered from the glomerulus per unit of time [4]. The renal afferent and efferent arteriole blood pressure change influences GFR measurement. GFR is calculated by the normalization of plasma and urine creatinine together. Creatinine has been identified as a waste by-product of creatine-phosphate breakdown from muscle and is secreted into the bloodstream. Creatinine is freely filtered by the kidney nephron with little reabsorption in the renal proximal tubule. As a result, it is used as a marker for renal filtration, and to evaluates the stage of renal function and damage over disease progression [5]. In normal kidney function, the GFR is quantified above 90 mL per minute. Moreover, the GFR value obtained is dependent on protein intake, level of exercise and diurnal activity of the body from day to night on renal function [6]. Therefore, during normal kidney function, apparent signs of healthy podocytes with non-injured foot processes filter the blood plasma particles smaller than 70 kD through the GBM [6]. In addition, the plasma flow filtered at the glomerulus is adequate, thus no leakage of oversized essential metabolites is assimilated, and the filtration of low molecular weight proteins is reabsorbed in the tubular system by active transport.

Furthermore, ACR is calculated by dividing urinary albumin concentration with the excreted creatinine concentration to establish kidney function. Thus, it is another gold standard method used to identify kidney damage [7]. Taken together, measurement GFR and or ACR is another

good method to properly assess kidney function injury and allows early detection of end-stage renal disease (ESRD).

The regulation of kidney function is maintained by proper osmolality of body fluids through the regulation of water, ions and small molecules balanced within the tubular compartment of the kidney [8]. *Vallon* characterized the tubulo-glomerular feedback (TGF) system in the kidney by its rapid responses and homeostasis stabilization throughout the filtration units [9]. Briefly, the TGF is a rapid responder exhibiting negative feedback on the renal system. In fact, tubular flow rate is maintained by the macula densa (MD) cells, specialized cells that sense sodium (Na^+) concentrations in the collecting duct prior to excretion in the urine. In responses to a decrease of blood flow interring the glomerulus or a vasoconstriction of the afferent arteriole, causing the decreases of GFR. The MD sense a concentration of Na^+ ions declines and the TGF response is generated by the production of nitric oxide (NO) accelerating vasodilatation of the afferent arteriole, thus equilibrating renal plasma flow (RPF), GFR and body hydration [9]. This fast responses of TGF limits stress to the kidney. However, a persistent disequilibrium on the kidney increases risk factors of kidney injury.

1.3 Impaired kidney function

Persistent kidney injuries are identified as chronic kidney disease (CKD). CKD is the leading cause of end-stage renal disease (ESRD) and characterized by the near to complete loss of renal function [10]. CKD leads to toxins accumulations in the body.

The improper perfusion of the GBM imbalances metabolic waste elimination such as creatinine and urea, but also increases larger protein loss in the urine, such as albumin, thus increases risk of CKD. *Hoyer and Seiler* were able to quantify and phenotype urinary proteins [11]. From normal and healthy patient, an average of 40 to 80 mg of urinary proteins is excreted over a duration of 24 hours, from which about 30 % are albumin protein (10-15 mg). The 70% leftover protein fraction is composed of metabolic waste from plasma and from Tamm-Horsfall protein

(epithelial cells shredding from the Loop of Henle limb) [11]. Therefore, secreted albumin is a good indicator of kidney injury and dysfunction, making it a reliable maker for analysis [11].

Albumin is a protein with a molecular weight above 67 kD produced in the liver and excreted in the bloodstream and mostly retained in the serum when blood is sent to the renal nephrons [12]. However, a small but still adequate fraction of albumin is freely filtered by the glomerulus and reabsorbed in the tubule. An overload in albumin concentration retained in the renal tubule, at moderate to a higher concentration, is a key indicator of kidney injury by apparent podocyte damage and resulting to tubulointerstitial fibrosis (TIF), tubular autophagy and macrophage infiltration [13].

A normal urinary albumin excretion rate, or non-albuminuric as shown is **Table I**, is estimated at less than 30 mg/d, thus indicating a proper kidney function. An elevation in urinary albumin excretion, represented as >30 mg/d over a period of 24 hours [14], is indication of kidney injury. The increases in albuminuria also favor protein casts formation in renal tubule cells (distal convoluted tubule and collecting ducts). Albumin forming proteinuria cast in the kidney is due to environment shifting, such as a decrease in urinary flow, its pH normal value and an increase in concentrated salts allowing protein denaturation [15].

Although secreted albumin in the urine is the key feature of kidney injury, many factors can influence its degree of albumin excretion, such as, sexes and gender differences [16]. Other factors affecting renal function includes lifestyle habits modifications (e.g., intensity of physical exercise) and health conditions (e.g., fever, hematuria, pyuria, increase in blood pressure and heart failure) [16, 17]. It is also well known that reduction of urinary albumin excretion is observed at night due to the independent decreases in renal filtration pressure in the organ. The kidney function is regulated by the quantity and concentration of extracellular fluid ions, but also by the RPF and the total volume filtered per day [16, 17]. Impairments in

the renal functions decreases its ability to eliminate the waste product of body metabolisms, while increasing the risk of body toxicity and resulting in chronic kidney disease (CKD).

1.4 Chronic Kidney Disease (CKD)

The investigation of chronic kidney disease (CKD) is well established by the risk increases of global health burden and in the prevalence data factors. CKD is characterized by a gradual loss of kidney function over a period of time [18]. The renal function progression is measured and classified into 5 different stages of GFR as illustrated in **Table I** and the estimated GFR (eGFR) deterioration lower GFR measured values via glomerular malfunction. Thus, when eGFR decreases to <15 ml/min, we observe kidneys failure, and the patient is in stage 5 of CKD. ESRD patients only requires treatment is dialysis therapy to eliminate toxic metabolic waste products from the body or renal transplant. Therefore, transplantation and dialysis are the only therapies to CKD allowing the patients to have a decent life.

Moreover, infiltration of macrophages in the kidney during CKD releases various damage associated with molecular patterns and pro-inflammatory/ fibrotic cytokines [19, 20]. TNF-α (Tumor necrosis factor-a) production is achieved by various renal endothelial tissues to regulate function and blood pressure [21]. It has been shown that podocytes, mesangial cells, and the epithelial cells from the proximal tubules, thick ascending limbs and the collecting ducts but also infiltrating inflammatory cells are all sources of TNF-α production in response to hypertension, renal failure and diabetic nephropathy [22–24]. Overall, CKD by itself activates inflammatory, oxidative and fibrosis pathways increasing innate immunity macrophage activation within the kidney [25]. However, the population is adopting an unhealthy lifestyle increasing the risk of advanced-CKD via metabolic syndrome inducing hypertension, hyperglycemia and obesity phenotypes.

Table I: Identification of CKD outcomes from eGFR and albuminuria.

				Albuminuria		
				1	2	3
				Normal to mild	Moderate	Severe
				<30 mg/g	30-300 mg/g	>300 mg/g
eGFR categories (mL/min/ 1.73 m^2	1	Normal to high	>90	Low	Moderate	High
	2	Mild	60-89	Low	Moderate	High
	3a	Mild to moderate	45-59	Moderate	High	Very High
	3b	Moderate to severe	30-44	High	Very High	Very High
	4	Severe	15-29	Very High	Very High	Very High
	5	Kidney failure ESRD	<15	Very High	Very High	Very High

Table adapted from KDIGO 2012 (www.kdigo.org/clinical_practice_guidelines/ckd.php)

Metabolic syndrome (MS) is a cluster of conditions induced by hypertension, hyperglycemia and obesity and are risk factors of cardiovascular (CV) disease, stroke, and type-2 diabetes mellitus (T2DM) [10]. The American Heart Association (AHA) established that MS is identified when a person has three or more of following criteria's: an increase in obesity (waist circumference is greater than 35-40 inches in men and women), elevated level of plasma triglycerides (greater than 150 mg/dL), elevation of fasting blood glucose (70-99 mg/dL) and

of hypertension (SBP of 130 mmHg or greater, or DBP of 85 mmHg or greater) but also by the decreases of HDL cholesterol (less than 60 mg/dL) [10]. Taken together, hypertension, hyperglycemia and obesity are MS major factors contributing to renal injury if left untreated and leading to CKD progression.

Hypertension is characterized by the elevation in systemic blood pressure (BP) overwhelming vascular hemodynamics load affecting organ puncture and causing micro-injuries [26]. The increased BP enhances hemodynamic load to the vasculature, first encountered by the endothelial cell (EC) layer. The changes in the EC caused by CVD enhances the activity of various ion channels, integrins, tyrosine kinases and hormone production (including Ang II in the kidney) and growth factors [27, 28]. The hemodynamic overload in the glomerulus by the kidney afferent arteriole can leads to an overproduction of extracellular matrix, ROS generation and VSMC proliferation. These changes also promote vessels permeabilities to leukocyte infiltration and local inflammation [29]. The risk associated with hypertension in the context of renal injury is expected when CV hemodynamic load is not corrected, thus leading to chronic kidney disease and to ESRD. MS by itself doubles the risk of CV complications and triples the risk of CV mortality. Moreover, the atherosclerosis and arterial stiffness increasing hypertension represents a risk factor of renal injury. The hemodialysis (HEMO) study (1995-2001) investigated mortality and mobility of hemodialysis patients after dialysis dose delivery modifications. This study demonstrated 80% CVD complications prevalence is observed in hemodialysis patients in correlation with age, presence of diabetes and with the duration of dialysis treatment [30]. A dialysis treatment only attenuates the progression of the disease without curing it and thus increases longevity of disease progression. The addition of various external risk factors induced by MS, such as diabetes, obesity and lifestyle habits affect the renal function. Taken together, there is a close relationship between CV disease induced via MS and CKD.

Diabetes mellitus is a worldwide health burden with increased prevalence. It is estimated that by 2045, over 693 million of the worldwide population will suffer from diabetes. The consumption of exceeded daily quantities of carbohydrate lead to an unhealthy lifestyle habits and health conditions. The risks associated with CV complications related to CKD can also shifts the CKD conditions into a diabetic kidney disease (DKD) stage if the renal health conditions are compromised (e.g., insulin resistance or glucose tolerance). The maladaptive response of carbohydrate is the key feature of diabetes. DKD is caused by either type-1 (T1DM) or DKD (T2DM). DKD is a multifactorial disease, characterized by fibrotic lesions in the kidney, persistent inflammation, oxidative stress and renal microvascular injury. The high blood glucose (hyperglycemia) also promotes dyslipidemia and obesity via the accumulation of fat in adipocytes, and obesity by itself is a risk factor for MS inducing diabetes. The worldwide population is adopting an unhealthy lifestyle and because of the levels of obesity keep rising, thus increasing the risk for DKD [31].

Obesity is another cause of MS inducing CKD well characterized by the lack of physical activities and unhealthy lifestyle habits [32]. It was shown that MS caused by dyslipidemia increases by 4-fold the risk of renal injury leading to CKD. Thus, a close parallel is obtained when correlating the rise in ESRD incidence and CV risk factors with obesity. It is of crucial importance to implement the obesity factor and parameters in the presence of hypertension and diabetes for bias human renal injury reproducibility. Moreover, the estimated GFR values have a strong correlation with kidney injury when measured independently from CV complications, hypertension, and obesity parameters [30, 31]. To this end, it is also known that fat accumulation in other organs increases the risk of multifactorial and complex diseases. For instant, liver fat accumulation induces nonalcoholic fatty liver disease (NAFLD) development thus increasing the risk CKD.

1.5 Liver injury induced by obesity

The liver is an important organ with many functions, including the productions of protein like (albumin) and blood clot factors, production of triglycerides and cholesterol and the elimination of toxins by enzyme metabolism activities [33, 34]. It also plays a role in maintaining glucose level by removing excess carbohydrates from the bloodstream and storing it in glycogen form. Moreover, the liver plays an important role in fat metabolism by breaking down fat molecules and ATP degradation for cell energy [33]. However, the excess of lipid accumulation in the hepatocyte increases liver toxicity and dysregulating cell mechanisms and increases risk of liver diseases [34].

Fatty liver disease is characterized by the accumulation of lipids in hepatocytes and chronic liver disease is a risk factor contributing to NAFLD. Clinical diagnosis of NAFLD is initially established by radiological imaging techniques when ≥5% of hepatic fat accumulation is present in the liver with absence of alcohol, drugs, virus or autoimmunity factors [35, 36]. Hence, chronic fat accumulation in liver injury is a facilitating risk to induced NAFLD.

NAFLD is not age associated but is most often diagnosed in patients between the age of 40 to 60 years old and its prevalence is increased in men at 30-40% compared to 15-20% for women [37]. Most patients diagnosed with NAFLD have apparent signs of obesity, glucose intolerance or T2DM, CVD and/ or hypertension contributing to metabolic syndrome making it a multifactorial disease [35, 36]. The meta-analysis published by *Musso. G et al.* evaluated causes specific mobility and mortality liver-related disease. A 57% increase in mortality from NAFLD and CVD factors was observed and a twofold increase in incidence related to risk factors with T2DM [38]. This same meta-analysis showed that liver injury inducing NAFLD also increased by twofold the risk of CKD [38]. However, with no current treatment and liver transplantation being the only solution to mitigate the problem, NAFLD ranked on the North American chart at the top three for liver transplantation [39]. Again, liver transplantation only

attenuates the disease progression without curing the problem, thus increasing longevity of the patient.

The liver injury and its progression can now be identified by using different blood tests. The most common assay to validate liver function decline and injury is performed by alanine aminotransferase (ALT) assay. ALT is an enzyme with high expression in the liver cytosol and released in the bloodstream when the liver is injured, thus making it a reliable marker for analysis [40]. ALT level can reach up to 50 times its basal level in presence of severe liver damage [41]. To validate severity of liver damage without other organs interference, comparison with biochemistry blood work analysis such as the total protein and the albumin-to-globulin values is often performed. Moreover, the ALT test is often co-analyzed with the aspartate aminotransferase (AST) test to validate level of liver damage. AST assay is less commonly used due to its cytosolic and mitochondrial forms and its expression in various tissues such as liver, kidney, heart, skeletal muscle, brain, white and red blood cells [40]. The identification of secreted AST enzymes from the liver helps screen and diagnose liver disease [41]. A study underlying NAFLD found that 83% of patients with high ALT levels also revealed signs of steatosis and steatohepatitis from biopsy samples [42]. Taking together mild to elevated values of ALT and AST indicates liver damage and both tests are well crosslinked. However, it was shown that NAFLD, obesity and insulin resistance are common factors associated with high levels of ALT and AST [43] and lifestyle modifications can correct such abnormalities to counter liver disease progression [40].

In addition, other possible mechanisms of steatosis affecting liver function have been shown to be implicated in the synthesis of hepatic triglycerides and the decline in low density lipoprotein (LDL) synthesis [44, 45] when compared to essential high density lipoprotein (HDL). The change in cellular mechanisms is possibly due to a decrease in fatty acids oxidation or an increase in free fatty acids deliveries to the liver [46]. *Ozaki et al*. demonstrated a close

correlation between albumin mRNA significant reduction and hepatic failure despite the presence of other mechanisms of albumin production, suggesting that albumin main site of production is regulated in the liver [47]. Hence, steatosis induced in the liver changes instinct mechanisms have not yet well been established. To also validates liver damage, biopsy samples identified steatosis, sign of hepatocytes apoptosis and inflammation throughout the organ. The biopsy samples are analyzed by colorimetric staining before giving corresponding pathology results. A biopsy from an NAFLD liver revealed visual appearance of liver mild to severe deterioration due to injury when compared to a healthy specimen [47].

1.6 Current treatment

The treatment for hypertension and hyperglycemia inducing-CKD currently available mainly triggers the control of glycemia and blood pressure from a recurrent to a continuous pharmacology drug usage, without curing the underlying disease [48]. While these therapeutic drug treatments may prove to be beneficial, simply targeting hypertension and glucose may not be enough to prevent renal injuries. Therefore, additional strategies are needed to treat this multifactorial and complex disease.

As the main key causes of CKD are diabetes and hypertension, treatments for patients with CKD includes designing drugs to control glycemia and BP. Regarding BP, uncontrolled parameters can have serious consequences on the kidneys' ability to regulates electrolyte and fluid handling, which ultimately promotes hypertension through volume expansion and increased vascular stress, leading to CVD and renal problems. The renin-angiotensin-aldosterone system (RAAS) pathway is a major player in this regard [49, 50]. Thus, the current first line of BP lowering agents includes angiotensin-converting enzyme inhibitors (ACEi), angiotensin type 1 receptor blockers (ARB) and renin inhibitors are effective in lowering albuminuria in hypertensive patients with concomitant ACR values of 200 mg/g [51]. These treatments are often combined with additional drugs, such as beta-blockers, calcium channel

blockers and vasodilators to achieve ideal BP, usually below 130 mmHg systolic and 80 mmHg diastolic. A proper BP control translates to a reduction in renal injury in patients with diabetic nephropathy (DN) [51]. However, these drugs can only slow disease progression and do not completely attenuate it. In addition, these drugs may lead to hypotension if higher concentration are used [51]. Therefore, the search remains for the quest of effective DN therapies which are BP-independent.

Diabetes is a disorder in which circulating plasma glucose levels are increased due to either: an incapacity of pancreatic beta cells to produce endogenous insulin (T1DM) or caused by insulin resistance (T2DM) to take up extracellular glucose and metabolize it into energy [52]. The cause of T1DM still remains unknown, however the combination of genetics with environmental factors both play majors fundamentals roles. However, patients diagnosed with T1DM require continuous blood glucose monitoring (continuous control of glycated hemoglobin HbA1C) and the use of human synthetic insulin to maintain proper health. Moreover, the current treatment of T2DM includes the use of biguanides, thiazolidinediones and sulfonylureas [53, 54]. These drugs lower liver glucose production, enhances tissue glucose reuptake, and stimulates pancreatic insulin secretion. Moreover, these drugs are effectives to restore blood glucose levels to a normal range, found between 80-110 mg/dL or 4.5-6.0 mM limiting CVD and CKD progressions [54]. Since then, many drugs' findings for hypertension and hyperglycemia monitoring have been investigated, however the renal ability to reabsorbed glucose play in important role.

Recently, a new class of antiglycemic drugs, 'flozins' have emerged as promising new therapies for DKD patients. These drugs act by inhibiting sodium glucose transporter 2, blocking glucose reabsorption along the renal proximal tubule, and promotes glucose elimination in the urine [48]. While these treatments may prove to be beneficial, simply targeting glucose may not be enough to prevent renal injury in the context of that disease.

Hyperglycemic patients are in glomerular hyperfiltration due to excess of glucose and sodium reabsorption in the proximal tubule, thus increasing systematically GFR from the TGF system. Moreover, hyperfiltration increasing GFR induced glomerular damage, accelerating cells ER and oxidative stress, inflammation and mesangial cells proliferation and fibrosis. These drugs only attenuate plasma glucose but cannot remediates to decreasing GFR by the TGF response. From the Flozin family, Canagliflozin (Cana) developed by Janssen pharmaceuticals (Johnson and Johnson) is of high therapeutic interests. Cana has shown promising therapeutic effects to reduce renal injury and impact macrophage infiltration in mouse models of obesity [55]. Like all other Flozin drugs, Cana mode of action acts on blocking the sodium-glucose cotransporter 2 (SGLT-2) [48].

The SGLT-2 receptors are located at the proximal tubule and are hyperactivated in the presences of high glucose environment, allowing sodium and glucose reabsorption from the apical side to the basolateral [56]. The SGLT-2 cotransporter by itself is responsible for 90% of glucose reabsorption in the renal proximal tubule, thus leading glucose plasma concentration to increase at a higher level when the cotransporter is shifted from normal to hyperactivated. *Moses et al*. review article underlined the concept that normal renal glucose reabsorption is 180 mg/dL of plasma. In a T2DM patient, glucose reabsorption threshold is up regulated by SGLT-2 maladaptive response [57], thus underlying the importance of the receptor inhibition in hyperglycemic patients. In hyperglycemic conditions, the hyperactivation of the receptor is increased by both glucose and sodium reabsorption and impairing the TGF system. The reduction in Na^+ delivery in the MD leads to a TGF maladaptive response, thus increasing renal perfusion by inadequate arterial hemodynamic tone [58, 59] and leading to glomerular hyperfiltration. Inhibition of the SGLT-2 cotransporter increases Na^+ delivery to the macula densa and restores TGF and reduce glomerular hypertension [60]. The changes result in plasma

flow and hyperfiltration reduction [59]. Hence, glucose and sodium aren't reabsorbed by the SGLT-2 receptor along the proximal tubule, leading to urine glucose increase (glycosuria).

In 2014, the canagliflozin and renal endpoints in diabetes with established nephropathy clinical evaluation (CREDENCE) human clinical trial evaluated the effect of Cana and renal outcomes in T2DM [61, 62]. This study consisted of a pretreatment phase and a double-blinded treatment phase that lasted up to 66 months randomized in a 1:1 Cana to placebo ratio and with approximately 4,200 participants. During pretreatment, all participants received a specific diet and exercise for assessing their blood pressure and lipid and evaluating the CV risks. Hence, the CREDENCE study lasted 5.5 years and provided primary composite outcomes that favor Cana. All participants on Cana showed a reduction in ESRD, a delay to initiate dialysis or kidney transplantation and therefore a decrease in renal death. Also, Cana showed excellent outcomes in reducing CV death or hospitalization for health failure and stroke [60]. Taken together, Cana provides positive outcomes from the CREDENCE study [61, 62]. Patients taking Cana experience an increase of glycosuria and natriuresis from the sodium and glucose inhibition drug action on the SGLT-2 cotransporter.

1.7 Animal model of metabolic syndrome induced CKD

To study CKD and its pathophysiological progression, various tools are needed. These include *in vitro* cell culture systems or characterization of the disease process *in vivo* in murine models of CKD. The use of rodent models for modulation DN disease progression has been refined over the years and the replication and time efficiency of disease progression on rodents have been shown to occur more rapidly. The studies on diabetic mice showed to induce renal injury after approximately 20 to 26 weeks of age [63, 64]. Hence, mice models are useful tools to study therapeutic, pharmacological, and molecular pathways involved in the progression of complex disease, when compared to human clinical studies for primary results.

The current animal models of obesity in research have showed to replicate human obesity progression by specific mutation, such as the monogenic mutation in the leptin pathway (ob/ob mouse have a leptin deficiency, db/db mouse have a leptin receptor deficiency or Zucker rats have mutated leptin receptor) [65, 66]. Moreover, dyslipidemia can be induced on animal models by the exposures of obesogenic environments, such as being maintained on high-fat diet for long periods of time [67]. In addition, the increase in obesity in the animal is also shown to induce hyperphagia and the changes in metabolism energy favoring significant body weight increase.

Even though mouse models are widely used, most mouse models of CKD do not fully recapitulate human disease progression and only a limited number of available models meet the Animal Models of Diabetic Complications Consortium (AMDCC) criteria's [67]. The AMDCC stipulates that a 50% decline in GFR, a 10-fold increase in albuminuria compared to age and gender-matched healthy controls, a 50% increase in glomerular mesangial matrix, hyalinosis of the arterioles, a 25% thickening of the GBM and the presence TIF are all characteristics that should be display in an adequate murine model of DN [68]. Since most current murine models of DN do not fully recapitulate all these criteria's, this field of research area remained yet quite active. Currently, great efforts are undertaken to generates a rodent model of CKD which meets all AMDCC criteria [68].

Rodent models of T1DM, where mice are either born or rendered hypo-insulinemic, include intraperitoneal injections of alloxan or β-cell toxin streptozotocin (STZ) or through, β-cell specific overexpression respectively in OVE26 and Akita models [69–71]. T2DM rodent models are typically obtained by rendering these animals obese using a HFD, or by disrupting the satiety hormone leptin via mutations within the leptin gene (ob/ob mice), or leptin receptor (db/db mice, Zucker rats). While the above models display abnormalities associated with early DN, such as albuminuria, renal hypertrophy, and glomerular scarring, they fail to develop late

features related to human disease, including declining GFR and arteriolar hyalinosis [72]. The differences found in the severity of renal injury observed in rodent models may explains why some treatments are effective in experimental animal models but fail to replicate the effects of human diseases in trials.

Several factors must be taken into consideration when choosing to study a specific mouse model to another one [63]. Of these, the susceptibility imparted by the strain of rodent chosen and whether the model develops hypertension or not are major requirements [63, 73]. In mice, it is well established that obese and hyperglycemic type-2 diabetic db/db mice develop substantially more renal injury when bred onto an FVB/n background, compared to the C57BL/6J mouse strain. Hence, T1DM OVE26 mice bred onto the susceptible FVB/n background demonstrated glomerulosclerosis and albuminuria [63, 73]. Finally, hypertension is not observed in murine DN models. The RAAS-activation through either exogenously or endogenously enhanced renin-dependent Ang II production has also provided hypertension increase onto a diabetic phenotype [74]. One example, the TTRhRen mice developed by Dr. Reudelhuber at the Montreal Research Clinical Institute, expresses a modified human pro-renin gene specifically expressed in the liver which leads to an overproduction of active renin and thus promotes Ang II- dependent on hypertension [75].

The current mouse models of advanced-CKD do not fully mimic human renal disease and cellular mechanisms dysfunctions. It was found that pro-renin has a direct correlation with microvascular disease and nephropathy in patients with common diabetes [76]. From this knowledge, *Thibodeau et al*. previously generated a novel mouse model of advanced CKD by superimposing type-1 diabetes with genetic RAAS dependent hypertension [67] on the TTRhRen mouse model. This transgenic mouse model is genetically hypertensive by the expression of a human pro-renin cDNA under the control of a 3-Kb region of the transthyretin gene promoter (also called LinA3+ mice) in the liver. Pro-renin is the precursor of renin, a

surge in renin promotes systemic hypertensive and thus renal hypertension through the RAAS pathway activation dependent [76]. This model also showed signs of glomerular sclerosis and significant albuminuria 20 weeks post T1DM induction via STZ pancreatic beta cells death when compared to their TTRhRen littermates, normal db/db diabetes mice and wildtype mice groups. Taken together, the disease progression showed that hypertension and hyperglycemia combination are the leading cause of CKD and development of renal dysfunction takes time. The strategy of combining hypertension with hyperglycemia resulted in a model of CKD, however lacking an important characteristic of human CKD, the presence of dyslipidemia via fat accumulation for cellular mechanisms shifting toward a hypertensive model genetically activated by the RAAS system.

1.8 Rationale

Hypertension, hyperglycemia, and obesity are hallmarks contributing to MS inducing renal injury and thus leading causes to CKD. To study MS associated with CKD in humans, multiple rodent models have previously been used. Of which, *Glastras et al*. identified renal outcomes when comparing T1DM (via low dose STZ, 55 mg/Kg body weight daily intraperitoneal, for 5 consecutive days) and obesity phenotypes inducing-MS on C57BL/6J male mice [77]. The results obtained from their study demonstrated that glucose and HFD surge to the kidney significantly increase urinary ACR and serum creatinine level, with apparent sign of TIF visible by Periodic Acid Schiff (PAS) staining at 30 weeks of age compared to regular chow-fed mice [77]. However, this study was missing an important characteristic of human MS inducing advanced-CKD, the presence of hypertension. Moreover, *Touyz et al*. previously established the TTRhRen mice model with distinct phenotypes of elevated systemic chronic hypertension by the RAAS system activation through the insertion of a liver specific human pro-renin transgene [75]. Furthermore, *Thibodeau et al*. established a novel mouse model displaying genetic hypertension using the TTRhRen mice model and superimposing T1DM by low-dose STZ [78]. The combination of hyperglycemia and hypertension led to induced CKD by the development of glomerulosclerosis and significant albuminuria at 20-weeks post streptozotocin injections [67]. However, the generation of a mouse model with distinct features of disease takes time and this previous mouse model lacked an important characteristic, dyslipidemia. In the current study, we first aimed to obtain a novel mouse model of metabolic syndrome induced CKD mimicking human disease with hyperglycemia and dyslipidemia phenotypes combination in the TTRhRen mouse and have disease proliferation time frame shortened in animals of 20 weeks of age. We also aimed to validate other potential chronic organ injury caused by MS induced via hypertension, hyperglycemia and dyslipidemia.

Furthermore, the CREDENCE human clinical trial revealed beneficial effects of Cana usage in T2DM patients with distinct renal injury, such as the reduction in ESRD, a delay to initiate dialysis or kidney transplantation, reducing CV death or hospitalization for health failure and stroke [60]. Patients taking Cana resulted in an increase of glycosuria and natriuresis from the effect of Cana on the SGLT-2 transporter after couples' weeks of treatment [60–62]. These observations found correlates with recent findings suggesting that Cana is a reno-protective anti-glycemic therapeutic drug. To this end, we aimed to validate the SGLT-2 inhibitor effect on the sodium and glucose reabsorption in the kidney proximal tubule in hypertensive/T1DM mice model within 3 weeks of treatment.

1.9 Purpose

The purpose of this study is to generate a novel model of metabolic syndrome inducing CKD, with apparent phenotypes of hypertension, hyperglycemia and dyslipidemia and characterize Canagliflozin treatment on renal damage.

1.10 Hypothesis

The two hypotheses of this study are:

A) The superimposition of dyslipidemia phenotype on the previously generated genetically-hypertensive/ type-1 diabetic mouse model would mimic features of human metabolic syndrome.
B) The SGLT-2 inhibitor (Canagliflozin) treatment will be beneficial for the LinSTZ mouse model by blocking the reabsorption of glucose and sodium in the proximal tubule.

1.11 Objectives

Objective 1: Establish and characterize a novel mouse model of metabolic syndrome inducing-CKD by combining the genetically-hypertensive/type-1 diabetic with a high fat regimen.

1) Generating genetically liver specific human renin hypertensive male mice and WT littermates.
2) Induce T1DM via pancreatic beta cells death at 8 weeks of age.
3) Feed a 60% kCal HFD regimen to induce dyslipidemia for 8 consecutive weeks.
4) Measuring in mice physiological parameters, such as, systolic blood pressure, fasted blood glucose or urine volume.
5) Quantify the level of kidney injury in the different groups.

*This animal study timeline (**Figure 1A**) illustrates mice allocation in 4 groups (**Table II**) according to baseline systolic blood pressure and hyperglycemia.*

Objective 2: Quantify the level of other organ damage (liver injury) in the novel mouse model of metabolic syndrome inducing-CKD.

1) Examine the liver injury from collected tissue.
2) Quantify the activity of liver function via enzymatic assay.

A |

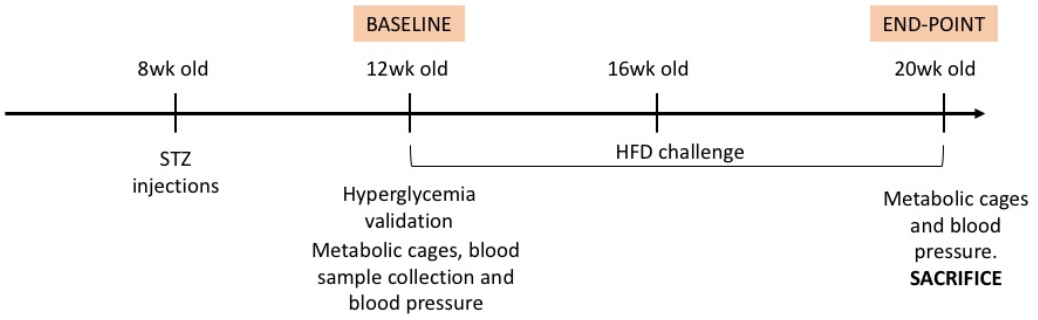

B |

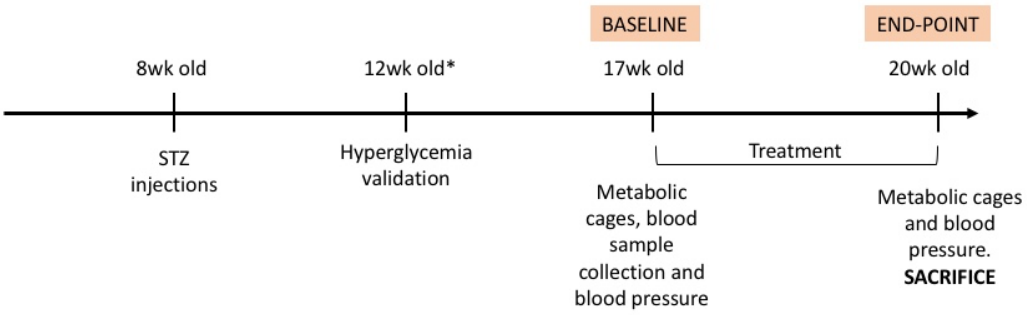

* Waited 4 more weeks for disease progression in model and reproducibility from previous study (LinSTZHFD)

Figure 1 **| Mice study timelines.**
A) Study timeline illustrating a novel model of MS inducing-CKD via hypertension (TTRhRen mice), hyperglycemia and fat accumulation phenotypes. B) Study timeline illustrating Canagliflozin treatment on the TTRhRen mice with distinct hyperglycemia phenotypes.

Objective 3: Determine if fat accumulation inducing hepatocyte injury affects the liver human renin transgene.

1) Generate custom pair oligonucleotide primers for human and mouse renin.
2) Isolate RNA from snap-freeze liver and kidney samples.
3) Quantify human and mouse renin samples.

Objective 4: Compare the effects of SGLT-2 inhibitor (Canagliflozin) treatment on renal injury in the LinSTZ mouse model.

1) Induce T1DM via pancreatic beta cells death at 8 weeks of age and let hypertension and hyperglycemia phenotype disease progress in animals.

2) Treat mice with a dose of 30 mg/Kg.BW dose Canagliflozin compound for a duration of 3 weeks, at 17 weeks of age.
3) Measure in mice physiological parameters, such as, systolic blood pressure, fasted blood glucose or urine volume from treated and vehicle group
4) Quantify the level of kidney protection by drug.

*This animal study timeline (**Figure 1B**) illustrates mice allocation in 2 groups (**Table II**) according to baseline systolic blood pressure and hyperglycemia.*

Table II: Mice allocation in groups according to hypertension and hyperglycemia values.

Study A: Novel model of MS inducing-CKD via hypertension (TTRhRen mice), hyperglycemia and obesity.				
Group	**Genotype**	**Challenges**		**Number of mice (n =)**
1	WT	Saline	Regular diet	8
2	WT	Saline	HFD	8
3	LinA3+	STZ	Regular diet	9
4	LinA3+	STZ	HFD	23*

Study B: Canagliflozin treatment on the TTRhRen mice with distinct hypertension/ hyperglycemia phenotypes.					
Group	**Genotype**	**Challenges**		**Treatment**	**Number of mice (n =)**
1	LinA3+	STZ	Regular diet	Vehicle	8
2	LinA3+	STZ	Regular diet	Canagliflozin	8

** N number elevated due to sub-division into subgroups for treatments with drugs. However, this milestone did not happen due restriction with the animal care facility.*

Animals

Hypertensive TTRhRen (or also named LinA3+) mice have been previously described according to the literature [79, 80]. Briefly, liver-specific expression of a modified human pro-renin cDNA transgene was achieved under the control of a 3-Kb region of the mouse transthyretin promoter. The synthesis of active human renin was optimized by introducing a furin cleavage site between the pro and active segments of the human renin transgene. Cleavage of the pro segment from the renin transgene occurs by the ubiquitously expressed furin enzyme in cells expressing this construct. Hyperreninemic LinA3+ mice on an FVB/n background display elevated systolic blood pressure (140-150 mmHg) and develop cardiac hypertrophy by 4 months of age [80] that may be attenuated by ACE inhibition or ARBs [75, 79, 80]. Hypertensive LinA3+ mice do not display a renal hypertrophy phenotype.

Briefly, 8-10 weeks-old LinA3+ and their wildtype (WT) littermate male mice on a FVB/n background were subjected to 5-day intraperitoneal (i.p.) injections of STZ (50mg $kg^{-1}BW^{-1}$; Sigma-Aldrich, Oakville, ON.) or 0.1 M Na-citrate buffer pH 4.5 as vehicles respectively to induce hyperglycemia via pancreatic beta cell death [81–83]. After 4 weeks post-STZ injection, mice were allocated in corresponding groups and fed either a regular diet (10% kilocaloric (kCal); Teklad, Mississauga, ON.) or a high-fat diet (HFD; 60% kCal; Teklad, Mississauga, ON.) for 8 weeks for body weight gain [84, 85].

All mice were subjected to baseline and endpoint metabolic cages. Food consumption, water intake and urine output were measured at 24 hours metabolic cages for baseline and after 12 hours for endpoint. Values of 12 hours metabolic cages were extrapolated to obtain 24 hours values comparisons.

Mice were administered Canagliflozin at 30 mg/kg body weight dose suspended in vehicle solution containing 0.5% w/v methylcellulose in saline solution with 0.025% v/v Tween-20

[86]. The Cana drug was administered by daily gavage at 8:00 AM for a duration of three (3) weeks before sacrifice. Mice had *Ad libitum* access to food and water before and after the procedure. Dehydrated signs in the hypertension/ hyperglycemic mice were supplemented with i.p. saline solution and with heat pad for up to 8 hours at the time.

Experimental animals (male, 8-20 weeks) were housed and carried at the Animal Care Facility at the University of Ottawa with free access to food and water. Protocols were approved by the University of Ottawa Animal Care Committee (CMM – 2209) and conducted according to the guidelines of the Canadian Council on Animal Care.

KIDNEY INJURY ANALYSIS

Blood pressure measurement

Systolic, diastolic and pulse reading were measured by tail-cuff plethysmography (BP 2000, Visitech systems, Apex, NC) throughout the study [67]. Mice were trained for 5 consecutive days at 11 weeks of age (5 preliminary readings, 10 actual readings/ day). Later BP measurement in the study was obtained within 2 consecutive days on 12- and 20-weeks old mice. False results from unread blood pressure instrument and outliers measured according to the average +/- two-times standard deviation of sample were removed from data analysis to obtained sample average.

Physiological data

Baseline blood samples were collected by saphenous vein bleed into heparinized capillaries (Fisher Scientific, Pittsburgh PA). The capillaries were centrifuged 5000 g for 10 minutes at 4°C to measure hematocrit fraction before sampling plasma and place immediately -80°C until

subsequent analysis. Sacrifice blood samples were collected via cardiac puncture into heparinized syringes, kept on ice and centrifuged at 5000 g for 10 minutes at 4°C. Collected plasma was immediately frozen at -80°C until subsequent analysis. Plasma glucose levels were determined by glucometry (Nova StatStrip Xpress Glucose CR Meter. Nova Biomedical, Waltham, MA).

At sacrifice, kidneys were removed, individually weighted and normalized to tibia length. The right kidneys were cut sagittal. A section of the right kidney and white adipose tissue (WAT) were placed in 4% paraformaldehyde fixation solution for 24 hours, transferred to 70% ethanol before embedded in paraffin. The other sagittal right kidney sections were placed in 30% sucrose for 24 hours and embedded in the OCT frozen section compound. The left kidneys and WAT were snap-freezed for protein and quantitative PCR (qPCR) analysis.

Biochemistry analysis

Plasma and urine biochemistry values were measured according to Cres17 (sodium, chloride, total protein, albumin, globulin, creatinine, glucose, cholesterol, triglycerides) and Cres18 (urine sodium, urine chloride, urine total protein, urine urea nitrogen, urine creatinine, urine glucose) respectively test type from IDEXX inc. (IDEXX, Westbrook, Maine). Briefly, 180 ul of plasma and 300 ul of urine volume per sample were sent to IDEXX to measure general biochemistry composition from each group. The values of the urine obtained for biochemistry were standardized for the 24 hours urine output.

Albuminuria

Albuminuria was measured using the Mouse Albumin Elisa Kit (Bethyl labs, Montgomery, TX.) following manufacturer's protocol and measured A_{450} nm wavelength spectrophotometry (FLUOstar Galaxy. BMG LABTECH, Cary, NC). Albumin levels were determined by

normalizing to creatinine concentration, determined by high pressure liquid chromatography (HPLC) creatinine area under the curve (AUC) concentration quantification by fluorescence detection and with the polar bonded-phase 300-SCX ZORBAX narrow-bone 5-micron column (Agilent Technologies 1100 series, Santa Clara, CA) with 15 mM sodium acetate, 40% methanol and 10% acetonitrile (pH 4.2) for creatinine migration into column [5].

Insulin test

Baseline plasma insulin level was measured using Ultra-Sensitive Mouse insulin Elisa kit (Crystal Chem, Elk Grove Village, IL) following manufacturer's protocol. Plate was measured using the spectrophotometry (FLUOstar Galaxy. BMG LABTECH, Cary, NC). Insulin concentration was measured by subtracting A_{630} to A_{450} nm and interpolated using the standard curve.

Histology and α-SMA immunohistochemistry

At sacrifice, mice were anesthetized under isoflurane and kidneys were excised, dissected and immediately fixed in 4% paraformaldehyde (PFA). PFA Paraffin-embedded kidney sections (3 μm), liver (4μm) and WAT (4 μm) were obtained and stained with periodic-acid Schiff (PAS) or Masson's Trichrome reagent [67, 77]. All sectioning, paraffin embedding, and staining were performed by the University of Ottawa's Department of Pathology. The sections were viewed using a light microscope at either 200X or 400X magnification (Axioskop 2 Imager A1, Zeiss, Germany). Kidney glomerular (20-25 glomeruli/ mice) were analyzed using imaging software (Axiovision v4.8, Carl Zeiss, Germany) was used to calculate relative mesangial matrix/ glomerular area, whereby the area of the mesangial scar as a percentage of total glomerular area was determined. Visual degree of kidney and liver damage was scored using the following

qualitative scale: 0 - no damage in tissue, 1 - minimal, 2 - mild, 3 - moderated, 4 - marked and 5 - severed damage and injury. A total of (20-30) representative visual areas were analyzed in a blinded manner for each group.

Kidney and liver α-smooth muscle actin (α-SMA; Santa Cruz Biotechnology, Dallas, TX.) immunofluorescence was performed on paraffin-embedded sections mounted on glass slides. Sections were deparaffinized in mixed xylenes (Fisher Scientific, Pittsburgh, PA.), and rehydrated through a gradient of ethanol and distilled water. Sections were washed 3x in PBS, boiled for 20 minutes in 0.1 M Na-citrate buffer (pH 9.0) for antigen unmasking. Sections were blocked in PBS containing 10% donkey serum/ 1% BSA for 1 hour and incubated with mouse anti-α-smooth muscle actin (1:200) overnight at 4°C. Slides were washed and treated with a FITC-labelled donkey anti-mouse secondary antibody (1:1000; Molecular Probes, Burlington, ON.) for 1 hour, followed by 4,6-diamidino-2-phenylindole (DAPI; Sigma-Aldrich, Oakville, ON.) for nuclear localization. Sections were covered with fluorescent mounting medium (Vector laboratories, Burlington, ON.) and coverslips. Immunofluorescence sections were visualized under fluorescence microscopy at 400X magnification, whereby representative cortical profiles from each group were obtained in a blinded manner.

Quantitative Real-Time RT-PCR

Quantification of the human pro-renin liver specific transgene superimpose into the LinSTZ mice model and SGLT-2, tumor necrosis factor alpha (TNF-α) expressions was assayed to the wildtype (WT) littermates. Briefly, snap-freeze liver and kidney tissues collected at sacrifice from each group and RNA were isolated using QIAGen RNEasy Minikit with DNase treatment kit manufacturer's kit protocols (QIAGen, Toronto, ON.). Quantification of isolated RNA was performed using the Epoch Spectrophotometer with Take3 Micro-Volume Plate (BioTek,

Winooski, VT.) as described by the manufacturer. RNA analysis was undergone using Gen5 software (Version 2.09) (BioTek, Winooski, VT.) calibrated for RNA quantification. Extracted RNA was converted to cDNA using the High-Capacity cDNA Reverse Transcription kit (Applied Biosystems, Foster City, CA.) with 500 ng starting material per reaction before performing Real-Time RT-PCR. Reactions were carried using SYBR Advantage qPCR Premix (Clontech Laboratories, CA, USA) on an ABI Prism 7000 Fast Sequence Detection System (Applied Biosystem) and with corresponding pairs of primers found in **Table III**. Briefly, human renin (hRen) and mouse renin (mRen) primers were normalized to control mouse gene GAPDH, and the mouse SGLT-2 and TNF-alpha genes was normalized to the 18S control gene. The comparative threshold cycle method was used for data analyses. All samples were assayed in duplicate. Relative expressions were analyzed to the $2^{-\Delta\Delta}$CT qPCR threshold. A relative quantification was performed for each receptor and results are expressed as fold change control.

Isolation and stimulation of bone marrow-derived macrophages (BMM)

Mouse femurs and tibias were cleaned from muscles before centrifuges at 13 000 rpm to isolate fresh bone marrow. The bone marrow isolation was suspended into a warm RPMI 1640 lymphocyte medium containing 10% newborn calf serum and 1% Penicillin/Streptomycin, counted to. The cell suspension was seeded at 2 x 10^6 cells per well final concentration in BMM media containing lymphocyte medium supplemented with 10 ng/ml of macrophage colony-stimulating factor (ProSpec, East Brunswick NJ)), incubated at 37°C with a 5% CO_2/ 95% O_2 ratio. Media change was performed every other day and up to 7 days to differentiate monocytes into mature macrophages.

The macrophages polarization into M1 macrophages type was activated with 100 ng/ml lipopolysaccharides (LPS) (Sigma Aldrich, Oakville, ON, Canada) for 24 hours prior to RNA

isolation. A total of 500ng of RNA material was converted into complementary DNA and diluted 1:10 before undergoing mouse SGLT-2 quantification by qPCR as previously described. The results were normalized to the 18S control gene. All samples were assayed in duplicate. Relative expression was analyzed by the $2^{-\Delta\Delta}$CT method. A relative quantification was performed for each receptor and results are expressed as fold change control.

Table III: Primer sequence for qPCR with Tm values.

Product name	**Size (bp)**	**Primer sequences (DNA)**	**Tm value (°C)**
human Renin (hRen)	161	**Sense:** 5' -aagtgcagccgtctctacac- 3'	58
		Anti-sense: 5' -gtgattccacccacggtgat- 3'	
mouse Renin (mRen)	184	**Sense:** 5' -gcaccgctacctttgaacga- 3'	58
		Anti-sense: 5' -ccgtagtactgggtattcaggt- 3'	
mouse SGLT-2 (mSGLT-2)	72	**Sense:** 5' -gctggatttgagtggaattgc- 3'	60
		Anti-sense: 5' -cggtcagatacactggcaca- 3'	
mouse TNF-α (mTNF-α)	102	**Sense:** 5' -ccaccacgctcttctgtctac- 3'	60
		Anti-sense: 5' -agggtctgggccatagaact- 3'	
mouse GAPDH	151	**Sense:** 5' -actccactcacggcaaattc- 3'	58
		Anti-sense: 5' -tctccatggtggtgaagaca- 3'	
mouse 18S	61	**Sense:** 5' -atggtagtcgccgtgcctac- 3'	60
		Anti-sense: 5' -ccggaatcgaaccctgatt- 3'	

LIVER INJURY ANALYSIS

ALT and AST Elisa assay

Liver function was measured using the alanine aminotransferase (ALT) and liver damage was measured using aspartate aminotransferase (AST) according to the Elisa kits and following the manufacturer's protocol on sacrifice's plasma samples from each group.

Angiotensin II Elisa assay

Angiotensin II in plasma samples was measured using the Angiotensin II Elisa Kit (Enzo, Cedarlane distributor, Burlington, ON.) following manufacturer's protocol and measured A_{450} nm wavelength spectrophotometry (FLUOstar Galaxy. BMG LABTECH, Cary, NC).

Statistics

GraphPad Prism (Version 7.0a) was used to present the data and perform statistical analysis (Graphpad Prism, San Diego, Ca.). Values are expressed as means $\pm$ standard error of the means (SEM). Statistical analysis for one group variable was done using unpaired t-test with parametric Gaussian distribution test. Multiple groups analysis was statistically analyzed by ANOVA and multiple comparison corrected with Bonferroni's post test. A p-value < 0.05 with $n \geq 3$ was considered statistically significant.

3.1 Establish a novel model of metabolic syndrome inducing-CKD by combining the genetically-hypertensive/ type-1 diabetic phenotypes with a high fat regimen.

Hypertension, hyperglycemia and dyslipidemia are hallmarks of metabolic syndrome and if left untreated, can lead to CKD [87]. In order to determine whether superimposing obesity/ dyslipidemia onto the hypertensive/ T1DM phenotype present in LinSTZ mice would lead to a model of metabolic syndrome induced kidney injury that mimic human disease, we performed the following study. To this end, wildtype (WT) or LinSTZ mice were fed either a regular or HFD as illustrated in **Table II** and LinA3+ mice were rendered hyperglycemic via a low-dose streptozotocin challenge (50 mg/kg BW i.p. for 5 consecutive days) [69]. The obtained 4 subgroups from this study is WT mice non hyperglycemic on a regular diet (WT + Reg), WT mice non hyperglycemic induced obesity (WT + HFD), genetically hypertensive mice with hyperglycemia phenotype on a regular diet (LinSTZ + Reg) and genetically hypertensive mice induced T1DM and obesity (LinSTZ + HFD).

3.1.1 LinSTZ mice have elevated systolic blood pressure, blood glucose and confirmed obesity.

LinA3+ mice have induced hyperglycemia via pancreatic beta cell deaths with streptozotocin (STZ) cellular toxicity. At four weeks post STZ-injections (baseline), the blood glucose was measured in mice after 4 hours of nutritional food fasting and using a glucometer. A fasting blood glucose level exceeding 15 mmol/L is characterized as hyperglycemia. An increase in fasting blood glucose level was observed in the LinSTZ group compared to their WT littermates receiving only sodium citrate buffer as vehicle (**Figure 2A**). Accordingly, STZ led to reduced fasting insulin levels in LinSTZ mice, confirming beta cells injury-mediated hyperglycemia (**Figure 2B**). Blood glucose levels remained elevated and unaffected in both regular and HFD fed LinSTZ mice at endpoint (**Figure 2C**).

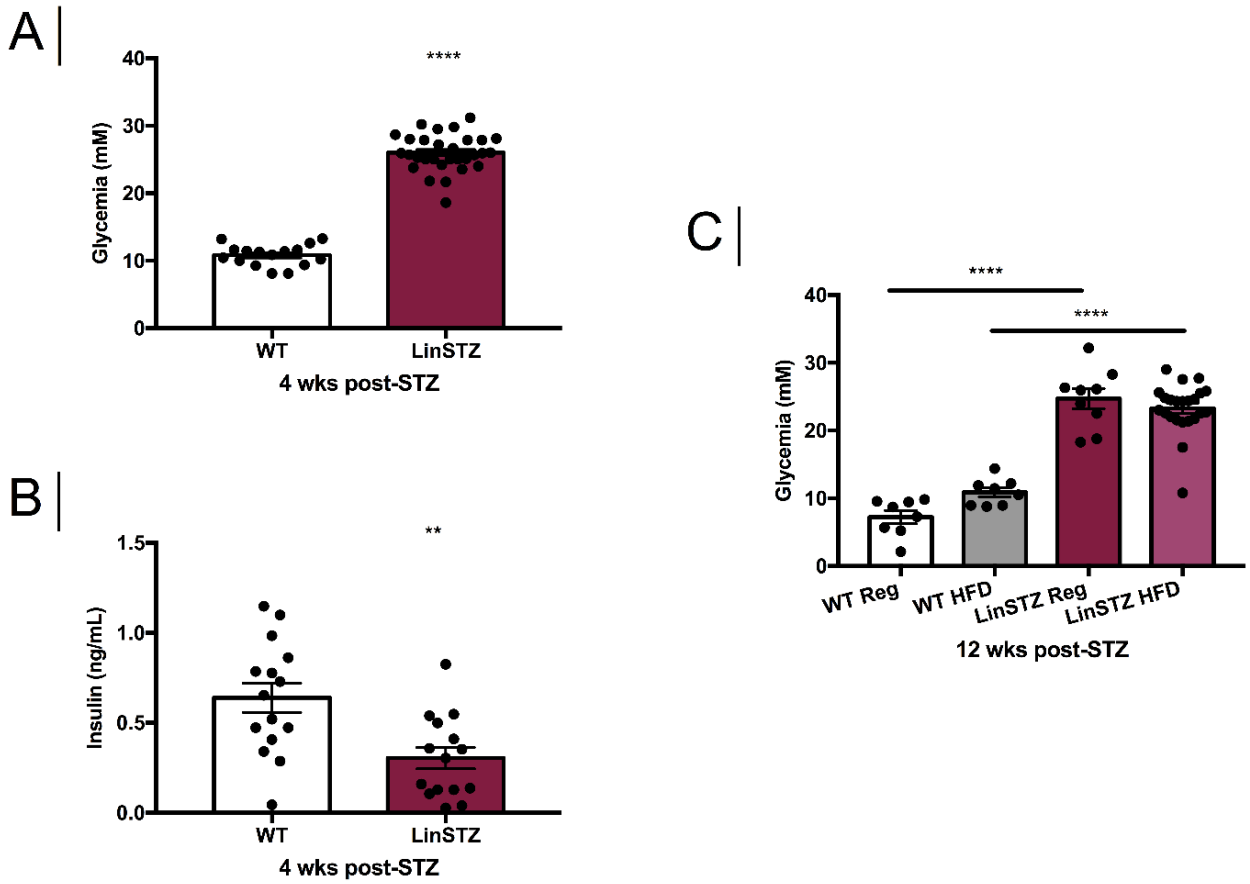

Figure 2 | Hyperglycemia and hypoinsulinemia is observed in LinSTZ mice.
A) Baseline fasted blood glucose is higher in LinSTZ. B) Plasma insulin is decreased in LinSTZ mice at 12 weeks of age. C) Endpoint blood glucose remained elevated in LinSTZ mice. The high blood glucose was induced in fasted mice through five consecutive daily low-dose STZ intraperitoneal injections (50 mg/kg BW/ day). Blood glucose results were obtained using glucometer via saphenous vein from 4 hours fasted mice. Data expressed as means ± SEM, A) unpaired t test, ****p<0.0001 B) unpaired t test, **p<0.001 C) ANOVA, ****p<0.0001

Hypertension leads to systemic and renal vascular injury and is the second leading cause of end-stage renal disease [88]. LinA3+ mice are hypertensive at birth, due to sustained increased renin-angiotensin system activity [67]. Using tail-cuff plethysmography-based systolic blood pressure measurements, we confirmed that systolic blood pressure (SBP) was higher in genetically hypertensive LinA3+ mice, given STZ (LinSTZ), at baseline (**Figure 3A**) compared to WT littermates, as expected. Moreover, the SBP remained elevated in LinSTZ mice fed a regular diet throughout the study. Unexpectedly, HFD-feeding reduced SBP in LinSTZ mice (**Figure 3B**), which was statistically significant at several time points. Whether the HFD-induced decrease in SBP would translate into decreased renal injury remains to be confirmed.

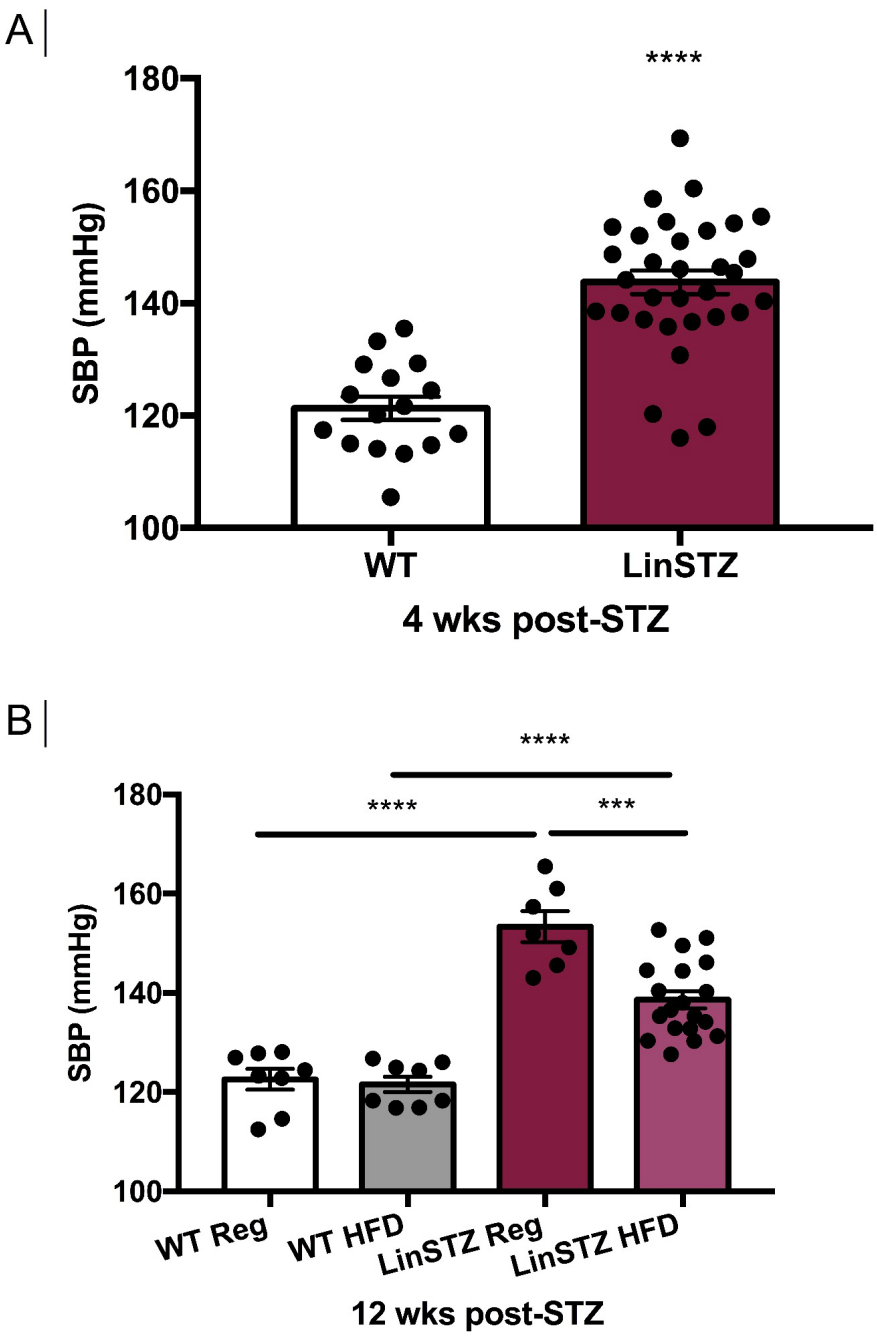

Figure 3 | Systolic blood pressure taken from WT and LinSTZ mice given a 60% kCal high fat diet (HFD).

A) High systolic blood pressure was confirmed at baseline. B) HFD shows a trend improving systolic blood pressure in LinSTZ after 8 weeks. Blood pressure was measured by tail-cuff plethysmography over 2 consecutive days with 5 preliminary readings and 10 actual readings per day. False results and outliers were removed from data analysis. Results represent mice aged from 12 (baseline) to 20 (endpoint) weeks of age. Data expressed as means ± SEM, A) unpaired t test, ****p<0.0001 B) ANOVA, ***p<0.001 or ****p<0.0001

Body weight was measured throughout the study to evaluate the effect of HFD feeding on obesity. Baseline (prior to HFD) body weight was taken as the first standardized measure. The genetically hypertensive LinA3+ mice were leaner than their WT littermates (**Figure 4A**). As expected, 8 weeks of HFD feeding led to significant increases in body weight in both WT and LinSTZ mice (**Figure 4B and *Figure 32, Appendices***), compared to mice fed a regular diet. LinSTZ mice fed a HFD were able to gain significantly more weight when compared to LinSTZ fed a regular diet, validating obesity on the model.

The state of obesity was further confirmed by histological assessment of white adipose tissue (WAT) morphology. For this, abdominal WAT was quantified at sacrifice, stained with H&E, and morphometric analysis performed in a blinded manner by a trained pathologist. Quantification of fat in white adipose tissues (WAT) revealed an increase of fat deposition in WT HFD, as expected. LinSTZ HFD also showed changes in adipose tissue morphology visual appearance (**Figure 5**).

Moreover, LinSTZ mice have low body weight accumulation but elevated circulating triglyceride levels (**Figure 6**). In addition, HFD increased plasma LDL cholesterol concentration in LinSTZ mice, confirming dyslipidemia (**Figure 7B**). The cholesterol level was further evaluated to determine the cholesterol ratio in mice by dividing the total cholesterol by the HDL (**Figure 7**). As expected, hypertensive/ T1DM mice have an elevated ratio compared to their WT littermates (**Figure 7D**).

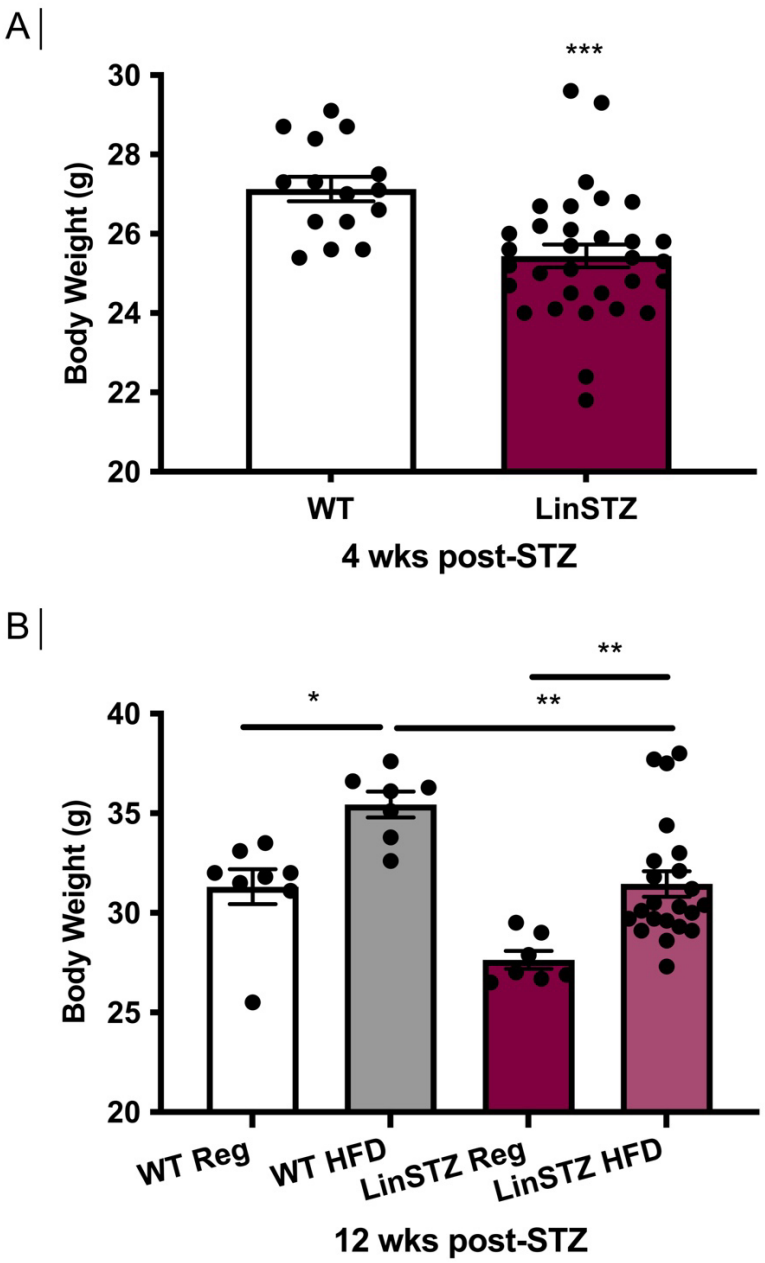

Figure 4 | HFD regimen increases mice body weight.
A) Baseline body weight measurements in grams (g). B) Endpoint body weight measurement is increased in HFD-treated groups after 8-weeks on regimen. Data expressed as means ± SEM, A) unpaired t test, ***p<0.001 B) ANOVA, *p<0.05, ***p<0.001 or ****p<0.0001

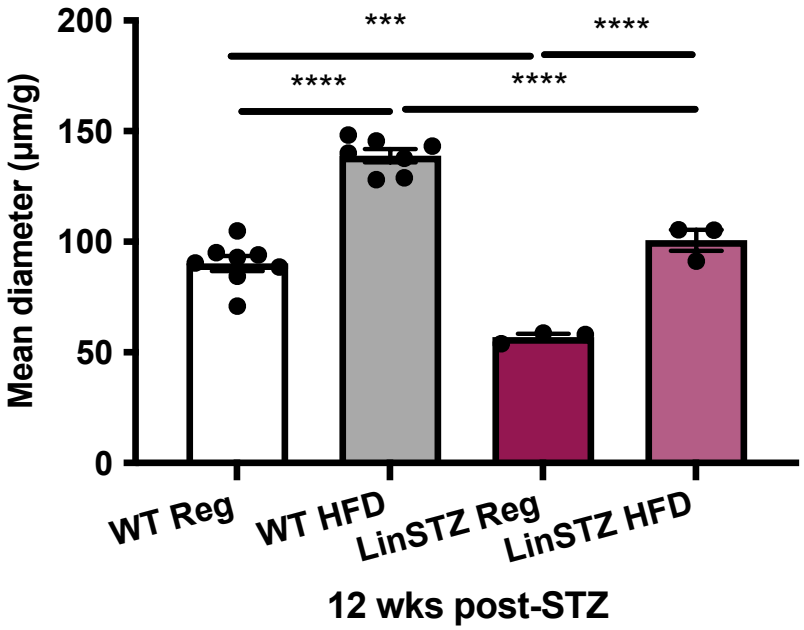

Figure 5 | HFD regimen induces white adipose tissue (WAT) deposition.
Quantification of WAT was measured from fixed H&E paraffin-embedded tissues and visualized at 400X magnification light microscopy. Measurement of adipose circumference was normalized to the total body weight. Data expressed as means ± SEM, ANOVA, ***p<0.001 or ****p<0.0001

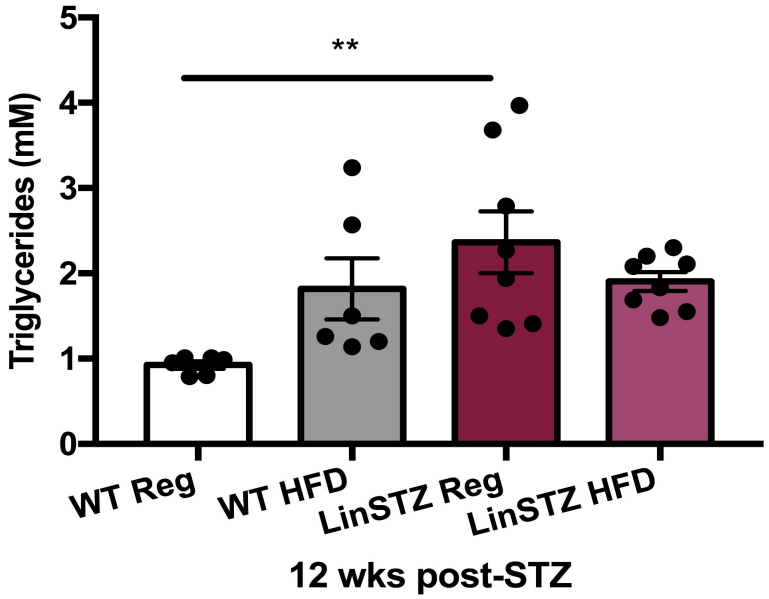

Figure 6 | Plasma triglyceride is increased in LinSTZ mice.
LinSTZ vehicle mice have an increase in plasmatic free triglycerides level. The samples were analyzed by the third party IDEXX inc. to limit the variations. Data expressed as means ± SEM, ANOVA, **p<0.01

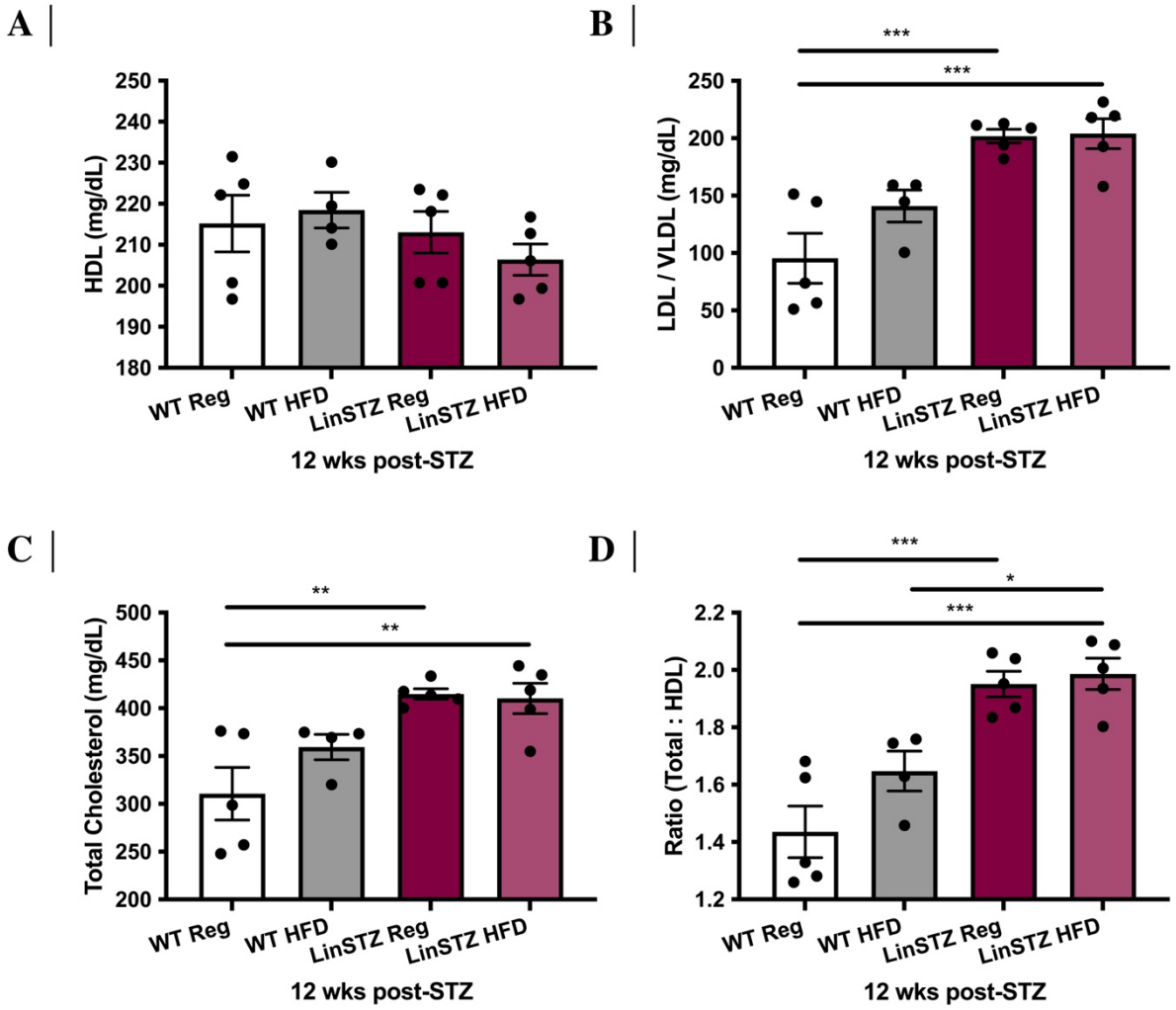

Figure 7 | Plasma cholesterol LDL/VLDL is increased in LinSTZ mice with no HDL changes at 12 weeks post-STZ injections.

A) Quantification for high density lipoprotein (HDL) from plasma samples. B) Low density and very-low density lipoprotein (LDL/ VLDL) quantification. C) Sum of HDL and LDL/ VLDL in plasma to obtain the total cholesterol concentration. D) Cholesterol ratio obtained by dividing the total cholesterols by the HDL values. The samples were analyzed by the third party IDEXX inc. to limit the variations. Data expressed as means ± SEM, ANOVA, *p<0.05, **p<0.01 or ***p<0.001

3.1.2 Evidence of polydipsia, polyuria and dehydration confirmed in LinSTZ mice.

Hyperglycemia impairs the kidney's ability to reabsorb water, and thus mice become dehydrated [89]. LinSTZ mice with confirmed hyperglycemia/ hypertension showed multiple signs of dehydration and polydipsia throughout the study. The LinSTZ mice with polydipsia symptoms observed a higher water intake and urine production, compared to WT mice (**Figure 8A, B)** at baseline. The increase in hematocrit fraction (red blood cells) was also observed in the LinSTZ groups (**Figure 8C**), as LinSTZ mice experienced a reduction in plasma fluid when measuring blood hematocrit. Moreover, another sign of dehydration was analyzed by measuring the urine osmolality in mice. Again, we observed significant reduction in urine osmolality in the LinSTZ mice group (**Figure 8D**) when compared to non-hypertensive and diabetic WT littermate.

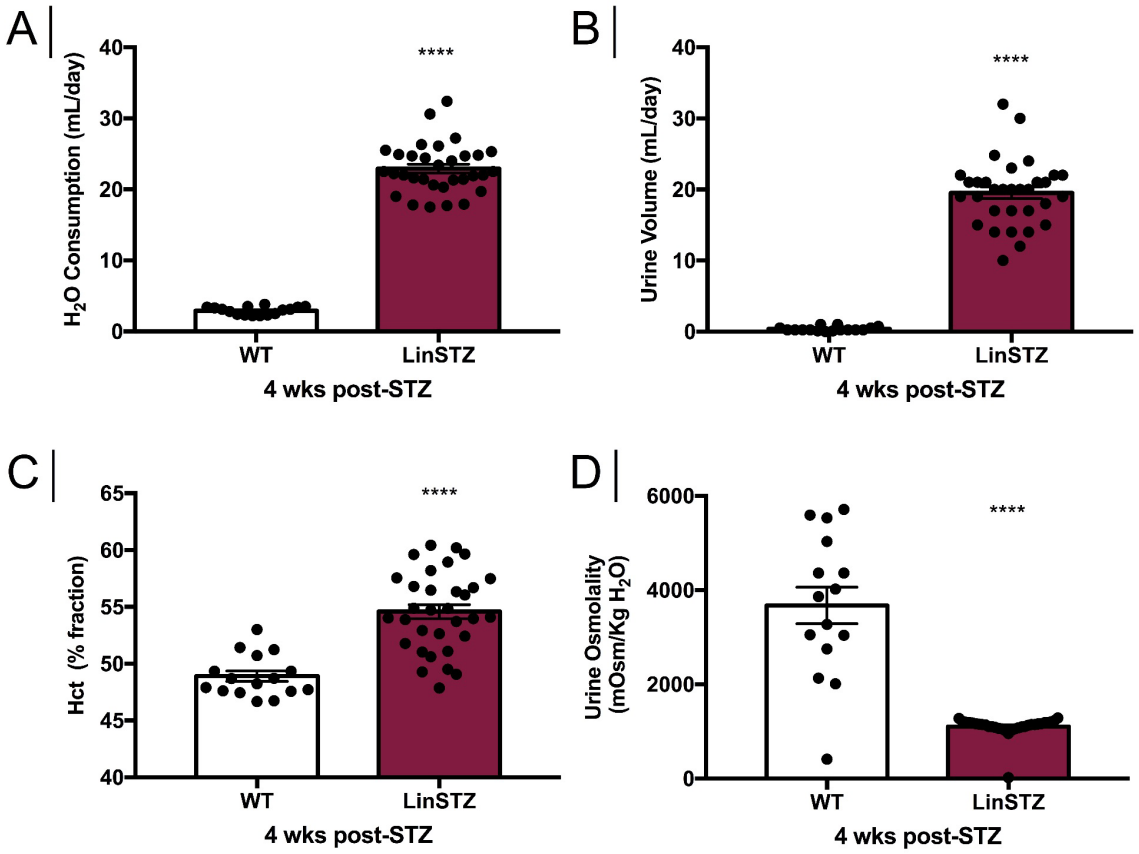

Figure 8 | LinSTZ mice shows evidence of polydipsia and dehydration.
A) LinSTZ are polydipsic by its higher water intake measurement taken by metabolic cages. B) Elevated urine output is observed in LinSTZ mice with shown characteristics of polydipsic and dehydration. C) Dehydration is quantified in LinSTZ by the increase in hematocrit fraction (Hct %). D) Urine osmolality is reduced in the LinSTZ group. Data expressed as means ± SEM, unpaired t test, ****p<0.0001

3.1.3 LinSTZ mice show ameliorated kidney function after 8 weeks on HFD regimen.

Kidney injury was also analyzed by measuring the albumin-to-creatinine ratio (ACR) at baseline (pre-HFD regimen) and endpoint (4 weeks post-HFD regimen). LinSTZ mice were already albuminuric at baseline with confirmed hypertension, hyperglycemic phenotypes (**Figure 9A**). At the endpoint, LinSTZ mice on fed HFD for a duration of 8 weeks showed a trend toward decreasing ACR when compared to regular diet LinSTZ mice (**Figure 9B**). Sustainably, blood urea nitrogen (BUN) was quantified as a surrogate of kidney function. The addition of a HFD regimen showed significant BUN reduction in both WT and LinSTZ mice (**Figure 9C**), thus ameliorating kidney function by eliminating toxins from the system.

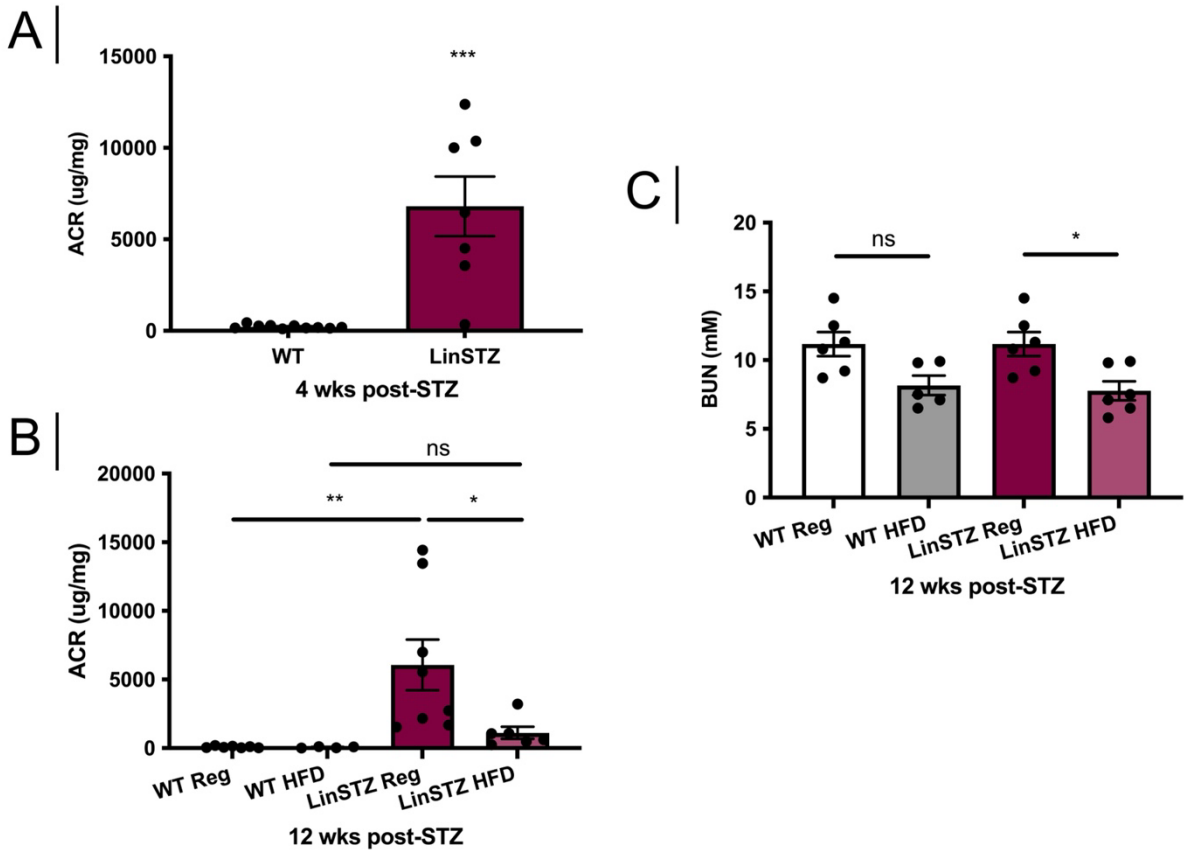

Figure 9 | LinSTZ mice have higher urinary albumin to creatinine ratio (ACR) and ameliorated BUN in presence of HFD.

A) Baseline ACR is higher in LinSTZ mice. B) LinSTZ mice show a trend towards decreasing ACR after 8 weeks of HFD. Urine albuminuria concentration was obtained from the Mouse Albumin Elisa Kit following manufacturer's protocol. C) Blood urea nitrogen illustrating kidney function amelioration with HFD. Data expressed as means ± SEM, A) unpaired t test, ***p<0.001 B) ANOVA, ns: not significant, *p<0.05, **p<0.01 or ***p<0.001 C) ANOVA, ns: not significant, *p<0.05

3.1.4 HFD-feeding reduced the degree of collagen accumulation in the kidney.

Histological assessment of kidney injury was performed on paraffin-embedded kidney sections stained with Masson's trichrome staining. The evidence of collagen proliferation and deposition, fibrotic glomerulopathy (CG) and tubulointerstitial fibrosis (TIF) quantified by Masson's trichrome was observed in the LinSTZ vehicle group (**Figure 10**). HFD-fed LinSTZ mice showed less renal injury as Masson's trichrome staining intensity by its reduction back to basal level, suggesting less fibrosis.

Moreover, alpha smooth muscle actin (aSMA) was quantified from immunohistochemistry kidney sections to validate progression of the disease. Alpha SMA has shown to be a relevant marker of reduced renal function as it can be identified in the renal glomerular mesangial cells and interstitial myofibroblasts. The amount of alpha SMA is significantly increased in the LinSTZ mice, but the expression is reduced when mice are on HFD (**Figure 11**), thus suggesting renal protection is obtained with HFD regimen.

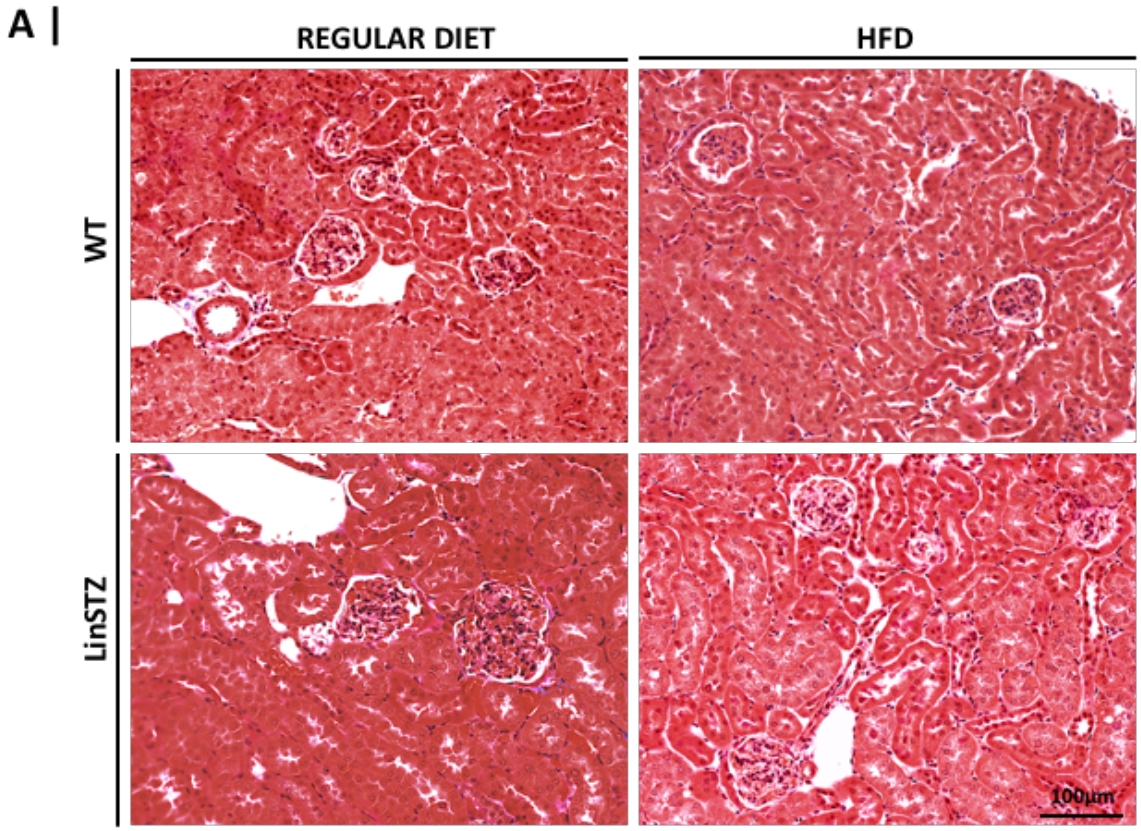

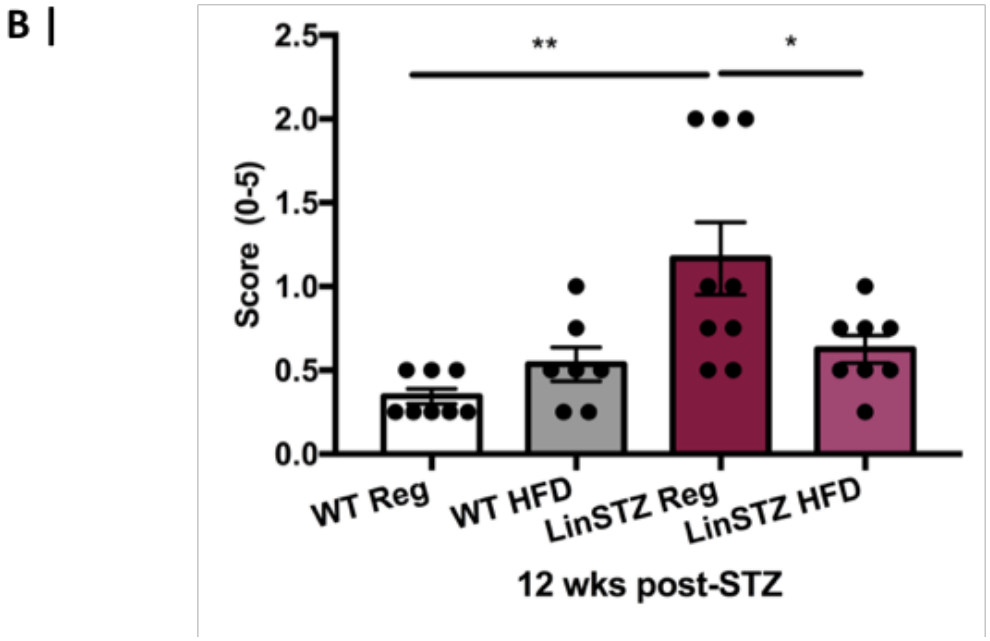

Figure 10 | LinSTZ mice significantly increased tubulointerstitial injury.
A) Visual representation of collagen deposition by Masson's trichrome staining. Magnification = 200X. B) Masson's trichrome scoring of kidney section revealing increase of collagen deposition in the glomeruli and tubulointerstitial of LinSTZ mice fed a regular diet Data expressed as means ± SEM, ANOVA, *p<0.05 or **p<0.01

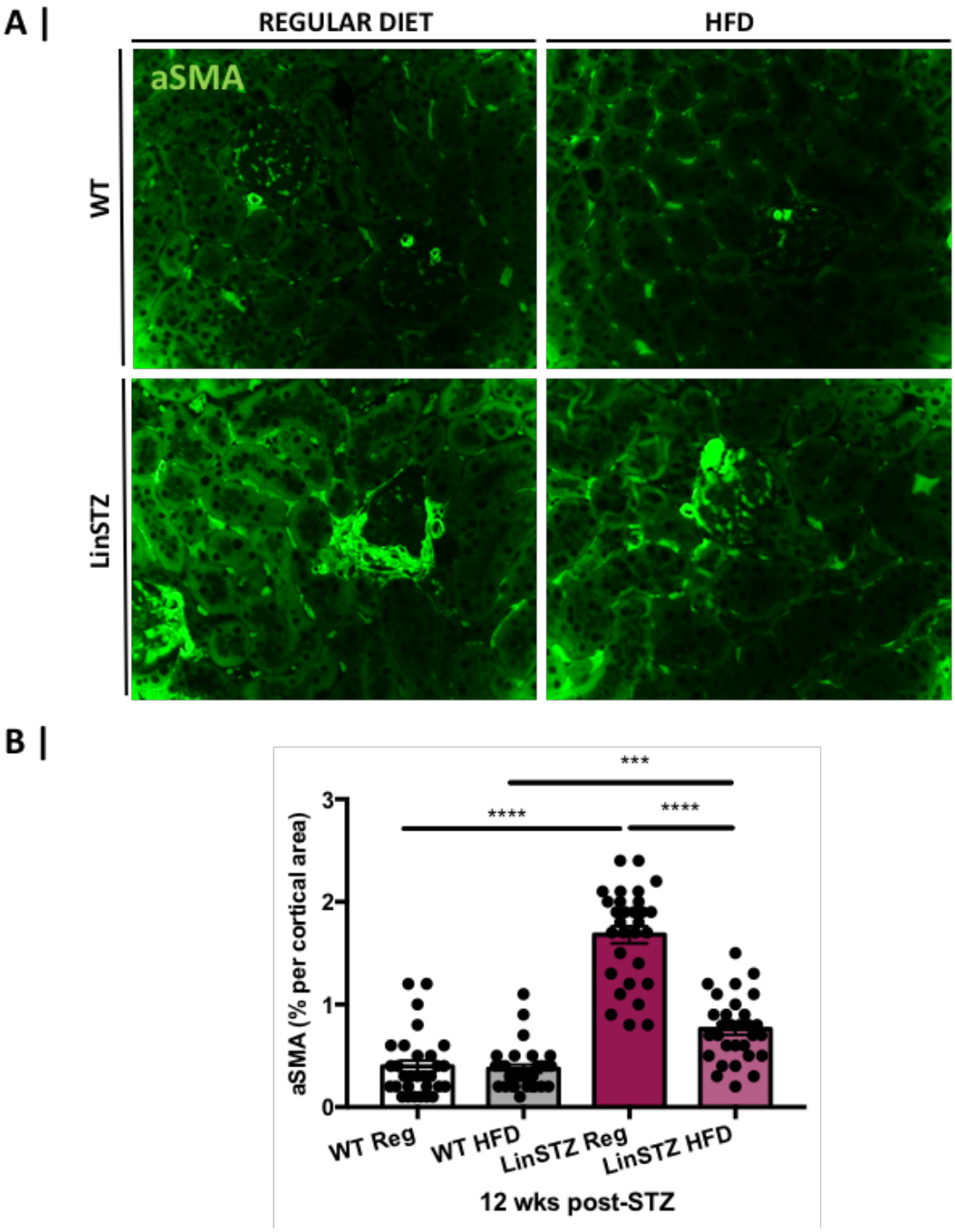

Figure 11 | alpha smooth muscle actin immunofluorescence on kidney section.
Immunofluorescent analysis of the renal cortex. The amount of alpha-actin is significantly increased in LinSTZ mice but reduced on a high fat diet. A) Primary antibody anti alpha-actin, 1:500, (Magnification = 400X, immunofluorescent light microscopy) B) Percentage of immunofluorescence of alpha SMA per cortical area of kidney section. Data expressed as means ± SEM, ANOVA, n=30, ***p<0.001 or ****p<0.0001.

3.1.5 Total kidney and glomerular hypertrophy is observed in the mouse model.

The increase observed in ACR, water intake and urine output suggest that LinSTZ mice glomerular segments are over-filtrating resulting in kidney hypertrophy. The total kidney weight was measured post sacrifice of each individual mice for normalization to the tibia length to obtain the kidney hypertrophy. It was shown that LinSTZ mice have increased kidney hypertrophy when compared to the WT mice (**Figure 12A**). The HFD regimen did not interfere with an increase in the kidney hypertrophy when comparing both LinSTZ on a regular and HFD regimen. The glomerular hypertrophy was also measured by confocal light microscopy visual analysis of glomerular measurements using a blind study. Surprisingly, HFD-fed LinSTZ mice developed significantly less glomerular hypertrophy (**Figure 12B**) at the endpoint than regular-diet fed littermates.

Moreover, the histological assessment of kidney injury was performed on paraffin-embedded kidney sections stained with PAS. The evidence of glomerular mesangial cell proliferation and expansion was observed by PAS staining in all LinSTZ mice (**Figure 13**) but also in HFD-fed WT group.

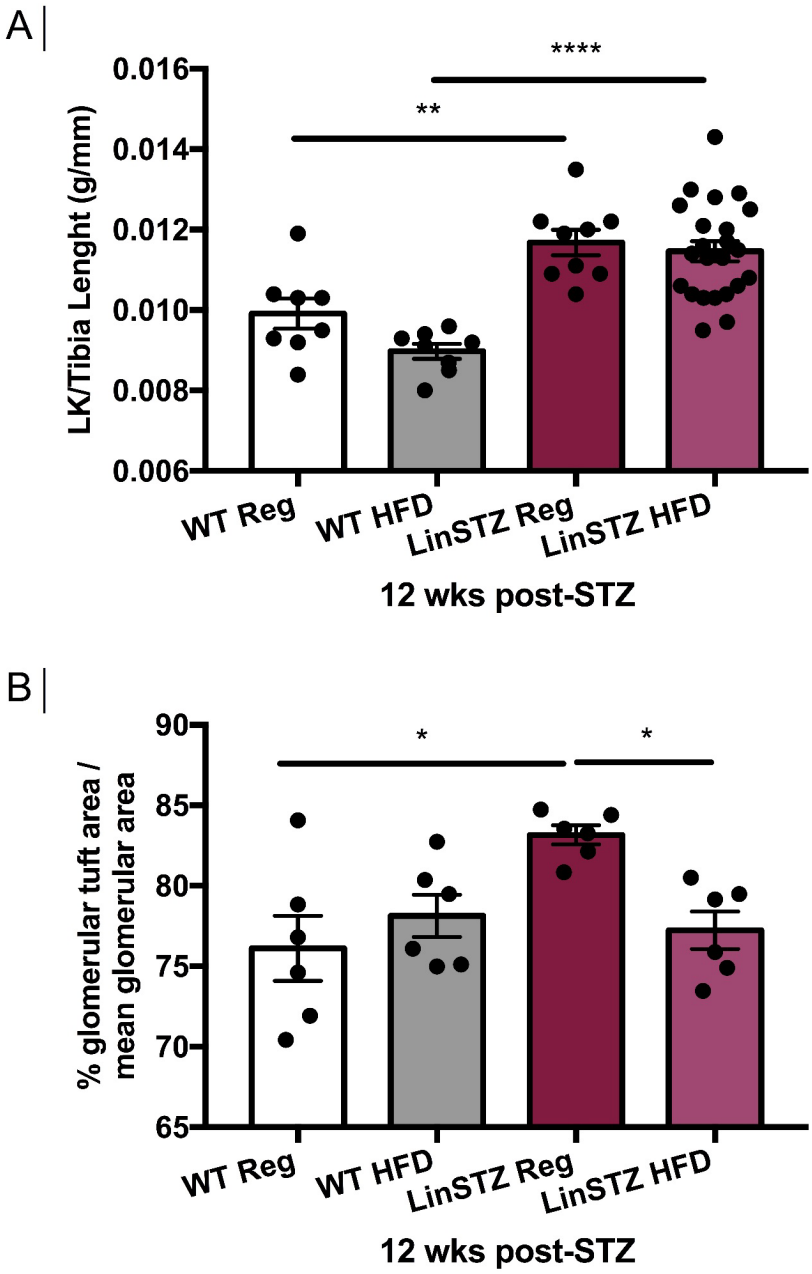

Figure 12 | Kidney hypertrophy and glomerular hypertrophy is increased in LinSTZ. **A)** Kidney hypertrophy was measured from normalizing the left kidney (LK) weight to the tibia length of the mice. **B)** Morphometric analysis of glomerular area was assessed to quantify kidney hypertrophy PAS-stained paraffin-embedded kidney sections. Data expressed as means ± SEM, ANOVA, *p<0.05, **p<0.01 or ****p<0.0001

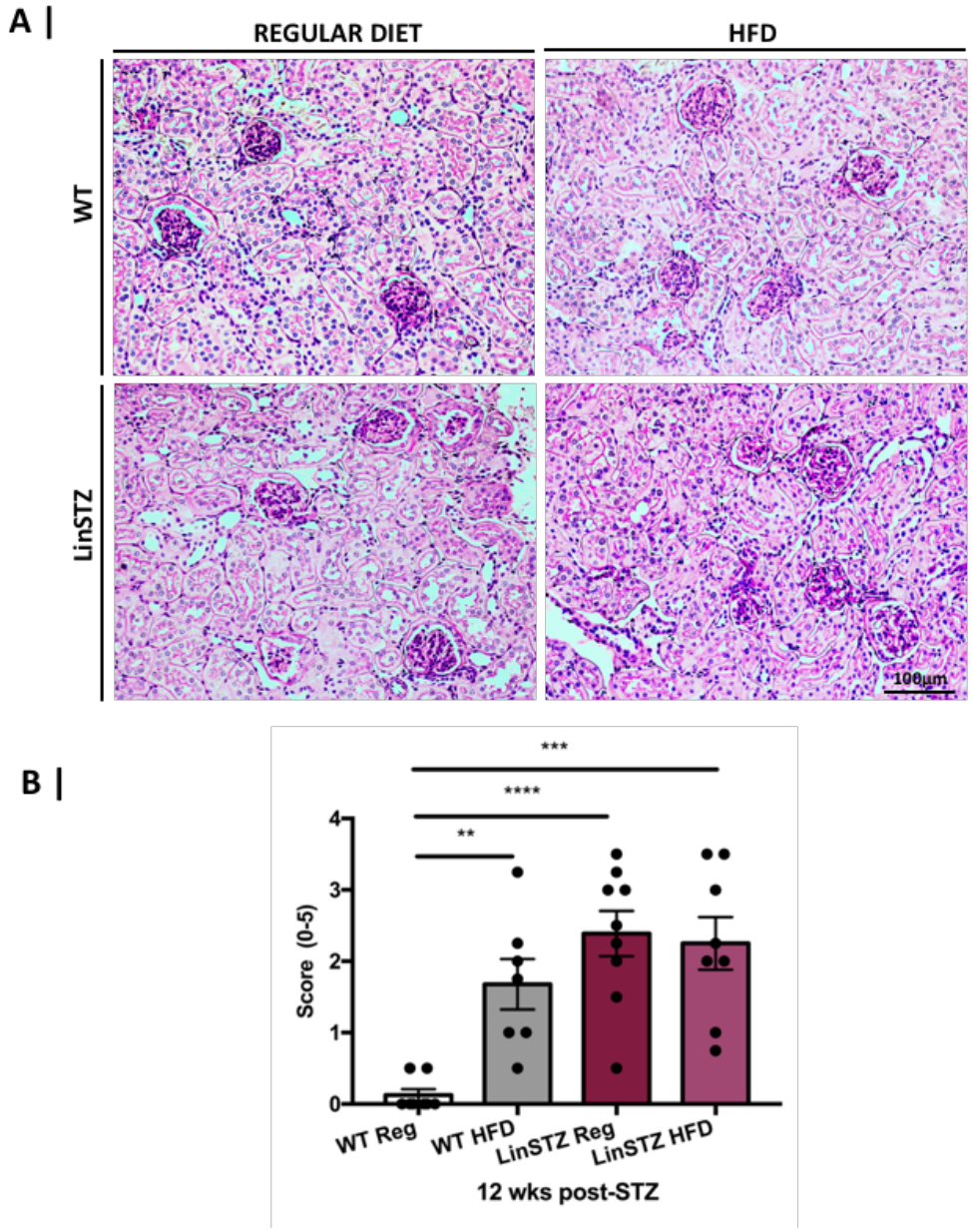

Figure 13 | LinSTZ vehicle and HFD-treated mice significantly increased glomerular injury.

A) Visual representation of paraffin embedded kidney section stained with PAS staining. Magnification = 200X, light confocal microscopy. B) PAS qualitative scoring revealed the presence of glomerular mesangial cell proliferation and expansion in LinSTZ and HFD-treated groups. Data expressed as means ± SEM, ANOVA, **p<0.01, ***p<0.001 or ****p<0.0001

3.1.6 HFD protect kidney from infiltrating inflammatory cells

Infiltrating inflammatory cells such as macrophages are sources of TNF-α production in response to hypertension, renal failure, and diabetic nephropathy. An increase in kidney cortex of TNF-α, not only from resident kidney cells, but from inflammatory cells validates M1 macrophage infiltration. To quantify the level of macrophage infiltration and activation in the kidney, we quantified level of expression of tumor necrosis factor alpha (TNF-α) as a pro-inflammatory/ fibrosis cytokine secreted from macrophages. From which, kidney RNA material was isolated before performing a quantitative RT-PCR on the complementary DNA with respective TNF-α pair primers. No significant increase was identified in LinSTZ mice (**Figure 14**) when compared to the WT groups.

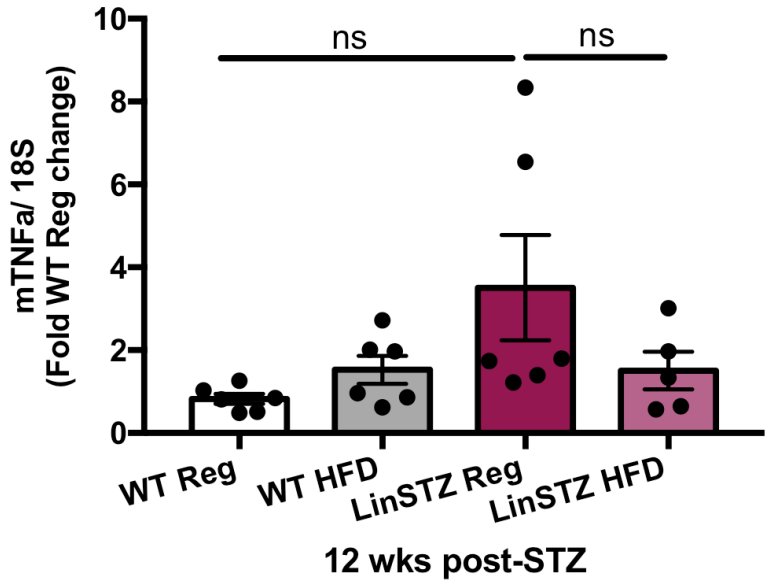

Figure 14 | Tumor necrosis factor alpha is not increase in LinSTZ mice.
Tumor necrosis factor alpha (TNF-α) was quantified from cDNA isolated from the kidney cortex and analyzed by qRT-PCR as source inflammatory cells infiltration in the kidney. Data was normalized to 18S and is presented as fold change WT Reg means ± SEM, ANOVA, ns: not significant

3.2 Quantify the level of liver injury in the novel model of metabolic syndrome inducing-CKD.

Since the humanized pro-renin transgene, responsible for the hypertensive phenotype in LinA3+ mice, is specifically expressed in liver hepatocytes via the transthyretin promoter, as previously described by Touyz et al. [75]. We wanted to know whether reno-protection seen in HFD-fed LinSTZ mice was merely due to the effect of HFD on the liver, and subsequently affecting the severity of the LinSTZ phenotype, leading to potential protection in the kidney.

3.2.1 Liver function is affected by fat accumulation in LinSTZ HFD-fed mice.

We first measured circulating albumin levels as a surrogate marker for liver function [90], as liver is the main site of albumin production. From our results, both regular diet and HFD-fed LinSTZ mice developed hypoalbuminemia (**Figure 15**) when compared to WT littermates, suggesting liver injury. The reduced serum albumin is often related with severe chronic liver disease, thus affecting albumin synthesis.

To better understand the level of liver damage onto the model, we performed alanine and aspartate aminotransferase enzymatic assays. As expected, the ALT level was changed by 2-fold in the LinSTZ model on regular diet and HFD (**Figure 16A**). Surprisingly, the level of AST in the LinSTZ model was not decreased in the model as expressed in **Figure 16B**. When comparing the ALT to the AST ratio, we observed liver damage similar to ALT quantification. The hypertension/ hyperglycemia and the HFD regimen induced on the mice seems to exacerbate early sighs of liver damage.

ALT is often compared with other biochemistry analysis, such as total plasma protein and albumin-to-globulin value to identify liver disease. From the IDEXX inc. plasma results, endpoint plasma revealed that total protein significantly decreased in both LinSTZ groups (**Figure 17**). There is also an early decline in the albumin to the globulin ratio (*Figure 33, Appendices*) revealing potential damage related to the liver.

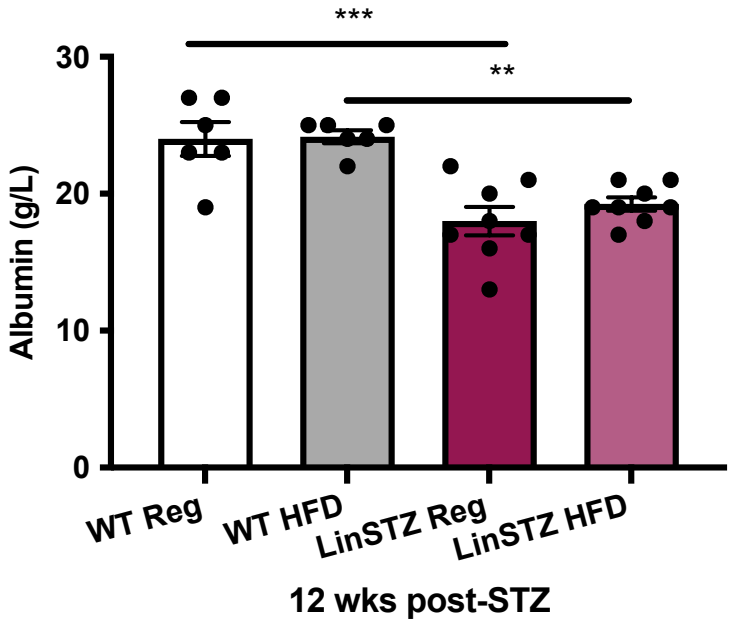

Figure 15 | LinSTZ vehicle and HFD-treated mice significantly reduced plasma albumin level.

The samples were analyzed by IDEXX labs. Data expressed as means ± SEM, ANOVA, **p<0.01 or ***p<0.001

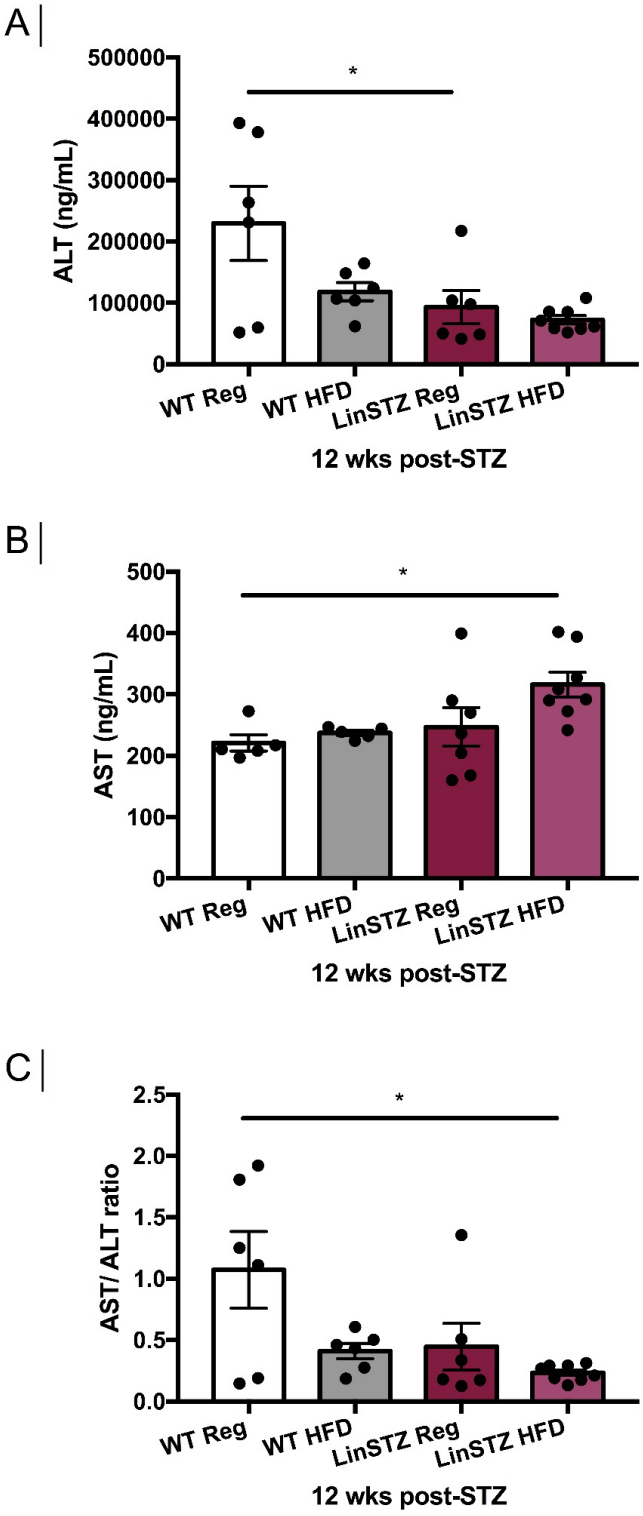

Figure 16 | Liver injury analysis.
A) Alanine aminotransferase is reduced in LinSTZ mice on Regular and HFD and WT HFD illustrating a decrease in liver function. B) Aspartate aminotransferase increased in LinSTZ HFD mouse model illustrating liver damage C) ALT to AST ratio. Data expressed as means ± SEM, ANOVA, *p<0.05

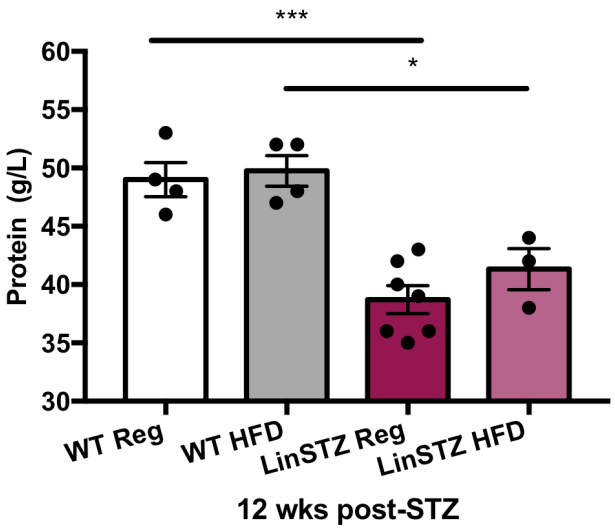

Figure 17 | Total plasma protein is decreases in LinSTZ mice.
The samples were analyzed by IDEXX labs. Data expressed as means ± SEM, ANOVA, *p<0.05 or ***p<0.001

3.2.2 HFD-fed LinSTZ mice led to pronounced hepatocyte ballooning, liver inflammation and fibrosis.

Liver damage was also visualized with PAS staining to better identify inflammation, fibrosis and apoptosis from sections' scoring by a pathologist. The histological assessment of liver injury revealed that both WT+HFD and LinSTZ+HFD mice developed steatosis (fat accumulation) lesions (**Figure 18A**) when compared to regular diet fed mice. In fact, we observed a 4-fold increase in steatosis when mice were fed 4 weeks a 60% kCal HFD, compared to regular diet fed mice. The liver histological scoring analysis revealed pronounced hepatocyte ballooning, liver inflammation and fibrosis (**Figure 18B**) in HFD-fed LinSTZ mice. Based on these findings, HFD-fed LinSTZ mice may be a suitable model of liver fibrosis and inflammation. Therefore, the combination of hypertension, hyperglycemia and obesity on these mice models induced NAFLD.

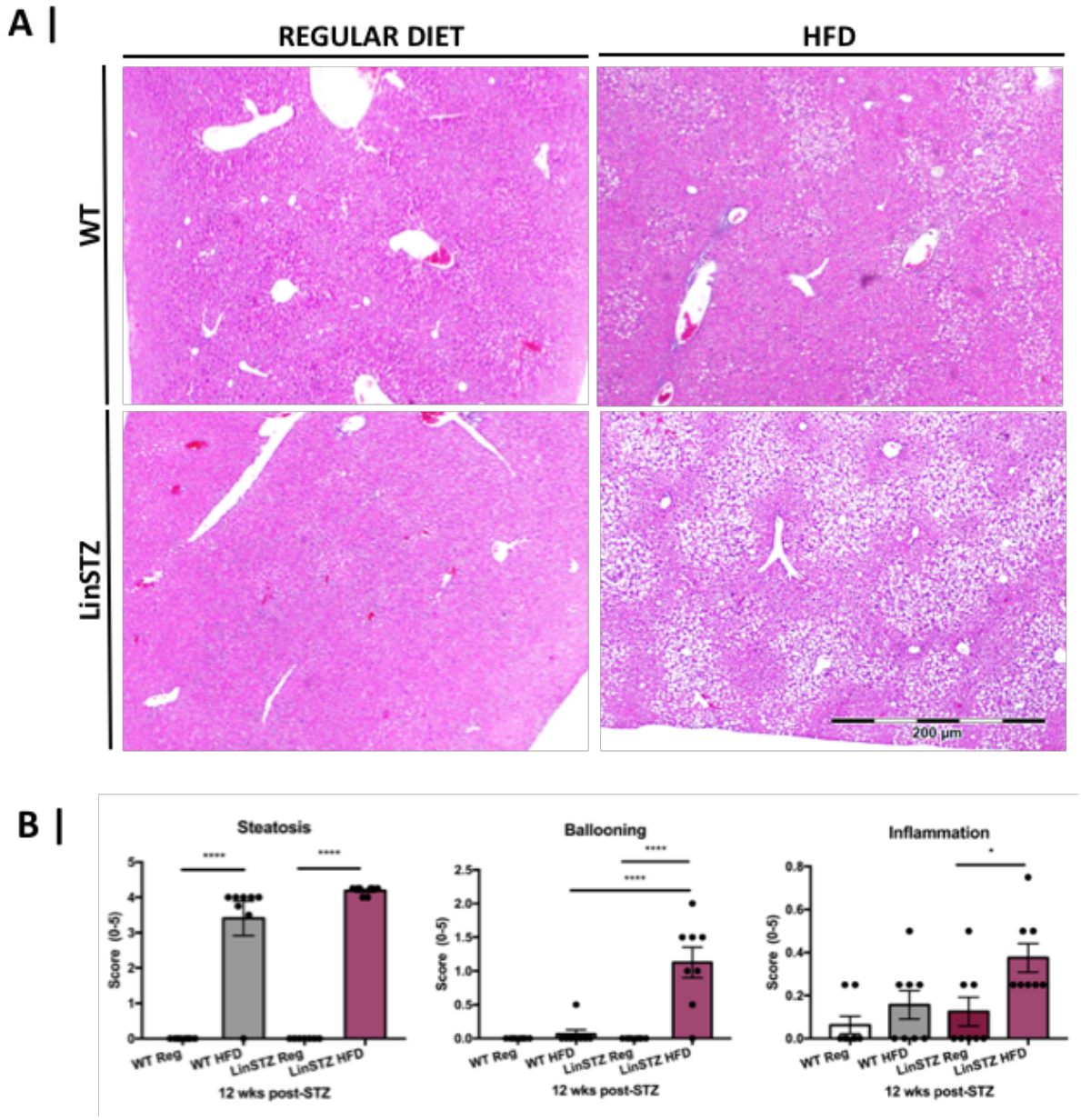

Figure 18 | Both WT HFD and LinSTZ mice significantly increased liver steatosis lesions. **A)** Hematoxylin and Eosin (H&E) Staining revealed the presence of steatosis lesions in the liver. Light confocal microscopy, Magnification = 400X. **B)** Scoring quantification of steatosis, ballooning and inflammation from liver section validating a NAFLD model. Data expressed as means ± SEM, ANOVA, *p<0.05 or ****p<0.0001

3.2.3 Liver injury does not exacerbate human pro-renin transgene depletion.

The humanized pro-renin transgene is specifically expressed in liver hepatocytes of LinA3+ mice. However, we questioned whether renoprotection seen in HFD-fed LinSTZ mice was due to HFD on the liver, and subsequently affecting the severity of the LinSTZ phenotype. To validate this hypothesis, we customized oligo pair primers to the human renin sequence and performed a quantitative PCR. As expected, WT littermate's level of detection is undetectable for human renin expression by qPCR since they do not express the transgene (**Figure not shown**). Moreover, the human renin mRNA level of expression was not affected by the degree of liver damage, as a 250- and 300-fold change is observed in LinSTZ regular and HFD-fed mice respectively (**Figure 19**). Surprisingly, liver damage did not interfere with the human liver specific pro-renin transgene and the hypertension reduction after 4 weeks of HFD does not come from the human renin transgene depletion on the model as it is normally expressed.

As we observed a drop in hypertension in the LinSTZ HFD mouse model, we also quantified Angiotensin II (Ang II) as a potential target to validate the RAAS system function. By enzyme-linked immunosorbent assay (Elisa), we quantified Ang II from endpoint plasma collected in LinSTZ mice fed a regular and HFD. Again, the Ang II plasma level was unaffected in the model (**Figure 20**). The Ang II protein is the end-product of the RAAS system, exacerbating the vasoconstriction via the Ang II receptor type 1, thus inducing constant hypertension in the model through the human pro-renin transgene and the continuous endogenous renin production.

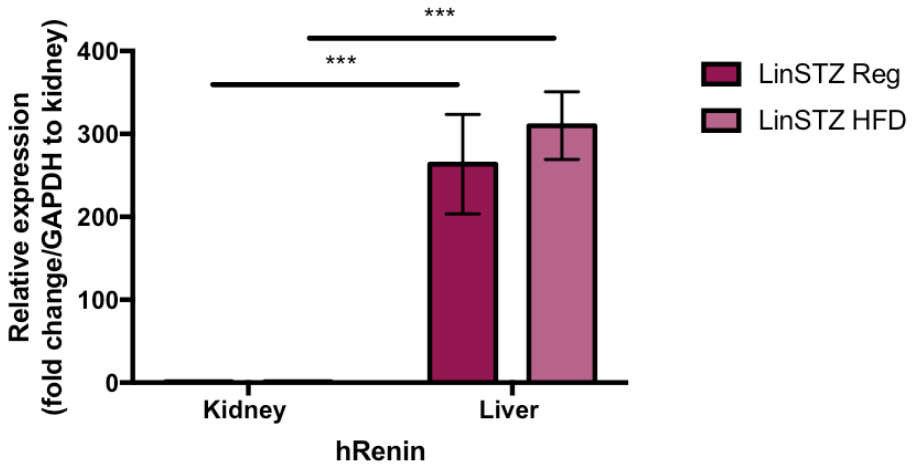

Figure 19 | Liver damage did not affect expression of the human liver specific pro-renin transgene.
Human renin (hRen) was quantified from RT-PCR cDNA isolated from the liver tissue and kidney cortex and analyzed by qRT-PCR. Data was normalized to GAPDH and is presented as fold change kidney means ± SEM, ANOVA, ***p<0.001

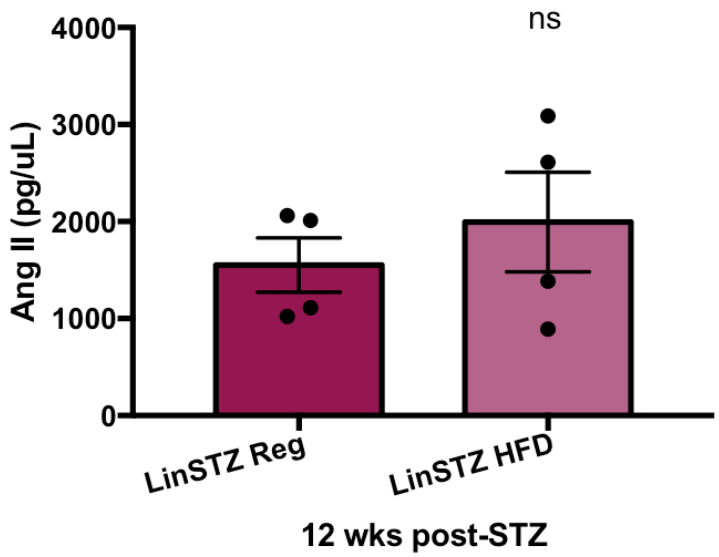

Figure 20 | Plasma angiotensin II quantification.
Plasma Ang II concentration is unchanged in LinSTZ HFD compared to LinSTZ fed a Regular regimen. Data expressed as means ± SEM, unpaired t test, ns: not significant

3.3. Effect of Canagliflozin treatment on LinSTZ mouse model with advance induce-CKD from hypertension and hyperglycemia.

As HFD showed a reno-protection effect despite inducting MS in the LinSTZ model with to induce of hypertension, hyperglycemia, and obesity. From this obtained result, we had to reinvestigate the model and opt-out the HFD regimen on the studied model. The previously studied LinSTZ mouse model from *Thibodeau et al*. showed advanced-CKD injury by 20 weeks post STZ [67]. The used of the genetically-hypertensive/ T1DM LinSTZ mouse model would allow us to perform Canagliflozin treatment with distinct phenotypes (**Figure 1 and Table II**). In this study, we compare the effect of Cana on genetically hypertensive mice with hyperglycemia (LinSTZ + Cana) and Vehicle group (LinSTZ +Veh) with advanced-CKD.

3.3.1 Body weight remains the same throughout the study.

Canagliflozin has shown to regulate body weight from previous animal and human clinical studies. Therefore, body weight was measured throughout the study. The genetically hypertensive LinSTZ mice are lean adult age mice confirmed at baseline (**Table IV**) with no significant changes when compared to non-diabetic animals (WT). Hence, body weight remains the same in a 20 weeks-old animal treated with a 30 mg/kg body weight daily Cana (**Table V**), compared to the vehicle treated group. Mice from this study remained at approximately 27.40 ± 0.50 g and 27.08 ± 1.45 g for the Vehicle and Cana treated group respectively.

3.3.2 LinSTZ mice are hypertensive with no changes when treated with Canagliflozin.

The LinA3+ mice are hypertensive at birth, due to sustained increased renin-angiotensin system activity from the liver specific human pro-renin transgene activation [67]. Previously described, using tail-cuff plethysmography-based SBP measurements, we confirmed that SBP induced in genetically hypertensive LinA3+ mice, given STZ (LinSTZ), at baseline (**Table**

IV), as expected. A 1.5-fold change is observed in SBP of the LinSTZ group when compared to a WT littermate. Surprisingly, Cana treatment did not reduce SBP phenotype in the LinSTZ mouse model (**Table V**). Cana mechanisms of action are independent of hypertension in this rodent model of hypertension/ T1DM and its translation into decreased renal injury remains to be confirmed.

3.3.3 Canagliflozin decreases hyperglycemia in LinSTZ mice.

The LinA3+ mice have induced hyperglycemia via STZ-pancreatic beta cell deaths. At four weeks post STZ-injections, a significant 2.5-fold change in fasted blood glucose level was observed in the LinSTZ group compared to their WT littermates (**Table IV**). The hyperglycemic LinSTZ mice from this study obtained a blood glucose of 27.79 ± 1.54 mM compared to 10.81 ± 0.40 mM for WT littermates, non-hypertensive and hyperglycemic confirmed. Blood glucose levels remained elevated in the untreated group throughout the study. As expected, Canagliflozin (SGLT-2 inhibitor) at 30 mg/kg body weight treatment for 3 consecutive weeks significantly decreased plasma glucose in the LinSTZ model (**Table V**). As a result, elevated glycosuria is also observed in the treated model (**Figure 21**). The Cana treated group had significantly more glucose excreted in the urine with a glucose to creatinine ratio of 146.2 ± 0.32 compared to 138.3 ± 0.25 for the vehicle group.

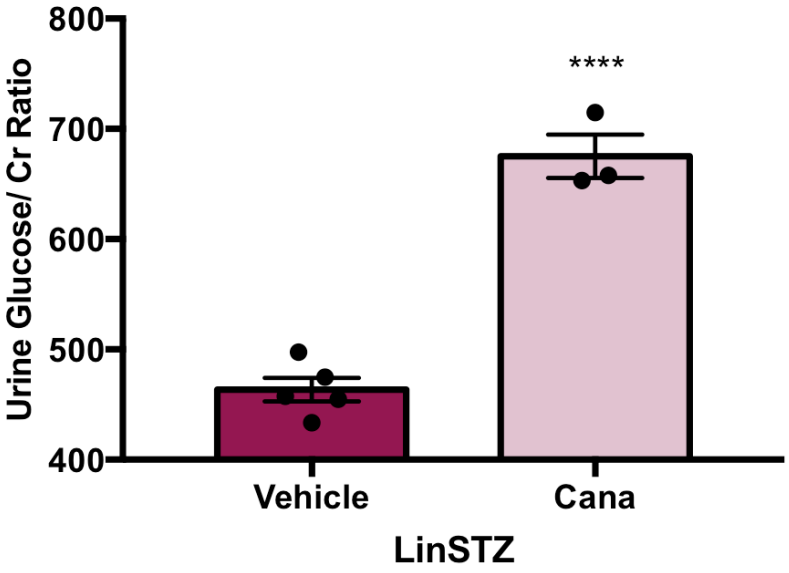

Figure 21 | Elevated glycosuria is observed in the Cana treated model.
The samples were analyzed by IDEXX labs. Data expressed as means ± SEM, unpaired t test, ****p<0.0001

3.3.4 Canagliflozin decreases metabolic demand in LinSTZ mice.

Metabolic demand in mice was measured using 24 hours metabolic cages where mice had access to plenty of food and water. As expected, LinSTZ mice with confirmed hyperglycemia/ hypertension showed multiple signs of dehydration and polydipsia with a higher water intake and urine production (**Table IV)** at baseline. After 3 weeks of treatment, Cana significantly decreased food and water intake in mice (**Table V**), and significantly decreased the urine volume output (**Table V**) when compared to the mice receiving the vehicle.

Table IV: Mice physiological data taken pre-treatment compared to WT mice.

Measurements	WT	LinSTZ
Body weight (g)	26.81 ± 0.43	27.97 ± 0.74
Blood glucose (mM)	10.81 ± 0.40	27.79 ± 1.54 #
SBP (mmHg)	121.30 ± 2.04	157.42 ± 6.53 #
Food consumption (g/ 24 hr)	2.91 ± 0.23	6.33 ± 0.38 #
Water intake (mL/ 24hr)	2.93 ± 0.14	31.58 ± 2.86 #
Urine excretion (mL/ 24hr)	0.37 ± 0.08	6.33 ± 0.38 #

SBP: Systolic blood pressure.
#: **** $P < 0.0001$

Table V: Post-Cana treatment (3 weeks) mice physiological data.

Measurements	LinSTZ	
	Vehicle	Canagliflozin
Body weight (g)	27.40 ± 0.50	27.08 ± 1.45
% Body weight	101.91 ± 0.64	96.72 ± 2.96
Blood glucose (mM)	30.17 ± 2.14	21.70 ± 3.48 #
SBP (mmHg)	157.73 ± 7.68	169.89 ± 10.29
Food consumption (g/ 24 hr)	7.20 ± 0.74	4.20 ± 1.15 #
Water intake (mL/ 24hr)	36.00 ± 6.83	19.68 ± 6.46 #
Urine excretion (mL/ 24hr)	28.80 ± 6.75	9.60 ± 4.70 #
LK/ Tibia length (g/ mm)	0.013 ± 0.001	0.014 ± 0.0004
LK/ BW ratio	0.009 ± 0.0004	0.009 ± 0.0007
RK/ Tibia length (g/ mm)	0.014 ± 0.001	0.014 ± 0.0004
RK/ BW ratio	0.009 ± 0.0004	0.009 ± 0.0005

SBP: Systolic blood pressure, LK: Left kidney, RK: Right kidney, BW: Body weight.
#: * $P \leq 0.05$

3.3.5 Canagliflozin treatment decreases SGLT-2 level of expression.

Canagliflozin blocks sodium and glucose reabsorption in the renal proximal tubule. Given a 30 mg/kg body weight daily dosage for three (3) weeks by gavages, LinSTZ mice experienced an increase in glucosuria (**Figure 21**). To better quantify the level of inhibition of the SGLT-2 cotransporter, kidney cortical RNA was isolated and converted into complementary DNA for qPCR with corresponding SGLT-2 pair primers. We identified that the inhibition of SGLT-2 by Cana reduced cDNA level of expression by 2-fold changes (**Figure 22**) when compared to the untreated group (LinSTZ + Veh). As an indicator of the success of the cDNA target gene quantified, the levels of the 18S ribosomal was used as the control gene.

Additionally, Cana has shown promising therapeutic effects to reduce renal injury and impact macrophage infiltration. Moreover, M1 macrophages play an important mediator in glucose metabolism suggesting SGLT-2 cotransporter direct link with macrophages. From which we isolated RNA material from LPS M1 polarized macrophages obtained from femur and tibia bone marrow from mice isolation and performed quantitative RT-PCR using respective mouse SGLT-2 pair primers to quantify SGLT-2 level of expression. As shown in **Figure 23**, macrophages do not express the SGLT-2 cotransporter when compared to renal cortex SGLT-2 level of expression. These results suggest that Cana's treatment is ineffective on macrophage glucose regulation.

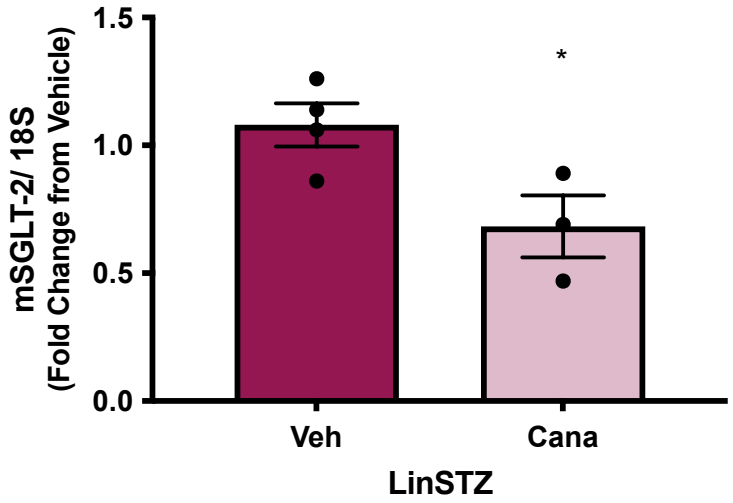

Figure 22 | Inhibition of SGLT-2 cotransporter by Canagliflozin at 30 mg/Kg body weight daily dose.
Mouse SGLT-2 was quantified from RNA isolated from the kidney cortex and analyzed by qRT-PCR. Data was normalized to 18S and is presented as fold change Vehicle means ± SEM, ANOVA, *p<0.05

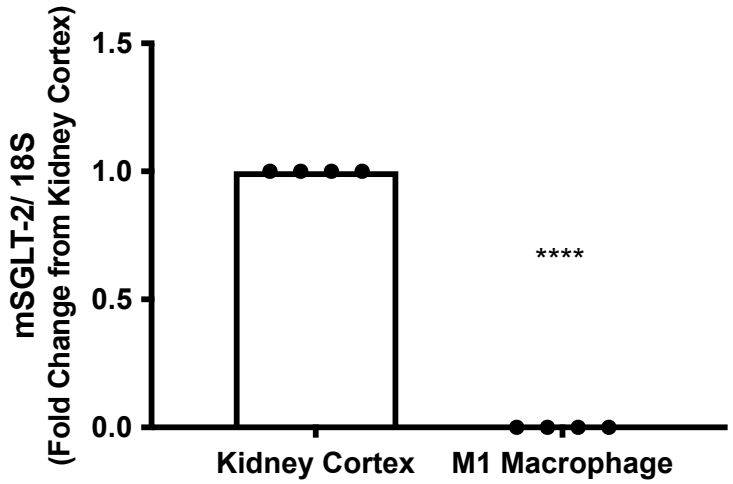

Figure 23 | LPS M1 polarized macrophages do not express the SGLT-2 cotransporter.
Mouse SGLT-2 was quantified from RNA isolated from M1-polarized BMM and analyzed by qRT-PCR. Data was normalized to 18S and is presented as fold change of kidney cortex means ± SEM, unpaired t test, ****p<0.0001

3.3.6 Hypernatriuresis is observed in the LinSTZ treated with Cana.

The SGLT-2 cotransporter is a secondary active transporter that depends on the maintenance of sodium gradient by the sodium-potassium pump ATP energy dependent and active transport. Thus, reabsorption of glucose by GLU2 (glucose transporter 2) and sodium molecules in the renal proximal tubule maintain homeostasis. However, inhibition of the cotransporter increases concentration of glycosuria and natriuresis excretion. The sodium concentration was quantified in plasma and urine. As expected, LinSTZ mice treated with Cana had significant increase in natriuresis when compared to the untreated group (**Figure 24A**). The plasma sodium was unaffected with Cana treatment (*Figure not shown*).

Moreover, the urine chloride concentration was also significantly increased in the LinSTZ model treated with Cana (**Figure 24B**). This increase in chloride concentration excretion is often related with dehydration or kidney injury. As shown in **Table V**, Cana treated mice are drinking less fluid than their vehicle littermates, however the volume consumed per day is still 10-fold higher compared to WT non-hypertensive and non T1DM mice (**Table IV**). Furthermore, the hyperglycemic phenotype activates the TGF system and increases the concentration of chloride delivery to the macula densa of the nephron which subsequently decreases GFR. However, Cana treated mice excreted more glucose and sodium in the urine, thus more free chloride.

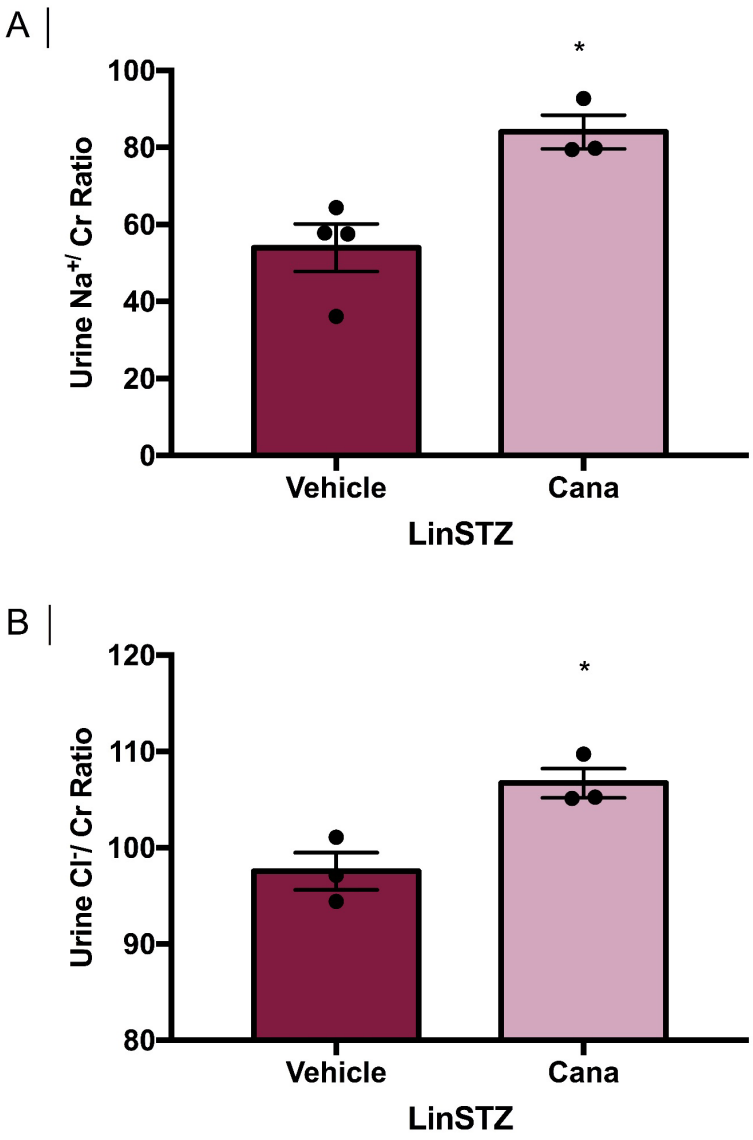

Figure 24 | Hypernatriuresis is increased after 3 weeks post-Cana treatment.
A) Urine sodium quantification. B) Urine chloride is also increased in the Cana treated mouse model. The samples were analyzed by IDEXX labs. Data expressed as means ± SEM, unpaired t test, *p<0.05

3.3.7 Canagliflozin is renal protective in the LinSTZ mice model.

The renal injury is easily measured by calculating the urine albumin to the concentration of creatinine. The results obtained revealed that renal injury worsened during treatment for the vehicle treated group. However, ACR was unchanged after treatment with the Cana for 3 consecutive weeks (**Figure 25**).

Moreover, the renal function is determined by measuring the glomerular filtration rate (GFR). Here, we assess the creatinine clearance measuring the volume of fluid filtered by the glomerulus during a time frame of 24 hours. The results obtained revealed that renal injury worsened during treatment for both groups but stayed unchanged at the endpoint in the Cana treated group when compared to the vehicle group (**Figure 26**). From histological assessment of kidney injury, LinSTZ mice treated with Cana had also significant glomerular hypertrophy increase when compared to the vehicle treated group (**Figure 27**). However, when comparing the kidney weight to the tibia length for normalization, results show no kidney hypertrophy in both groups (**Table V**).

Furthermore, urea is a product from protein degradation and filtered by the kidney for elimination. However, kidney injury reduces urea filtration and elimination from the body, thus increasing body toxicity. Urea was quantified from plasma collected at sacrifice in both vehicle and Cana LinSTZ groups. The plasma urea was significantly decreased in the Cana treated group (**Figure 28**) compared to the vehicle, showing a reno-protective effect on the mice.

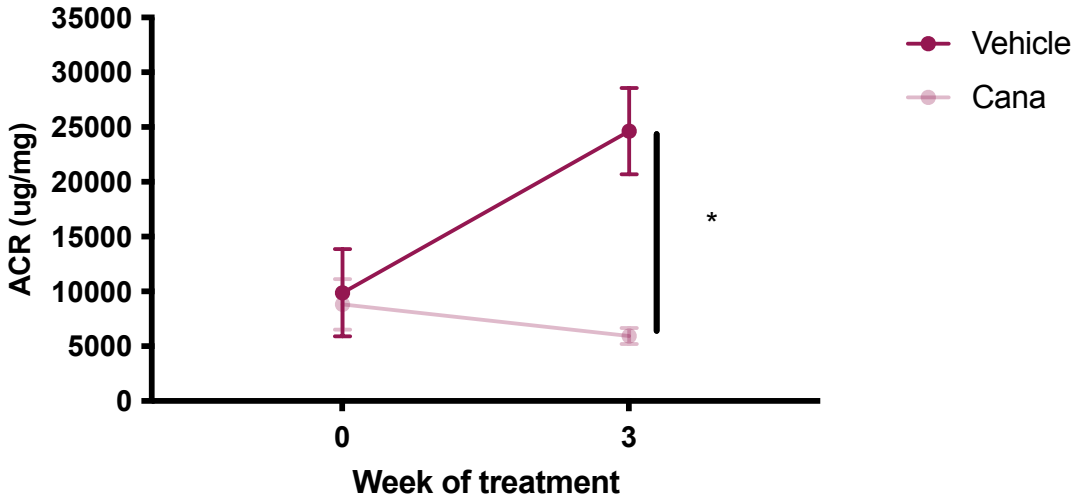

Figure 25 | Urinary albumin to creatinine ratio (ACR) show improvement with Cana treatment.
Longitudinal ACR is unchanged in the Cana group but worsened in the Vehicle group. Urine albuminuria concentration was obtained from Mouse Albumin Elisa Kit. This same albumin was normalized to the urine creatinine concentration measured by SCX-HPLC. Data expressed as means ± SEM, ANOVA, *p<0.05

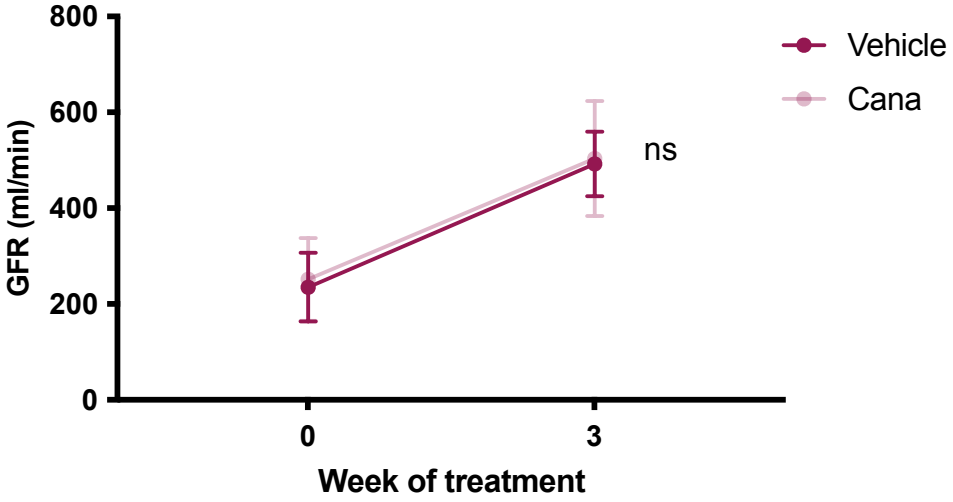

Figure 26 | Glomerular filtration rate (GFR) measurement quantify by creatinine clearance.
Longitudinal GFR is worsened but unchanged in the Cana group compared to the vehicle. Data expressed as means ± SEM, ANOVA, ns: not-significant

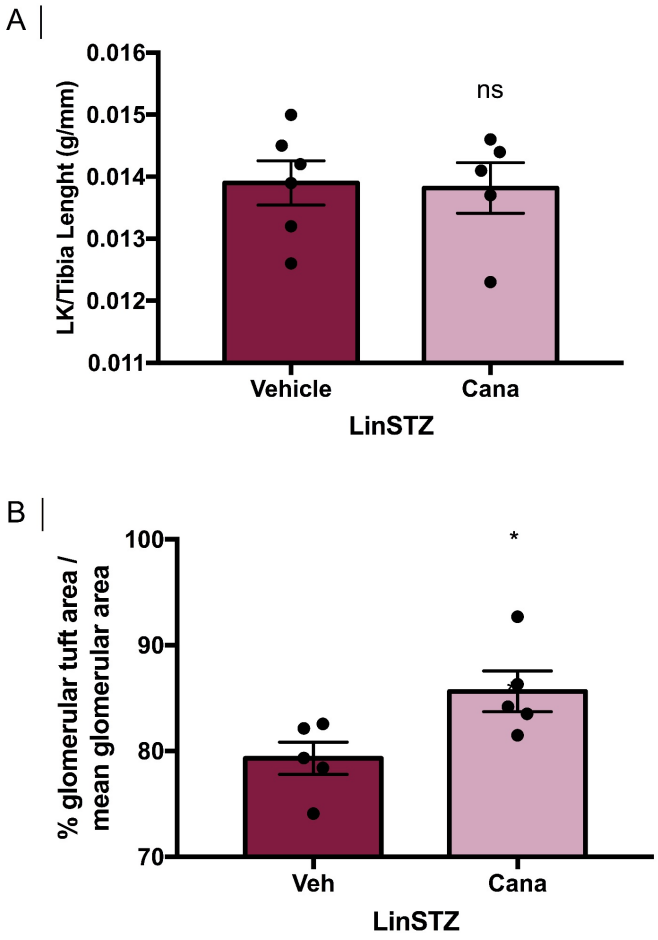

Figure 27 | Glomerular hypertrophy is increased with Cana with no apparent kidney hypertrophy.

The glomerular and kidney hypertrophy were measured 3 weeks post-Cana treatment. A) Kidney hypertrophy was measured from normalizing the left kidney (LK) weight to the tibia length of the mice. B) Morphometric analysis of glomerular area was assessed to quantify kidney hypertrophy PAS-stained paraffin-embedded kidney sections. Data expressed as means ± SEM, unpaired t test, ns: not significant or *p<0.05

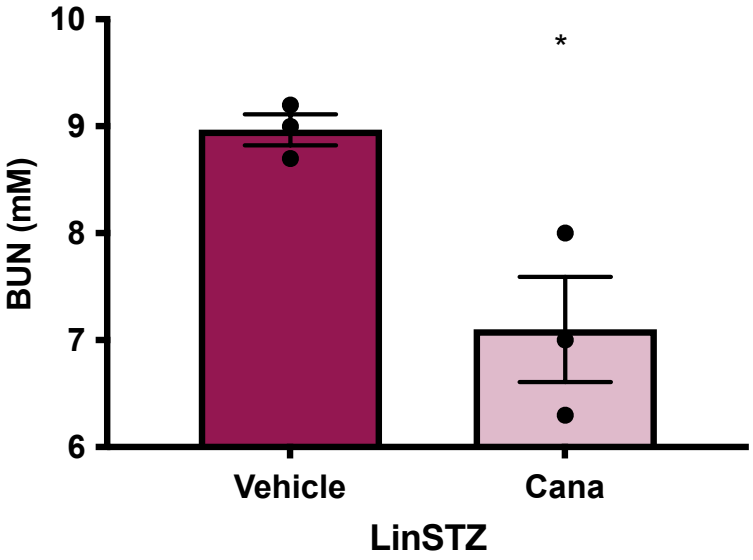

Figure 28 | Cana decreased plasma urea concentration after 3 weeks of treatment.
The samples were analyzed by IDEXX labs. The plasma urea values were normalized to the plasma creatinine concentration. Data expressed as means ± SEM, unpaired t test, *p<0.05

3.3.8 PAS-staining reveals glomerular injury in the Cana treated group.

The histological assessment of kidney injury was performed on paraffin-embedded kidney sections with PAS-staining. The evidence of glomerular mesangial cell proliferation and expansion was observed by PAS staining in the Cana treated group when compared to the vehicle group (**Figure 29**). This correlates with the glomerular hypertrophy results, as Cana modulates the TGF system through SGLT-2 inhibition to excrete more urine glucose and sodium.

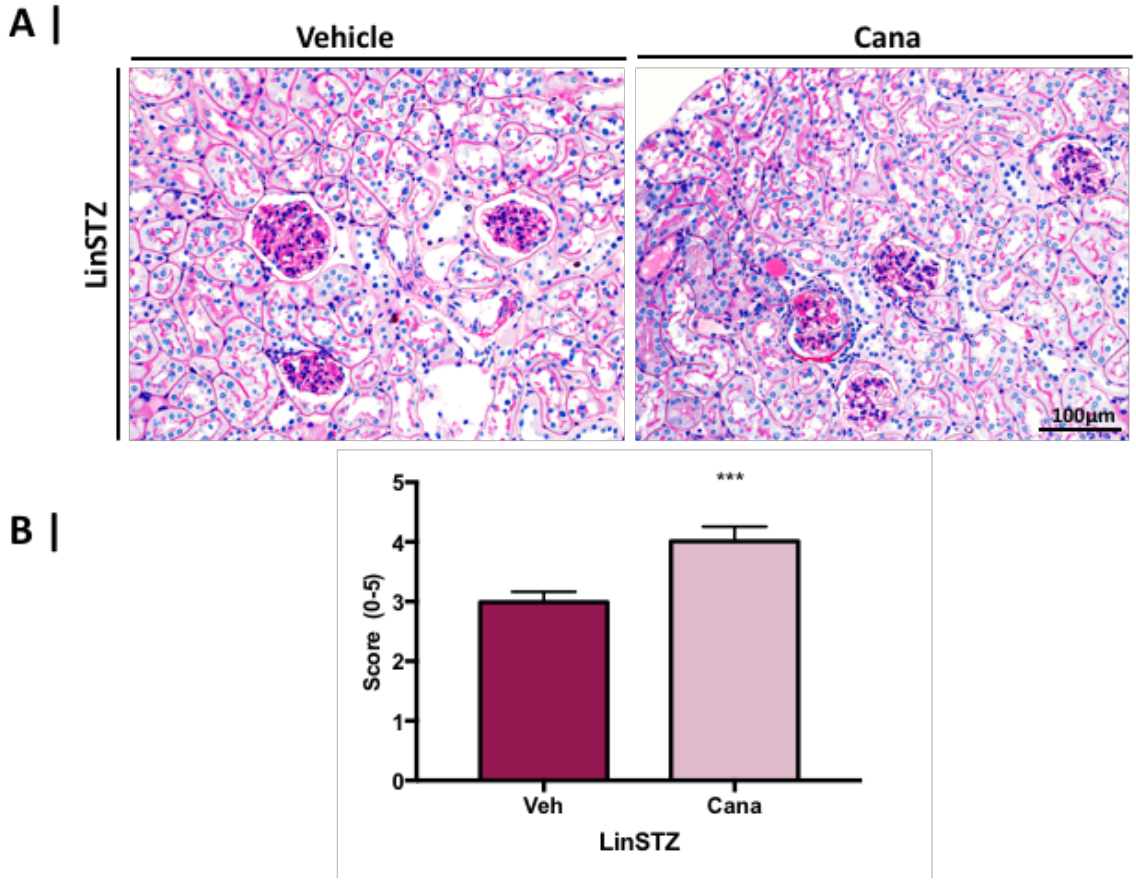

Figure 29 | Cana treated mice significantly increased glomerular injury.
A) Visual PAS staining on the paraffin embedded kidney section. Magnification = 200X, light confocal microscopy. B) PAS scoring reveals the presence of glomerular mesangial cell proliferation and expansion in LinSTZ and HFD-treated groups. Data expressed as means ± SEM, unpaired t test, ***p<0.001

3.3.9 Cana treatment reduced the degree of collagen accumulation in the kidney of LinSTZ mice.

Again, the histological assessment of kidney injury was performed on paraffin-embedded kidney sections stained with Masson's trichrome staining. The evidence of collagen proliferation and deposition, fibrotic glomerulopathy, CG and TIF was quantified by Masson's trichrome was observed in the LinSTZ vehicle group (**Figure 30**). A significant difference is observed in the Cana treated group, showing less renal injury, glomerular collagen deposition and suggesting less kidney fibrosis.

Moreover, alpha SMA was quantified from immunohistochemistry kidney sections to validate progression of the disease with Cana treatment. The amount of alpha SMA is significantly increased in the LinSTZ mice, but the expression is reduced when mice are treated with Cana for 3 consecutive weeks with a 30 mg/kg body weight (**Figure 31**).

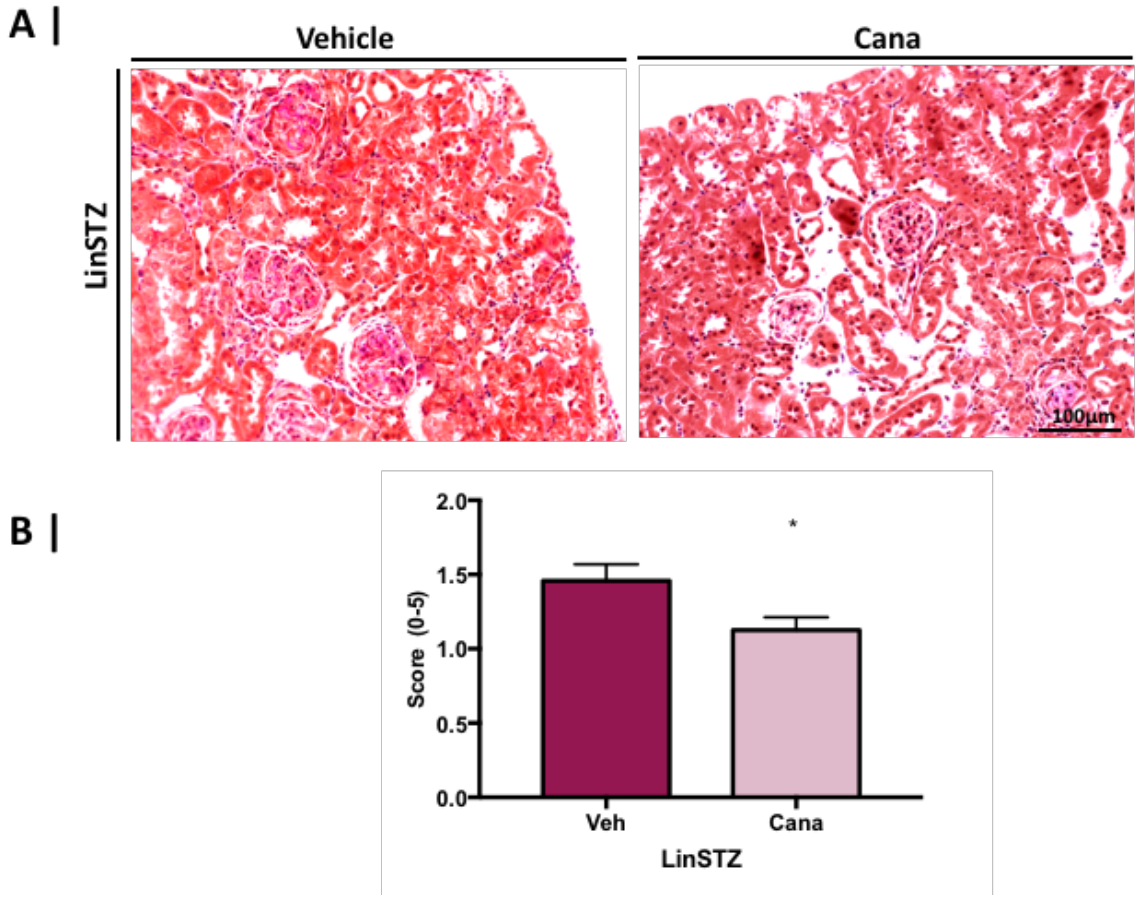

Figure 30 | Cana treated mice significantly reduced tubulointerstitial injury.
A) Visual Masson's trichrome staining of paraffin embedded kidney section. Magnification = 200X, light confocal microscopy. B) MT scoring reveals the presence of collagen deposition in the glomeruli and tubulointerstitial of kidney sections. Data expressed as means ± SEM, unpaired t test, *p<0.05

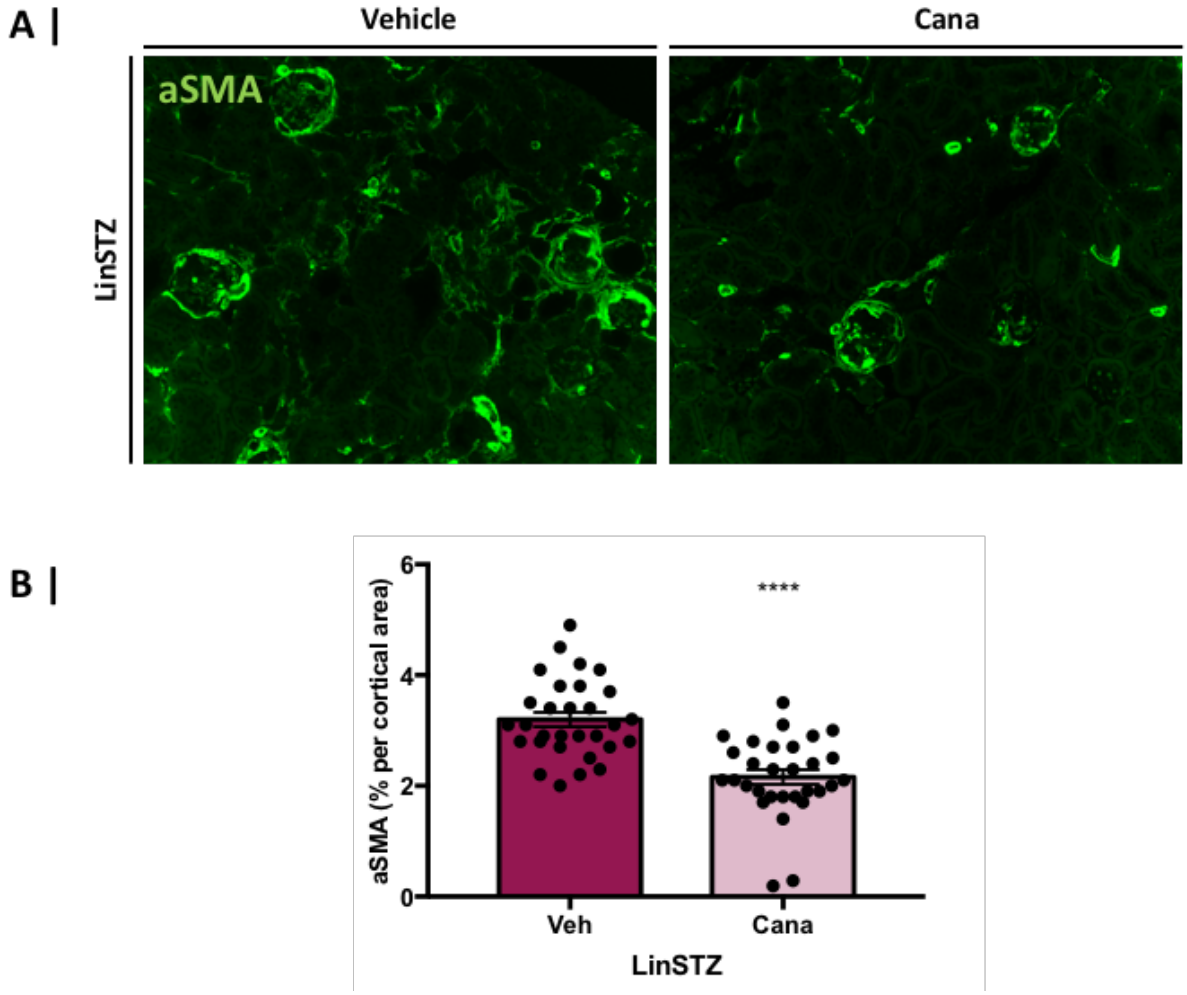

Figure 31 | alpha smooth muscle actin immunofluorescence is decreased in Cana treated mice kidney section.

A) Immunofluorescent analysis from alpha SMA performed on paraffin kidney sections. B) The amount of alpha-actin is significantly high in LinSTZ mice but reduced with Cana. Primary antibody anti alpha-actin, 1:500, (Magnification = 400X, immunofluorescent light microscopy) B) Data expressed as means ± SEM, unpaired t test, n=30, ****p<0.0001

4.1 Establish and characterize a novel mouse model with MS inducing advanced-CKD

The first objective of this study was to establish and characterize a novel mouse model of metabolic syndrome inducing-CKD that recapitulates human disease and therefore better study disease progression. It has been shown that the human disease progression in mouse models have multiple milestones during animal studies [91]. Moreover, the previous studies from the literature have demonstrated that mice were able to achieve MS phenotypes but fail to fully mimic human disease progression if the renal injuries were not reached. In fact, an estimated 24 to 30 weeks is required to generate renal diseases in a mouse model [63, 64]. Our research is unique in the way that the superposition of the genetically-hypertensive and type-1 diabetic (LinSTZ) mouse model previously generated in combination with a high fat regimen regulates MS and within a timeframe of 20 weeks. The used of the LinSTZ model is beneficial to study MS cellular mechanisms, to better understand the pathways using pharmacological tools on renal injuries. The LinSTZ mouse shows distinct features which are similar to MS criteria with the increase of body weight accumulation on a HFD, STZ beta cell inducing extended hyperglycemia and the elevated SBP maintenance by the human liver specific renin transgene. However, the generated LinSTZ mouse model resulted to a decrease in blood pressure, ACR, glomerular injury and in the tubulointerstitial fibrosis, thus validating reno-protection when we added it to a HFD for 8 consecutive weeks. These results obtained contradict the current literature demonstrating renal damage progression in HFD-fed mouse models [92–94]. Therefore, based upon our finding, the LinSTZ mouse model with HFD is not a suitable mouse model of MS.

First, the use of the genetically human pro-renin liver specific transgene induced systemic hypertension at birth, activating the RAAS by the overexpression of renin. This mouse model

is different from phenotype-driven mouse model (e.g., natural variation among inbred) and mouse models that surgically induced hypertension (e.g., Ang II microdiffusion) leading to a surge of blood pressure which plateaus with time and followed by the decreases of body metabolisms over a time period, and get eliminated from the system [95]. Therefore, the genetically human pro-renin liver specific transgenic mouse model studied in this thesis is a great model to study related systemic hypertension throughout my graduate work.

Our results also indicated a hyperglycemic phenotype in the mice model similar to T1DM [96]. As indicated by *Yin et al*., the induction of type-1 diabetes in mice with a low-dose STZ increases difficulties to stimulate insulin production when pancreatic beta-cells are nearly absent [96], thus increasing plasma glucose concentration. Consequently, hyperglycemia impairs the kidney's ability to reabsorb water and mice become dehydrated [89]. LinSTZ mice with confirmed hyperglycemia had multiple signs of dehydration and polydipsia throughout the study such as drinking and urinating more than their body weight volume per day compared to the non-hyperglycemic animals, as illustrated in the current literature [78, 97].

Moreover, feeding mouse *Ad libitum* HFD is shown to induce overconsumption and dysregulation of the daily caloric intake [84], thus favoring fat accumulation in hepatocyte cells and increasing significantly body weight in mice. In fact, the results from our study are in perfect harmony with the literature [45]. Mice fed a HFD gained weight, apparent to obesity phenotype and with corresponding triglyceride, total cholesterol, and LDL fraction increase. The hypertensive and T1DM mouse model develop dyslipidemia over the course of the study when added to a HFD for 8 consecutive weeks, validating cellular pathways dysfunctions associated with hypertension, hyperglycemia, and obesity phenotypes. However, the degree of MS phenotypes inducing CKD on the mouse model to develop gradual loss of kidney function was not as persistent. Thus, rejecting the validation to generate a novel mouse model with MS features of hypertension, hyperglycemia and obesity inducing CKD.

The AMDCC established specific criterions to validate novel diabetic mouse models that mimic features of human renal pathophysiology [98]. The genetically hypertensive, T1DM and dyslipidemia respect the AMDCC and replicate some features seen in human kidneys by its apparent albuminuria after 4 weeks of the induction of hyperglycemia (baseline). The criterions were also respected when we studied the renal pathology of this mouse model. Our results showed in mice mesangial sclerosis, and TIF on the kidney morphology [93] when compared to a non-hypertensive and hyperglycemic WT animal on a regular diet [67]. However, HFD showed to have a reno-protective effect on the hypertensive and diabetic kidney mice. In fact, the risks are increases with liver damage associated with non-alcoholic fatty liver disease (NAFLD) progression when LinSTZ mice are fed HFD for 8 consecutives weeks.

4.2 Validate liver damage in the mouse model of MS

The second objective of this study was to quantify the level of liver injury in the novel mouse model of metabolic syndrome inducing-CKD. We suggested depletion in the human liver specific pro-renin transgene affecting the systemic blood pressure in the LinSTZ mouse model fed HFD due to the potential increases of liver damage. Studies have shown that hypertension, hyperglycemia, and dyslipidemia are hallmarks that contributes to liver injury and if left untreated can lead to NAFLD [99–101].

The hepatocyte damage is characterized by visual appearance of steatosis, ballooning and inflammation. Our study demonstrated liver damage by liver function deterioration in LinSTZ mice with MS and a decrease in liver albumin production. Moreover, our results confirmed liver damage by performing a standardized aspartate to alanine aminotransferase plasma ratio, correlating with the current literature [40, 41, 44]. ALT results are often compared with other biochemical analysis to validate the degree of liver disease such as the albumin to the globulin ratio and to the total plasma protein concentration [40]. Our results confirm again the presence

of liver injury by the significant decrease in plasma protein concentration and the early trend of albumin-to-globulin *(Figure 33 illustrated in Appendices)*. The liver is the primary organ responsible of making and releasing most of the proteins in the blood. In addition, globulin in the body help with the immune system, help fight infection and play a role in the transport of nutriment [40]. The fluctuation in protein and globulin to albumin concentration is the cause of persistent liver injury. However, the level of liver injury was consistent in LinSTZ hypertensive and hyperglycemic mice on a regular diet and HFD limiting our approach to generate a more accurate injury with MS.

In addition, our morphology analysis from liver staining led to induced hepatic damage by the development of significant steatosis, ballooning and inflammation at 20-weeks post-streptozotocin injections inducing hyperglycemia, confirming a NAFLD mouse model. The liver damage characterized in the LinSTZ mouse model fed a HFD shows similar phenotypes that recapitulates the NAFLD, such as an increase 5% or more in liver steatosis quantify by histology with no other possible cause of steatosis, such as an insulin resistance in the model and also no significant alcohol consumption [102]. Liver damage is apparent in the LinSTZ model fed a regular diet or HFD thus suggesting blood pressure regulation in this model is linked with the human pro-renin human liver specific transgene and the increases of liver damage directly affects the expression of the transgene.

More importantly, the LinSTZ model is a genetically hypertensive mouse model with a specific human pro-renin transgene expressed in the liver and when cleaved into active renin induced systemic hypertension [75]. However, our results showed that the human liver specific renin transgene was not affected by the liver injury. In fact, the renin level of expression was overexpressed in the liver by 200 to 300-fold when compared to the kidney expression level. Moreover, Ang II plasma concentration was not affected in the LinSTZ mouse model fed a

regular or HFD diet, indicating that the RAAS pathway is well regulated. The blood pressure in this model is not affected by the degree of liver injury.

Based on our research, the genetically hypertensive and hyperglycemic LinSTZ mouse fed 8 consecutive weeks of HFD showed reno-protection by decreasing blood pressure without affecting the renin-driven transgene, ACR, glomerular injury and TIF. However, it is a more suitable mouse model of NAFLD by the increases of liver disease. For this, HFD was not continued onto the LinSTZ mouse model and Cana drug treatment was fulfill on the previously studies (*Dr. Thibodeau et al.*) LinSTZ mouse model [67].

4.3 Canagliflozin treatment on the renal SGLT-2 cotransporter

The last objective of this study was to compare the effects of Canagliflozin treatment on renal injury in the novel mouse model of MS, as it regulates the reabsorption of sodium and glucose. Cana has shown excellent efficacy in reducing DKD-induced renal injury in both rodents and humans. The CREDENCE human clinical trial provided positive results on Cana usage and renal outcomes in type-2 diabetes mellitus [60–62]. However, its impact in advanced-CKD remains unclear on the proximal tubule segment. The Cana treatment on the LinSTZ mouse model attenuates renal inflammation, renovascular damage and fibrosis by its capacity to blocks glucose reuptake in the proximal tubule.

Hyperglycemia and hypertension contribute to renal injury that altered hemodynamic and filtration barrier dysfunction. The SGLT-2 cotransporters reabsorb over 90% of filtered glucose contributing to hyperglycemia [103]. SGLT-2 is considered a key regulator target for hyperglycemic and multifactorial disease therapy [104]. In fact, *Jurczak et al.* examined the effects of SGLT-2 gene (SLC5A2) deletion on db/db mouse pancreas and other organs, and found that metabolic and renal outcomes were improved, but renal outcomes were not studied

with a SGLT-2 inhibitor drug [105]. The major novel finding of our study is that Cana (SGLT-2 inhibitor) significantly increased urine glucose in the mouse LinSTZ genetically renin-driven hypertensive and hyperglycemic. Consequently, plasma glucose was reduced in the same group. Our results also indicates that Cana play an important role in the mechanisms that regulate daily caloric intake [84]. In fact, many hormonal and neuronal factors are implicated in the regulation of food intake [106] and MS are risk factors of CKD, however the relationship of body weight changes and kidney disease progression mechanisms have not yet been established [107]. The LinSTZ mouse model from our study have shown reduced food and water intake with decrease in urine volume excretion. The reduction in daily caloric intake illustrates an amelioration in the LinSTZ genetically renin-driven hypertensive and hyperglycemic physiology. We suggested that hypertension and hyperglycemia are factors implicated in the participation of mitochondria dysfunction and limits cellular energy demands. Cana treatment may be a modulator of mitochondrial activity in renal endothelial cells by blocking SGLT-2 cotransporter in the proximal tubule cells and regulating mice energy demand and food intake. The potential effect of Cana on mitochondrial activity on the LinSTZ mice beg for further investigation.

The SGLT-2 inhibitor mechanisms of action on the cotransporter are to inhibit glucose and sodium reabsorption in the renal proximal tubule and to reduces the renal hyperfiltration [56]. To reduce hyperfiltration, Cana has showed to play an important role to restore TGF renal system by regulating afferent arteriole vasoconstriction from the increases of sodium delivery in the MD, thus restoring GFR [108]. Our research demonstrated that Cana was enabled to reduce GFR in mice treated at 30 mg/Kg bodyweight thus maintaining hyperfiltration higher. However, our research demonstrated SGLT-2 depletion by highlighting a decrease in genetic expression in presence of Cana treatment was reno-protective on the LinSTZ mouse model when considering an increase of glucosuria and natriuresis, glomerular collagen reduction, TIF

attenuation, myofibroblasts and blood urea nitrogen reduction. Moreover, the renal morphology data collected from Cana treated mice also showed renal protection in the LinSTZ model. Furthermore, the results obtained from our study are in perfect agreement with the publish literature [9, 108, 109]. Taken together, even if hyperfiltration was not corrected by Cana, many other results lead us to conclude that the Cana drug dose response was effective at 30 mg/kg bodyweight.

The SGLT-2 cotransporter was suggested by *Xu et al*. to be expressed on LPS-M1 polarized macrophages cell surface and play an important role in anti-inflammatory mechanisms [110]. Cana treatment could serve to mediate renal inflammatory disease such as CKD by its anti-inflammatory benefit effects. The hypoglycemia environment caused by the inhibition of SGLT-2 with Cana suggests that it reduces intracellular glucose metabolism, and it promotes immune cells autophagy [110]. The hypothesis made by *Xu et al*. and the current literature fails to fully investigate this objective [110]. The result obtained from this study demonstrates that polarized M1 macrophages isolated from mouse bone marrow do not express SGLT-2. Our result clarified that macrophages don't express SGLT-2 cotransporter on its cell surface membrane. In fact, macrophage infiltration in the kidney is independent from the activation of the SGLT-2 cotransporter and glucose regulation [19, 20], thus rejecting *Xu et al*. hypothesis [110]. Moreover, our results demonstrated that SGLT-2 is primary expressed in kidney cortex cells, more importantly on renal proximal tubule epithelial cells and is responsible for 90% of glucose reabsorption [111]. In addition, macrophage infiltration at the site of injury is either caused by persistent inflammation or by cytokine (e.g., TNF-α) release from injured endothelial cells [112]. As shown by our results, TNF-α is highly expressed in hypertensive and hyperglycemic LinSTZ mice, but expression is reduced in presence of HFD. This result is another indicator of renal protection from HFD in this model of MS inducing-CKD from hypertension, hyperglycemia, and dyslipidemia.

CHAPTER 5: SUMMARY

Taken together, the mouse models of advanced-CKD do not fully mimic human disease progression and do not correlate with the AMDCC criterions. In this current study we showed that HFD is reno-protective primary via the reduction in glomerular hypertrophy, scarring and albuminuria parameters. The major finding showed that HFD-fed LinSTZ did not lead to a more robust model of MS-induced CKD. In fact, several indices of liver injury resulting in a NAFLD were observed in the LinSTZ fed with HFD. In this study we showed that HFD induced liver injury with significant increase in liver steatosis, ballooning and inflammation. Moreover, the LinSTZ genetically renin-driven hypertensive and hyperglycemic mouse showed anti-glycemic and beneficial effects when treated with Canagliflozin. In fact, Cana plays a role of reno-protection in the LinSTZ mouse model by inhibiting the glucose and sodium reabsorption in the renal proximal tubule.

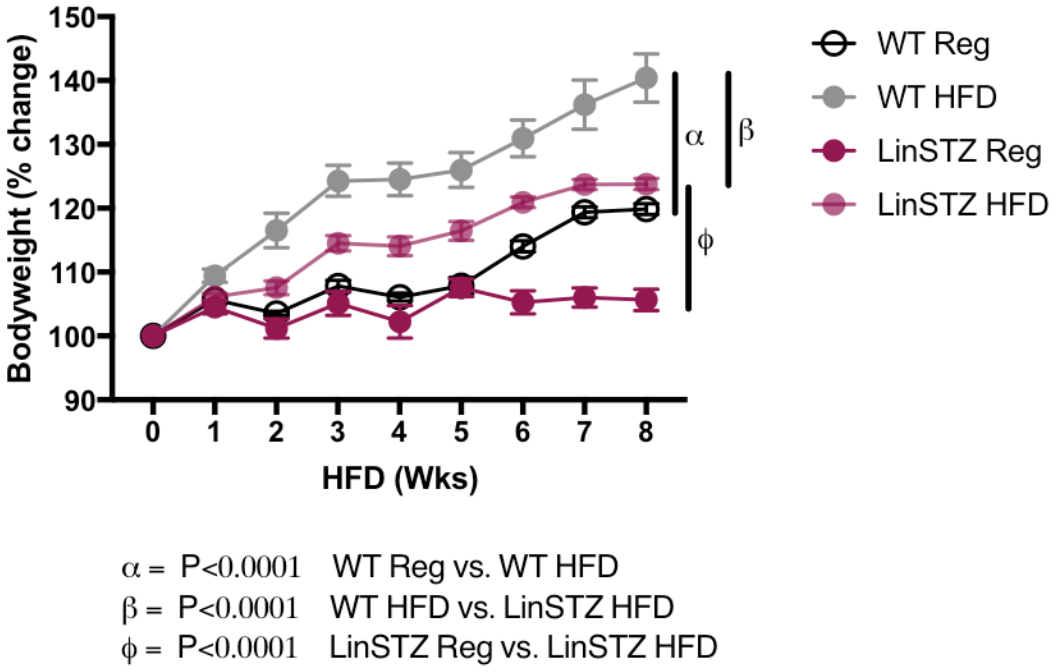

Figure 32 | Longitudinal body weight change taken weekly during 8 weeks of HFD regimen.
Percentage body weight change normalized to weeks 0 of HFD challenge. Data expressed as means ± SEM, ANOVA. ****p<0.0001

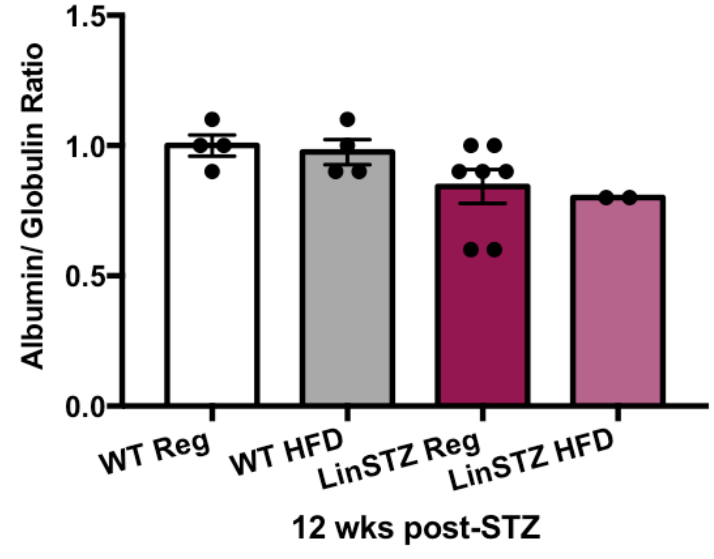

Figure 33 | Plasma albumin-to-globulin ratio trend to decrease in LinSTZ fed with HFD.
The samples were analyzed by IDEXX labs. Data expressed as means ± SEM, n= 2-7, unpaired t test.

1. Robertson GL, Norgaard JP. Renal regulation of urine volume: potential implications for nocturia. BJU Int. 2002;90 Suppl 3: 7–10.

2. López JI, Larrinaga G, Kuroda N, Angulo JC. The normal and pathologic renal medulla: a comprehensive overview. Pathol Res Pract. 2015;211: 271–280.

3. Kaufman DP, Basit H, Knohl SJ. Physiology, Glomerular Filtration Rate (GFR). StatPearls. Treasure Island (FL): StatPearls Publishing; 2019.

4. Qi Z, Whitt I, Mehta A, Jin J, Zhao M, Harris RC, et al. Serial determination of glomerular filtration rate in conscious mice using FITC-inulin clearance. Am J Physiol Renal Physiol. 2004;286: F590–6.

5. Moore JF, Daniel Sharer J. Methods for Quantitative Creatinine Determination. Current Protocols in Human Genetics. 2017. doi:10.1002/cphg.38

6. Stevens LA, Levey AS. Measured GFR as a Confirmatory Test for Estimated GFR. Journal of the American Society of Nephrology. 2009. pp. 2305–2313. doi:10.1681/asn.2009020171

7. Erman A, Rahamimov R, Mashraki T, Levy-Drummer RS, Winkler J, David I, et al. The Urine Albumin-to-Creatinine Ratio: Assessment of Its Performance in the Renal Transplant Recipient Population. Clinical Journal of the American Society of Nephrology. 2011. pp. 892–897. doi:10.2215/cjn.05280610

8. Reiser J, Altintas MM. Podocytes. F1000Research. 2016. p. 114. doi:10.12688/f1000research.7255.1

9. Vallon V. Tubuloglomerular feedback and the control of glomerular filtration rate. News Physiol Sci. 2003;18: 169–174.

10. Thompson S, James M, Wiebe N, Hemmelgarn B, Manns B, Klarenbach S, et al. Cause of Death in Patients with Reduced Kidney Function. Journal of the American Society of Nephrology. 2015. pp. 2504–2511. doi:10.1681/asn.2014070714

11. Hoyer JR, Seiler MW. Pathophysiology of Tamm-Horsfall protein. Kidney International. 1979. pp. 279–289. doi:10.1038/ki.1979.130

12. Artigas A, Wernerman J, Arroyo V, Vincent J-L, Levy M. Role of albumin in diseases associated with severe systemic inflammation: Pathophysiologic and clinical evidence in sepsis and in decompensated cirrhosis. J Crit Care. 2016;33: 62–70.

13. Agrawal S, Smoyer WE. Role of albumin and its modifications in glomerular injury. Pflugers Arch. 2017;469: 975–982.

14. Snyder S, Pendergraph B. Detection and evaluation of chronic kidney disease. Am Fam Physician. 2005;72: 1723–1732.

15. Fan S-L, Bai S. Urinalysis. Contemporary Practice in Clinical Chemistry. 2020. pp. 665–680. doi:10.1016/b978-0-12-815499-1.00038-7

16. Kazancioğlu R. Risk factors for chronic kidney disease: an update. Kidney International Supplements. 2013. pp. 368–371. doi:10.1038/kisup.2013.79

17. Kassem H, Jaar BG. Risk Factors for Chronic Kidney Disease. Kidney Protection. 2019. pp. 29–38. doi:10.1093/med/9780190611620.003.0004

18. Chapter 1: Definition and classification of CKD. Kidney Int Suppl. 2013;3: 19–62.

19. Cao Q, Harris DCH, Wang Y. Macrophages in kidney injury, inflammation, and fibrosis. Physiology. 2015;30: 183–194.

20. Rodríguez-Prados J-C, Través PG, Cuenca J, Rico D, Aragonés J, Martín-Sanz P, et al. Substrate Fate in Activated Macrophages: A Comparison between Innate, Classic, and Alternative Activation. The Journal of Immunology. 2010. pp. 605–614. doi:10.4049/jimmunol.0901698

21. Ramseyer VD, Garvin JL. Tumor necrosis factor-α: regulation of renal function and blood pressure. American Journal of Physiology-Renal Physiology. 2013. pp. F1231–F1242. doi:10.1152/ajprenal.00557.2012

22. Meng X-M, Tang PM-K, Li J, Lan HY. Macrophage Phenotype in Kidney Injury and Repair. Kidney Diseases. 2015. pp. 138–146. doi:10.1159/000431214

23. Jevnikar AM, Brennan DC, Singer GG, Heng JE, Maslinski W, Wuthrich RP, et al. Stimulated kidney tubular epithelial cells express membrane associated and secreted TNFα. Kidney International. 1991. pp. 203–211. doi:10.1038/ki.1991.201

24. Al-Lamki RS, Mayadas TN. TNF receptors: signaling pathways and contribution to renal dysfunction. Kidney Int. 2015;87: 281–296.

25. Liu Y. Cellular and molecular mechanisms of renal fibrosis. Nat Rev Nephrol. 2011;7: 684–696.

26. Luft FC, Mervaala E, Müller DN, Gross V, Schmidt F, Park JK, et al. Hypertension-Induced End-Organ Damage. Hypertension. 1999. pp. 212–218. doi:10.1161/01.hyp.33.1.212

27. Davies PF. Mechanisms involved in endothelial responses to hemodynamic forces. Atherosclerosis. 1997;131 Suppl: S15–7.

28. Davies PF. Overview: temporal and spatial relationships in shear stress-mediated endothelial signalling. J Vasc Res. 1997;34: 208–211.

29. Mervaala EMA, Müller DN, Park J-K, Schmidt F, Löhn M, Breu V, et al. Monocyte Infiltration and Adhesion Molecules in a Rat Model of High Human Renin Hypertension. Hypertension. 1999. pp. 389–395. doi:10.1161/01.hyp.33.1.389

30. Di Lullo L, House A, Gorini A, Santoboni A, Russo D, Ronco C. Chronic kidney disease and cardiovascular complications. Heart Fail Rev. 2015;20: 259–272.

31. Pi-Sunyer FX, Xavier Pi-Sunyer F. Obesity and Hypertension. Obesity Management. 2009. pp. 57–61. doi:10.1089/obe.2009.0204

32. Lerman LO, Lerman A. [The metabolic syndrome and early kidney disease: another link in the chain?]. Revista espanola de cardiologia. 2011. pp. 358–360.

33. Trefts E, Gannon M, Wasserman DH. The liver. Curr Biol. 2017;27: R1147–R1151.

34. Alamri ZZ. The role of liver in metabolism: an updated review with physiological emphasis Zaenah Zuhair Alamri. IJBCP. 2018;7: 2271.

35. Ábel T, Lengyel G. Nonalcoholic Fatty Liver Disease (NAFLD). Bentham Science Publishers; 2017.

36. Byrne CD, Targher G. NAFLD: a multisystem disease. J Hepatol. 2015;62: S47–64.

37. Bertolotti M, Lonardo A, Mussi C, Baldelli E, Pellegrini E, Ballestri S, et al. Nonalcoholic fatty liver disease and aging: epidemiology to management. World J Gastroenterol. 2014;20: 14185–14204.

38. Musso G, Gambino R, Cassader M, Pagano G. Meta-analysis: natural history of non-alcoholic fatty liver disease (NAFLD) and diagnostic accuracy of non-invasive tests for liver disease severity. Ann Med. 2011;43: 617–649.

39. Charlton MR, Burns JM, Pedersen RA, Watt KD, Heimbach JK, Dierkhising RA. Frequency and outcomes of liver transplantation for nonalcoholic steatohepatitis in the United States. Gastroenterology. 2011;141: 1249–1253.

40. Giboney PT. Mildly elevated liver transaminase levels in the asymptomatic patient. Am Fam Physician. 2005;71: 1105–1110.

41. Huang X-J, Choi Y-K, Im H-S, Yarimaga O, Yoon E, Kim H-S. Aspartate Aminotransferase (AST/GOT) and Alanine Aminotransferase (ALT/GPT) Detection Techniques. Sensors. 2006. pp. 756–782. doi:10.3390/s6070756

42. Daniel S, Ben-Menachem T, Vasudevan G, Ma CK, Blumenkehl M. Prospective evaluation of unexplained chronic liver transaminase abnormalities in asymptomatic and symptomatic patients. Am J Gastroenterol. 1999;94: 3010–3014.

43. Malakouti M, Kataria A, Ali SK, Schenker S. Elevated Liver Enzymes in Asymptomatic Patients – What Should I Do? Journal of Clinical and Translational Hepatology. 2017. pp. 1–10. doi:10.14218/jcth.2017.00027

44. Alves-Bezerra M, Cohen DE. Triglyceride Metabolism in the Liver. Compr Physiol. 2017;8: 1–8.

45. Choi SH, Ginsberg HN. Increased very low density lipoprotein (VLDL) secretion, hepatic steatosis, and insulin resistance. Trends Endocrinol Metab. 2011;22: 353–363.

46. Puig-Jové C, Castelblanco E, Falguera M, Hernández M, Soldevila B, Julián MT, et al. Advanced lipoprotein profile in individuals with normal and impaired glucose metabolism. Rev Esp Cardiol . 2021. doi:10.1016/j.rec.2021.02.006

47. Ozaki I, Motomura M, Setoguchi Y, Fujio N, Yamamoto K, Kariya T, et al. Albumin mRNA expression in human liver diseases and its correlation to serum albumin concentration. Gastroenterologia Japonica. 1991. pp. 472–476. doi:10.1007/bf02782816

48. Donnan K, Segar L. SGLT2 inhibitors and metformin: Dual antihyperglycemic therapy and the risk of metabolic acidosis in type 2 diabetes. Eur J Pharmacol. 2019;846: 23–29.

49. Kobori H, Nangaku M, Navar LG, Nishiyama A. The intrarenal renin-angiotensin system: from physiology to the pathobiology of hypertension and kidney disease. Pharmacol Rev. 2007;59: 251–287.

50. Navar LG, Gabriel Navar L. Counterpoint: Activation of the Intrarenal Renin-Angiotensin System is the Dominant Contributor to Systemic Hypertension. Journal of Applied Physiology. 2010. pp. 1998–2000. doi:10.1152/japplphysiol.00182.2010a

51. Toto RD. Treatment of hypertension in chronic kidney disease. Semin Nephrol. 2005;25: 435–439.

52. Mitrofanova A, Sosa MA, Fornoni A. Lipid mediators of insulin signaling in diabetic kidney disease. Am J Physiol Renal Physiol. 2019;317: F1241–F1252.

53. Krentz AJ, Bailey CJ. Oral antidiabetic agents: current role in type 2 diabetes mellitus. Drugs. 2005;65: 385–411.

54. Betônico CC, Titan SM, Correa-Giannella ML, Nery M, Queiroz M. Management of diabetes mellitus in individuals with chronic kidney disease: therapeutic perspectives and glycemic control. Clinics. 2016. pp. 47–53. doi:10.6061/clinics/2016(01)08

55. Day EA, Ford RJ, Lu JH, Lu R, Lally JS, Schertzer JD, et al. Canagliflozin Directly Reduces Macrophage Inflammation via AMPK in a Mouse Model of Atherosclerosis. Atherosclerosis Supplements. 2018. p. 115. doi:10.1016/j.atherosclerosissup.2018.04.354

56. Hsia DS, Grove O, Cefalu WT. An update on sodium-glucose co-transporter-2 inhibitors for the treatment of diabetes mellitus. Curr Opin Endocrinol Diabetes Obes. 2017;24: 73–79.

57. Moses R, Colagiuri S, Pollock C. SGLT2 inhibitors: New medicines for addressing unmet needs in type 2 diabetes. Australasian Medical Journal. 2014. pp. 405–415. doi:10.4066/amj.2014.2181

58. Stanton RC. Sodium Glucose Transport 2 (SGLT2) Inhibition Decreases Glomerular Hyperfiltration. Circulation. 2014. pp. 542–544. doi:10.1161/circulationaha.113.007071

59. Cherney DZI, Perkins BA, Soleymanlou N, Maione M, Lai V, Lee A, et al. Renal hemodynamic effect of sodium-glucose cotransporter 2 inhibition in patients with type 1 diabetes mellitus. Circulation. 2014;129: 587–597.

60. Majewski C, Bakris GL. Blood Pressure Reduction: An Added Benefit of Sodium–Glucose Cotransporter 2 Inhibitors in Patients With Type 2 Diabetes: Table 1. Diabetes Care. 2015. pp. 429–430. doi:10.2337/dc14-1596

61. Jardine MJ, Zhou Z, Mahaffey KW, Oshima M, Agarwal R, Bakris G, et al. Renal, Cardiovascular, and Safety Outcomes of Canagliflozin by Baseline Kidney Function: A Secondary Analysis of the CREDENCE Randomized Trial. J Am Soc Nephrol. 2020;31: 1128–1139.

62. Bakris G, Oshima M, Mahaffey KW, Agarwal R, Cannon CP, Capuano G, et al. Effects of Canagliflozin in Patients with Baseline eGFR <30 ml/min per 1.73 m: Subgroup Analysis of the Randomized CREDENCE Trial. Clin J Am Soc Nephrol. 2020;15: 1705–1714.

63. Azushima K, Gurley SB, Coffman TM. Modelling diabetic nephropathy in mice. Nat Rev Nephrol. 2018;14: 48–56.

64. Wong SK, Chin K-Y, Suhaimi FH, Fairus A, Ima-Nirwana S. Animal models of metabolic syndrome: a review. Nutr Metab. 2016;13: 65.

65. Wiley. Obesity and Overeating: Research Fundamentals. John Wiley & Sons; 2013.

66. Lutz TA, Woods SC. Overview of animal models of obesity. Curr Protoc Pharmacol. 2012; Chapter 5: Unit5.61.

67. Thibodeau J-F, Holterman CE, Burger D, Read NC, Reudelhuber TL, Kennedy CRJ. A novel mouse model of advanced diabetic kidney disease. PLoS One. 2014;9: e113459.

68. Alpers CE, Hudkins KL. Mouse models of diabetic nephropathy. Current Opinion in Nephrology and Hypertension. 2011. pp. 278–284. doi:10.1097/mnh.0b013e3283451901

69. Furman BL. Streptozotocin-Induced Diabetic Models in Mice and Rats. Curr Protoc Pharmacol. 2015;70: 5.47.1–5.47.20.

70. Zheng S, Noonan WT, Metreveli NS, Coventry S, Kralik PM, Carlson EC, et al. Development of late-stage diabetic nephropathy in OVE26 diabetic mice. Diabetes. 2004;53: 3248–3257.

71. Gurley SB, Clare SE, Snow KP, Hu A, Meyer TW, Coffman TM. Impact of genetic background on nephropathy in diabetic mice. Am J Physiol Renal Physiol. 2006;290: F214–22.

72. Brosius FC 3rd, Alpers CE, Bottinger EP, Breyer MD, Coffman TM, Gurley SB, et al. Mouse models of diabetic nephropathy. J Am Soc Nephrol. 2009;20: 2503–2512.

73. Xu J, Huang Y, Li F, Zheng S, Epstein PN. FVB mouse genotype confers susceptibility to OVE26 diabetic albuminuria. Am J Physiol Renal Physiol. 2010;299: F487–94.

74. Morimoto S, Cassell MD, Sigmund CD. The brain renin-angiotensin system in transgenic mice carrying a highly regulated human renin transgene. Circ Res. 2002;90: 80–86.

75. Touyz RM, Mercure C, He Y, Javeshghani D, Yao G, Callera GE, et al. Angiotensin II-dependent chronic hypertension and cardiac hypertrophy are unaffected by gp91phox-containing NADPH oxidase. Hypertension. 2005;45: 530–537.

76. Zhang J, Wu J, Gu C, Noble NA, Border WA, Huang Y. Receptor-mediated nonproteolytic activation of prorenin and induction of TGF-β1 and PAI-1 expression in renal mesangial cells. Am J Physiol Renal Physiol. 2012;303: F11–20.

77. Glastras SJ, Chen H, Teh R, McGrath RT, Chen J, Pollock CA, et al. Mouse Models of Diabetes, Obesity and Related Kidney Disease. PLOS ONE. 2016. p. e0162131. doi:10.1371/journal.pone.0162131

78. Wu KK, Huan Y. Streptozotocin-induced diabetic models in mice and rats. Curr Protoc Pharmacol. 2008; Chapter 5: Unit 5.47.

79. Burger D, Reudelhuber TL, Mahajan A, Chibale K, Sturrock ED, Touyz RM. Effects of a domain-selective ACE inhibitor in a mouse model of chronic angiotensin II-dependent hypertension. Clinical Science. 2014. pp. 57–63. doi:10.1042/cs20130808

80. Prescott G, Silversides DW, Chiu SM, Reudelhuber TL. Contribution of circulating renin to local synthesis of angiotensin peptides in the heart. Physiol Genomics. 2000;4: 67–73.

81. Graham ML, Janecek JL, Kittredge JA, Hering BJ, Schuurman H-J. The streptozotocin-induced diabetic nude mouse model: differences between animals from different sources. Comp Med. 2011;61: 356–360.

82. Saadane A, Lessieur EM, Du Y, Liu H, Kern TS. Successful induction of diabetes in mice demonstrates no gender difference in development of early diabetic retinopathy. PLoS One. 2020;15: e0238727.

83. Leiter EH. Multiple low-dose streptozotocin-induced hyperglycemia and insulitis in C57BL mice: Influence of inbred background, sex, and thymus. Proceedings of the National Academy of Sciences. 1982. pp. 630–634. doi:10.1073/pnas.79.2.630

84. Licholai JA, Nguyen KP, Fobbs WC, Schuster CJ, Ali MA, Kravitz AV. Why Do Mice Overeat High-Fat Diets? How High-Fat Diet Alters the Regulation of Daily Caloric Intake in Mice. Obesity. 2018. pp. 1026–1033. doi:10.1002/oby.22195

85. Wang C-Y, Liao JK. A mouse model of diet-induced obesity and insulin resistance. Methods Mol Biol. 2012;821: 421–433.

86. Hawley SA, Ford RJ, Smith BK, Gowans GJ, Mancini SJ, Pitt RD, et al. The Na+/Glucose Cotransporter Inhibitor Canagliflozin Activates AMPK by Inhibiting Mitochondrial Function and Increasing Cellular AMP Levels. Diabetes. 2016;65: 2784–2794.

87. Thomas R, Kanso A, Sedor JR. Chronic Kidney Disease and Its Complications. Primary Care: Clinics in Office Practice. 2008. pp. 329–344. doi:10.1016/j.pop.2008.01.008

88. Griffin KA. Hypertensive Kidney Injury and the Progression of Chronic Kidney Disease. Hypertension. 2017. pp. 687–694. doi:10.1161/hypertensionaha.117.08314

89. Triplitt CL. Understanding the kidneys' role in blood glucose regulation. Am J Manag Care. 2012;18: S11–6.

90. Garcovich M, Zocco MA, Gasbarrini A. Clinical use of albumin in hepatology. Blood Transfus. 2009;7: 268–277.

91. Polotsky VY. Mouse model of the metabolic syndrome: the quest continues. Journal of Applied Physiology. 2007. pp. 2088–2089. doi:10.1152/japplphysiol.00219.2007

92. Gorriz JL, Martinez-Castelao A. Proteinuria: detection and role in native renal disease progression. Transplant Rev. 2012;26: 3–13.

93. Saratlija Novakovic Z, Glavina Durdov M, Puljak L, Saraga M, Ljutic D, Filipovic T, et al. The interstitial expression of alpha-smooth muscle actin in glomerulonephritis is associated with renal function. Med Sci Monit. 2012;18: CR235–40.

94. Kramann R, Menzel S. Mouse Models of Kidney Fibrosis. Methods Mol Biol. 2021;2299: 323–338.

95. Lerman LO, Chade AR, Sica V, Napoli C. Animal models of hypertension: An overview. Journal of Laboratory and Clinical Medicine. 2005. pp. 160–173. doi:10.1016/j.lab.2005.05.005

96. Yin D, Tao J, Lee DD, Shen J, Hara M, Lopez J, et al. Recovery of islet beta-cell function in streptozotocin- induced diabetic mice: an indirect role for the spleen. Diabetes. 2006;55: 3256–3263.

97. R N, Nasrallah R, Zimpelmann J, Cheff V, Thibodeau JF, Burns KD, et al. Collecting duct PGE2 responses reduce water loss with empagliflozin in mice with type 2 diabetes mellitus. Journal of Clinical Nephrology. 2021. pp. 023–030. doi:10.29328/journal.jcn.1001069

98. Sullivan KA, Lentz SI, Roberts JL Jr, Feldman EL. Criteria for creating and assessing mouse models of diabetic neuropathy. Curr Drug Targets. 2008;9: 3–13.

99. Wahba IM, Mak RH. Obesity and obesity-initiated metabolic syndrome: mechanistic links to chronic kidney disease. Clin J Am Soc Nephrol. 2007;2: 550–562.

100. Chang A, Kramer H. Effect of Obesity and the Metabolic Syndrome on Incident Kidney Disease and the Progression to Chronic Kidney Failure. Nutritional Management of Renal Disease. 2013. pp. 445–456. doi:10.1016/b978-0-12-391934-2.00028-x

101. Nashar K, Egan B. Relationship between chronic kidney disease and metabolic syndrome: current perspectives. Diabetes, Metabolic Syndrome and Obesity: Targets and Therapy. 2014. p. 421. doi:10.2147/dmso.s45183

102. Leoni S, Tovoli F, Napoli L, Serio I, Ferri S, Bolondi L. Current guidelines for the management of non-alcoholic fatty liver disease: A systematic review with comparative analysis. World J Gastroenterol. 2018;24: 3361–3373.

103. Vallon V, Platt KA, Cunard R, Schroth J, Whaley J, Thomson SC, et al. SGLT2 Mediates Glucose Reabsorption in the Early Proximal Tubule. Journal of the American Society of Nephrology. 2011. pp. 104–112. doi:10.1681/asn.2010030246

104. Wang XX, Levi J, Luo Y, Myakala K, Herman-Edelstein M, Qiu L, et al. SGLT2 Protein Expression Is Increased in Human Diabetic Nephropathy: SGLT2 PROTEIN INHIBITION DECREASES RENAL LIPID ACCUMULATION, INFLAMMATION, AND THE DEVELOPMENT OF NEPHROPATHY IN DIABETIC MICE. J Biol Chem. 2017;292: 5335–5348.

105. Jurczak MJ, Lee H-Y, Birkenfeld AL, Jornayvaz FR, Frederick DW, Pongratz RL, et al. SGLT2 deletion improves glucose homeostasis and preserves pancreatic beta-cell function. Diabetes. 2011;60: 890–898.

106. Coll AP, Farooqi IS, O'Rahilly S. The hormonal control of food intake. Cell. 2007;129: 251–262.

107. Andres-Hernando A, Lanaspa MA, Kuwabara M, Orlicky DJ, Cicerchi C, Bales E, et al. Obesity causes renal mitochondrial dysfunction and energy imbalance and accelerates chronic kidney disease in mice. Am J Physiol Renal Physiol. 2019;317: F941–F948.

108. Fioretto P, Zambon A, Rossato M, Busetto L, Vettor R. SGLT2 Inhibitors and the Diabetic Kidney. Diabetes Care. 2016;39 Suppl 2: S165–71.

109. León-Jiménez D, Moreno-Obregón F, Beltrán-Romero LM, Miramontes-González JP. Is the joint use of diuretics and SGLT2 inhibitors beneficial in diabetic kidney disease? Kidney International. 2020. p. 213. doi: 10.1016/j.kint.2019.08.039

110. Xu C, Wang W, Zhong J, Lei F, Xu N, Zhang Y, et al. Canagliflozin exerts anti-inflammatory effects by inhibiting intracellular glucose metabolism and promoting autophagy in immune cells. Biochem Pharmacol. 2018;152: 45–59.

111. Abdul-Ghani MA, DeFronzo RA. Inhibition of renal glucose reabsorption: a novel strategy for achieving glucose control in type 2 diabetes mellitus. Endocr Pract. 2008;14: 782–790.

112. Calle P, Hotter G. Macrophage Phenotype and Fibrosis in Diabetic Nephropathy. Int J Mol Sci. 2020;21. doi:10.3390/ijms21082806